AD-A029 386

RIA-76-U519

USADACS Technical Library
5 0712 01010323 1

AD-A029 386

EDGEWOOD ARSENAL CONTRACTOR REPORT

EM-CR-76056

Report No. 1

ANALYSIS AND PRELIMINARY DESIGN OF A SUPPRESSIVE STRUCTURE FOR A MELT LOADING OPERATION

by

W. E. Baker

P. S. Westine

P. A. Cox

E. D. Esparza

TECHNICAL LIBRARY

May 1976

SOUTHWEST RESEARCH INSTITUTE

Post Office Drawer 28510, 8500 Culebra Road

San Antonio, Texas 78284

Contract No. DAAD05-74-C-0751

DAAA15-75-C-0083

DEPARTMENT OF THE ARMY

Headquarters, Edgewood Arsenal

Aberdeen Proving Ground, Maryland 21010

Approved for public release; distribution unlimited

19970930 050

DTIC QUALITY INSPECTED 3

Incl 4

Disclaimer

The findings in this report are not to be construed as an official Department of the Army position unless do designated by other authorized documents.

Disposition

Destroy this report when it is no longer needed. Do not return it to the originator.

REPORT DOCUMENTATION PAGE

READ INSTRUCTIONS BEFORE COMPLETING FORM

1. REPORT NUMBER: EM-CR-76056	2. GOVT ACCESSION NO.
3. RECIPIENT'S CATALOG NUMBER	
4. TITLE *(and Subtitle)*: ANALYSIS AND PRELIMINARY DESIGN OF A SUPPRESSIVE STRUCTURE FOR A MELT LOADING OPERATION	5. TYPE OF REPORT & PERIOD COVERED: Tech. Report: Jan. 1974 through March 1974
	6. PERFORMING ORG. REPORT NUMBER: Report No. 1
7. AUTHOR*(s)*: W.E. Baker, P.S. Westine, P.A. Cox, and E.D. Esparza	8. CONTRACT OR GRANT NUMBER*(s)*: DAAD05-74-C-0751, DAAA15-75-C-0083
9. PERFORMING ORGANIZATION NAME AND ADDRESSES: Southwest Research Institute, P. O. Drawer 28510, San Antonio, Texas 78284	10. PROGRAM ELEMENT, PROJECT, TASK AREA & WORK UNIT NUMBERS: PA, A 5751264
11. CONTROLLING OFFICE NAME AND ADDRESS: Commander, Edgewood Arsenal, Attn: SAREA-TS-R, Aberdeen Proving Ground, Md. 21010	12. REPORT DATE: May 1976
	13. NUMBER OF PAGES: 102
14. MONITORING AGENCY NAME & ADDRESS *(if different from Controlling Office)*: Commander, Edgewood Arsenal, Attn: SAREA-MT-H, Aberdeen Proving Ground, Md. 21010, (Mr. Bruce W. Jezek, CPO. 671-2201)	15. SECURITY CLASS. *(of this report)*: UNCLASSIFIED
	15a. DECLASSIFICATION/DOWNGRADING SCHEDULE: N/A

16. DISTRIBUTION STATEMENT *(of this Report)*

Approved for public release; distribution unlimited.

17. DISTRIBUTION STATEMENT *(of the abstract entered in Block 20, if different from Report)*

18. SUPPLEMENTARY NOTES

19. KEY WORDS *(Continue on reverse side if necessary and identify by block number)*

Suppressive structures	Dynamic structural response
Limit design	Plastic structural design
Blast loads	Blast scaling
Blast venting	Structural response

20. ABSTRACT *(Continue on reverse side if necessary and identify by block number)*

This report is the first in a series describing the development of methods for estimating dynamic loading and plastic response of suppressive structures. It covers application to containment of the blast from an accidental explosion in a melt loading operation, and includes preliminary developments of methods to predict blast loads and plastic structural response.

DD FORM 1 JAN 73 1473 EDITION OF 1 NOV 65 IS OBSOLETE

PREFACE

The work described in this report was authorized under PA, A 5751264, Preliminary Design of a Suppressive Structure for a Melt-Loading Operation. It was performed from January 1974 to March 1974.

Reproduction of this document in whole or in part is prohibited except with permission of the Commander, Edgewood Arsenal, Attn: SAREA-TS-R, Aberdeen Proving Ground, Maryland, 21010; however, DDC and the National Technical Information Service is authorized to reproduce the document for United States Government purposes.

This report was printed originally as Technical Report No. 1, Contract DAAD05-74-C-0751, in March 1974. It had a limited distribution of 15 copies. Because the work formed the basis for a number of later studies in loading and response of suppressive structures, it is reprinted here with only minor corrections, and given a much wider distribution.

The design concepts for the Category 1 structures presented here have evolved into rather drastically different structures, so one should *not* accept them as optimum designs. The report also contains no discussion of design for arresting fragments. The value of the report lies largely in the methods for prediction of internal and external blast loads, and methods for prediction of structural response using energy methods and allowing large plastic deformations. These methods, given in Appendices A, B and C, have been refined and modified in later reports, but the basic principles given in this report are largely unchanged in the later work.

TABLE OF CONTENTS

LIST OF ILLUSTRATIONS

LIST OF ILLUSTRATIONS (Cont'd)

ANALYSIS AND PRELIMINARY DESIGN OF A SUPPRESSIVE STRUCTURE FOR A MELT-LOADING OPERATION

I. EXECUTIVE SUMMARY

Guidelines

This report presents the results of a preliminary design study for a suppressive structure to suppress the blast effects from accidental detonation of a relatively large quantity of explosive. Guidelines are:

- Suppression of blast from 2500 lb of Comp B detonated in a melt kettle.
- Suppression desired to 50% or better of the peak side-on overpressure at the intraline distance (from DOD standards), and at all closer distances.
- Fragment containment will not be specifically considered in our design, although members are included which are primarily fragment stops.
- The desired floor working area is approximately 40 ft X 40 ft, and internal structure volume about 64,000 ft^3. This volume is assumed to be a simple shape, rather than a two- or three-tiered structure more typical of a melt loading plant.
- Past suppressive structures designs and test results will be used as much as possible in this study.
- We are to recommend structural configurations, size and overall design based on principles of limit design (plastic deformation). Curved structures as well as rectangular ones are to be considered.

Design Concepts

Two basic design concepts were considered. Concept A was a 40 ft X 40 ft X 40 ft rectangular box structure, with a false gridwork floor 10 ft above its base. Concept B was a 22.3 ft radius by 40 ft long horizontal cylinder, again with a false gridwork floor. As a limit to the concept of a curved structure, an unvented spherical shell was also considered. (In any blast containment structure, material is used most efficiently in the form of a pressure vessel, and the most efficient form of a pressure vessel is a sphere.)

Loading

An empirical method was developed, based on scaling of measurements of suppressed blast waves from past suppressive structure tests, to correlate vent panel designs with degree of blast suppression. A model analysis was also conducted for internal pressure rises in structures with various degrees of venting, but no applicable data were found for well-vented structures. Initial blast loads were predicted from sources of reflected blast data, accounting for

venting areas of innermost panels. The governing loads are quasi-static pressure rises of 145 psi for Concept A and 150 psi for Concept B, but these values may be reduced based on an ongoing test program.

Response

A number of design formulas were developed for prediction of plastic deformations of a variety of structural elements under impulsive and quasi-static pressure loading. Both bending and membrane deformations were considered. Structural elements included one-degree-of-freedom systems, simply-supported beams, clamped-clamped beams, rectangular plates, clamped-ended cylindrical shells, and spherical shells.

Results

Both Concepts A and B proved feasible. Structural weights for these structures were :

Structure	Weight, tons
Concept A (box)	799
Concept B (cylinder)	566

A comparison with a reinforced concrete rectangular structure, designed according to methods in TM5-1300, would perhaps be instructive. But, the structure closest to these containers in that TM is a four-wall cubicle with a frangible roof, with the walls designed for impulsive loading only. We have noted that the quasi-static pressure rise governs the current design, so it is entirely inappropriate to compare a concrete cubicle designed by the methods in TM5-1300 to the designs reported here.

Conclusions

The design, though feasible, is not yet optimized. Significant reductions in weight and cost would probably result from a further design effort. Further test and/or analyses were recommended to determine quasi-static pressure rises. A carefully-instrumented series of tests of a scale model structure to 1/4 or smaller scale was also recommended, prior to construction and test of the full-scale structure.

Fragment retention by the structure may or may not prove to be a problem—we did not address it in this study to date. Specific geometry of the melt kettle and nearby equipment will define the fragment hazard, with the most severe hazards probably being massive pieces of nearby equipment which are accelerated by the blast wave. Because of the fixed locations of melt kettles, such pieces can perhaps be best stopped by localized missile shields.

II. DESCRIPTION OF THE PROBLEM

The basic problem is one of design of a suppressive structure to suppress the air blast wave and contain the fragments from detonation of 2500 lb of Composition B explosive of hemispherical shape being processed in a melt kettle. Although present kettle designs involve the 2500 lb in three locations within the facility, for simplicity, we have considered the total amount in one structure of approximately the correct facility cubic footage. This work addresses only blast loading and design to withstand blast effects, however, with containment of kettle fragments being separately considered by others.

A floor working area of 40 ft × 40 ft is desired within the suppressive structure, with a structure height above the floor of 30 ft. A gridwork false floor can be allowed about 10 ft above the base of the structure, giving a total volume within the suppressive structure of about 40 ft × 40 ft × 40 ft = 64,000 ft^3.

Blast suppression desired is a reduction of at least 50% in peak sideon overpressure at all distances up to the intraline distance specified by DOD ammunition and explosive safety standards. From Table 5-6.4 of Reference 1, the intraline distance for an unbarricaded structure is given by the equation

$$R = 18\ W^{1/3} \tag{1}$$

where R is distance in feet and W is explosive charge weight in pounds. This distance is, for this study,

$$R = 18 \times 2500^{1/3} = 244 \text{ ft}$$

The peak side-on overpressure in the absence of a suppressive structure is, at this distance, (see Figure 6.1 in reference 2)

$$P_s = 3.5 \text{ psi}$$

Our goal for blast suppression is therefore

$$P_s = 1.75 \text{ psi at } R = 244 \text{ ft},$$

and 50% or better percentage reduction from free-air blast pressures at all distances closer to the structure.

Past suppressive structure designs and experimental data on attenuation of blast waves by these structures are largely the result of work sponsored by the Hazardous Materials Engineering Office, Edgewood Arsenal, and conducted at the NASA Mississippi Test Facility. References 3-6 are typical of recent designs and studies of this nature. As much as possible,

the technology developed during these and current studies is to be used as a basis for the current study, supplemented by other data and references available to us.

Another guideline which has governed our study is that principles of limit design should be used, i.e., the structure can be designed for large plastic deformation, rather than requiring that it be elastic and suffer no or negligible permanent deformation.

In conducting the design study, we are to do the following:

(1) Consider several different suppressive structural configurations, such as thin-walled cylindrical or curved structure, and box-shaped frame structure with internal panels. For each configuration, calculate transient blast loading on walls and quasi-static pressure rise for each of several sizes of structure. Blast loading estimates will be based on past suppressive structure studies and related work.

(2) Determine, using dynamic plastic structural response methods, strength and/or weights and stiffnesses of structures to contain the blast effects for each structural configuration. Energy methods and assumed deformed shapes will be used for these analyses as much as practicable.

(3) Recommend a structural configuration, size, and overall design based on results of the above analyses.

This report presents the results of the study.

III. DESIGN CONCEPTS AND LIMITATIONS TO DESIGN CONCEPTS

Suppressive structures are basically well-vented, multi-layered structures. Although they can conceptually be made in almost any conceivable geometry, requirements for ease and low cost of construction using readily available structural steel members have usually dictated rectangular box structures, with an alternative geometry being a cylindrical structure with flat ends. Doubly-curved structures such as spherical shells or domed ends for cylindrical shells require expensive fabrication methods, particularly when using the concept of a suppressive structure which requires multiple, spaced layers. Therefore the investigation was confined to two basic geometries, a rectangular box (Concept A) and a horizontal cylinder with flat ends (Concept B). The basic geometry and internal sizes assumed in this study are shown in Figure 1. A gridwork floor 40 ft $\times$ 40 ft in area is assumed for both configurations. Concept A has an internal volume $V_A = 40 \times 40 \times 40 = 64{,}000$ ft^3 while Concept B has a volume $V_B = \pi \times 22.3^2 \times 40 = 62{,}800$ ft^3. The melt kettle is assumed to be located in the center of either structure, about 5 ft above the gridwork floor. For estimation of blast loads, it will be assumed to be located in the *exact* center of each structure.

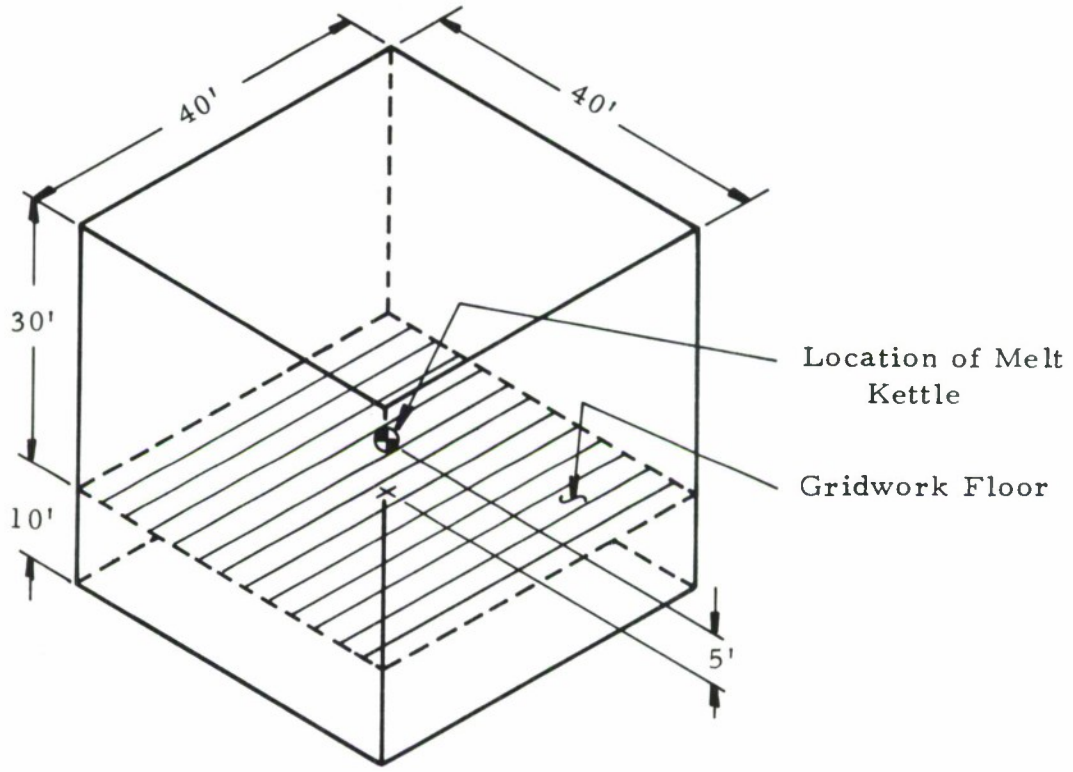

Concept A. Rectangular Box Structure

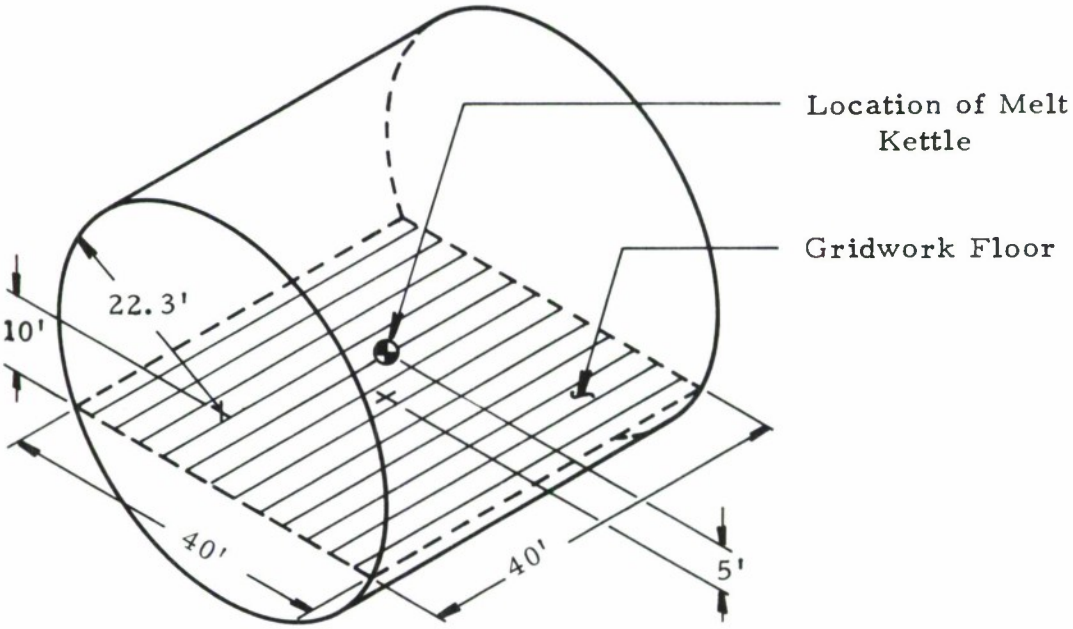

Concept B. Horizontal Cylinder Structure

FIGURE 1. BASIC CONFIGURATIONS

In applying the principles of limit design to each of these overall configurations, we will consider the ability of structural elements to absorb energy in plastic deformation by bending and membrane action, and will in general ignore the much smaller capability of these same elements to absorb energy by elastic deformation. Energies imparted to the structure by both the initial reflected blast loading (kinetic energy) and by the much longer duration quasi-static pressure resulting from addition of heat energy of the explosive to the air within the structure (plastic work) will both be considered.

A crucial question in the design of this particular structure is the degree to which the venting attenuates the quasi-static pressure rise after detonation of the explosive. We will address this question in some detail, based on available experimental data and analyses. We will also correlate existing designs with the degree of blast suppression measured outside the structure, and use this correlation as a basic design tool.

To use the results of the previous work on suppressive structures to the maximum extent possible, we will generally limit our panel elements to ones similar to those used already, i.e., angles, zees, perforated plates, and louvres. Support elements will be designed from readily available steel structural members such as I-beams, H-beams, angles, channels, circular tubing, or rectangular tubing. Because we wish also to plan a subscale test, we will be partially governed in our choice of structural members by the availability of smaller members of the same geometry which are nearly or exactly one-quarter scale sections of the prototype members. (In applying methods for subscale modeling of blast loading and structural response well into the plastic regime, we will *assume* that these methods are proven and well-known. References 7-10 provide ample evidence that this indeed is the case).

Although we have specifically excluded doubly-curved structures in this study, and also limit ourselves to well-vented structures, it seems wise to make a quick calculation to determine whether *any* structure of the assumed volume is feasible for containment of the blast and static pressure effects resulting from detonation of 2500 lb of Composition B. We consider an elastic-plastic steel sphere, completely unvented, with the charge detonated at the center. The internal volume is assumed to be $V = 64{,}000$ ft^3.

The analysis is based on References 11 and 12, and is presented in Appendix A. The results are:

(1) Design is controlled by quasi-static pressure, rather than initial reflected blast loading.

(2) Shell thickness $h = 0.432$ inch, at a radius $a = 298$ inches for mild steel with a yield stress $\sigma_y = 40{,}000$ psi.

(3) Weight of steel in the shell is $W_s = 136{,}000$ lb.

So, complete containment is feasible ignoring primary and secondary fragmentation with a shell weighing 68 tons. These results can be used as a rough basis to judge efficiency of suppressive structure design.

IV. METHODS OF ESTIMATING DYNAMIC AND STATIC LOADING

The loading from an explosive charge detonated within a vented or unvented structure consists of two almost distinct phases. The first phase is that of reflected blast loading. It consists of the initial high pressure, short duration reflected wave, plus perhaps several later reflected pulses arriving at times closely approximated by twice the average time of arrival at the chamber walls. These later pulses are attenuated in amplitude because of irreversible thermodynamic process, and they may be very complex in waveform because of the complexity of the reflection process within the structure, whether vented or unvented. We will assume in this study that the *first* blast pulse striking the walls is the important dynamic loading pulse, and neglect later ones. If the structure has solid walls, the blast loading can be accurately estimated by using sources of compiled blast data for normally reflected blast pressures and impulses such as Reference 2, and the well-known Hopkinson's blast scaling law (see Chapter 3 of reference 2). The effect of vented panels in the suppressive structures on reduction of the reflected blast loading will be addressed later.

As the blast waves reflect and re-reflect within the structure and as unburned detonation products combine with the available oxygen*, a quasi-static pressure rise occurs and the second phase of loading takes place. Proctor and Filler[12] present some data on these pressures, Proctor[13] has developed a computer program to calculate both blast and quasi-static pressure rises, and Sewell and Kinney[14] also present methods for estimating this later phase. In addition, Keenan and Tancreto[15] have made measurements of blast pressures emitted from rectangular box cubicles with various vent areas and pressure rises within the cubicles. Finally, Lasseigne[16] has measured static pressure rises in closed chambers to obtain design information for a specific suppressive structure. From these references, one obtains the answer that for the particular ratios of vent area to chamber volume tested, the venting has no effect on the peak quasi-static pressure. Thus, peak static pressures for unvented or poorly vented structures are the same. Unfortunately, essentially no data exist for quasi-static pressures within well-vented structures and the crucial question of the actual maximum pressure rise within such chambers remains unanswered. We must at present use the unvented pressure rise for design purposes. We have, however, conducted a model analysis and fitted curves to all data available to date to obtain the best possible estimate of this pressure. The model analysis and curve fits are presented in Appendix B.

A third important question regarding blast loading and suppressive structures is, "Can blast pressures outside these structures be predicted for specific designs?" Many of the past measurements of effectiveness of these structures have been based on blast attenuation which

*The amount of oxygen available within any complete structure is apparently little affected by venting, until venting area becomes very large.

they provide (see references 3, 5, 6, 16). Using these references and more recent data from MTF, we have generated a method of correlating emitted blast waves with suppressive structure design based on comparing free-field blast data to blast data for waves emanating from suppressive structures. This method introduces an effective vent area ratio, α_{eff}, which can be computed for any combination of vented elements in a suppressive structure panel. Using this parameter and least-squares curve fits to free-field and suppressive structures blast data, we have shown that the influence of the suppressive structure is to create an effective standoff distance R_{st}, less than the free-field standoff distance R_f at which side-on overpressure P_s is the same for a given blast source of energy W. Alternatively, this method will predict the reduction in overpressure over a considerable range of distances outside the structure. Details of the method are given in Appendix B.

The specific criterion which governs the blast loading of the particular structure we are considering is the goal noted in Section II of 50% or better blast overpressure reduction at R = 244 ft, and all closer distances. Using the methods of Appendix B, a value of α_{eff} = 0.0349 and a characteristic suppressive structure size of X = 40 ft, we achieve 50% blast reduction at R = 289 feet. Figure 2 shows the free-field and suppressed overpressures as a function of distance, with all of the suppressed pressures lying below 50% of free-field for $R \leqslant 289$ ft.

Because the effective vent area ratio is small, the quasi-static pressure rise has been assumed to be that for an unvented structure. The rectangular box structure (Concept A) with a volume of 64,000 ft^3, suffers a static pressure rise of ΔP = 145 psi, while the cylindrical structure (Concept B) with the smaller volume of 62,800 ft^3 has a higher pressure rise of ΔP = 150 psi. These values were read from Figure B-5 in Appendix B.

Impulsive loads on either of the structures are calculated from scaled curves in Figures 6-1 and 6-2 of Reference 2. Only the reflected impulses I_r are important, because wall response times are much longer than blast loading times*.

Loading is summarized in Table 1.

TABLE 1. LOADING OF SUPPRESSIVE STRUCTURES

Structure	α_{eff}	ΔP, psi	$(I_r)_{max}$, psi-ms
Concept A	0.0349	145	910**
Concept B	0.0349	150	783**

*These times are longer for flat walls and cylindrical shells than for spherical shells. We show in Appendix A that impulsive loading is appropriate for spherical shells.

**The values for I_r in this table were later found to be incorrect. They should be multiplied by a factor of 1.630.

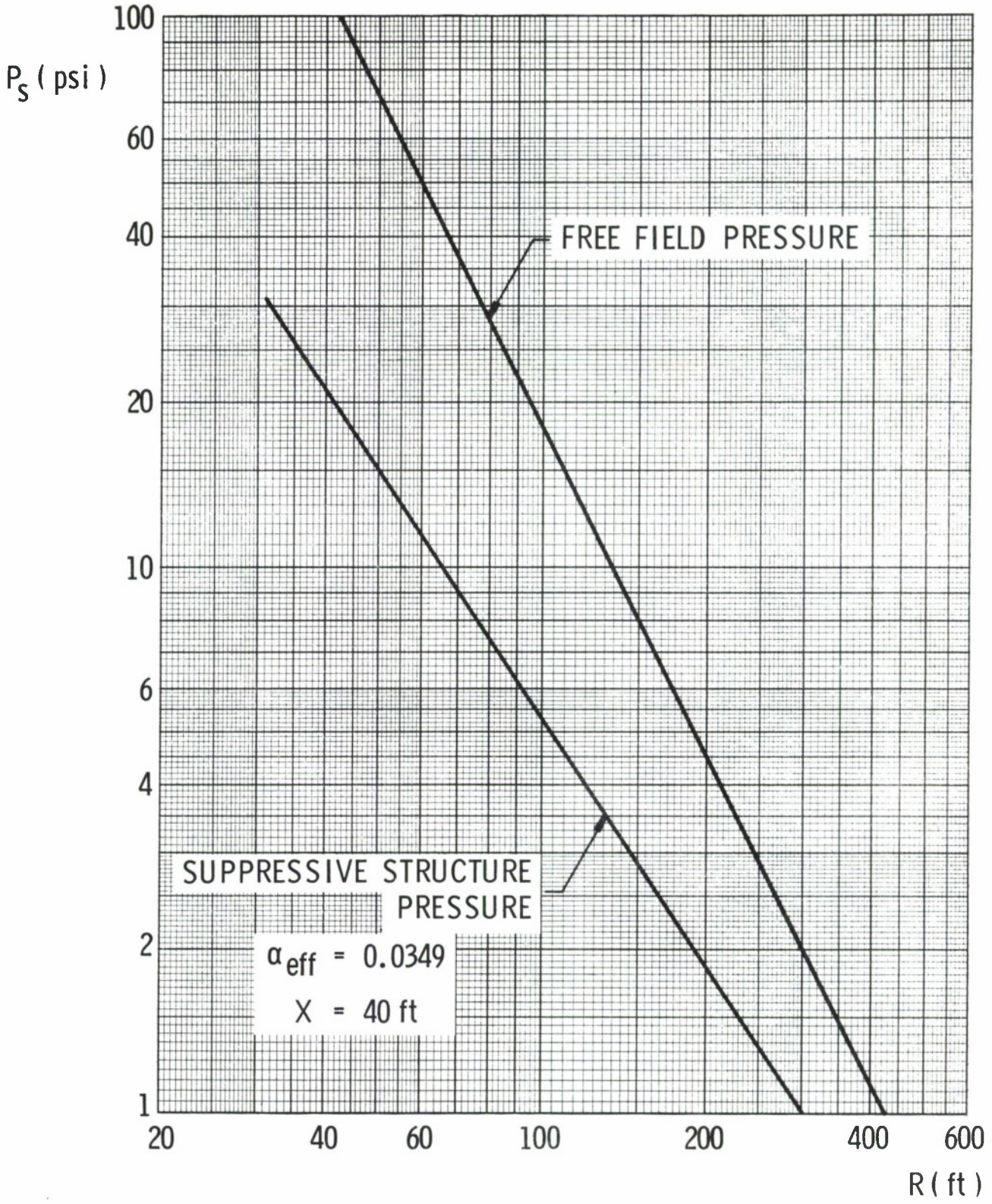

FIGURE 2. ESTIMATED BLAST SUPPRESSION FOR A 40 FT STRUCTURE

V. METHODS OF ESTIMATING RESPONSE OF STRUCTURES AND STRUCTURAL ELEMENTS

A number of limit design formulas were developed during the course of this study for calculating the ability of suppressive structural elements to withstand impulsive and quasi-static blast loads. Most of these formulas are based on energy balance techniques, equating initial kinetic energy from impulsive loading or work from quasi-static loading to plastic strain energy absorbed by the structural element. For some of the structural elements the deformed shapes of the impulsively loaded elements and predicted energy absorbing capabilities were compared with data available in the literature such as References 17-19, and were shown to yield accurate predictions. In all cases, the analyses yielded *explicit* expressions for nondimensional deformations in terms of nondimensional loading parameters. No involved solutions to complex differential equations were required—only integrations of works and strain energies per unit volume of material of each structural element. Table 2 summarizes the types of structural element considered, loading realm, method of plastic energy absorption, etc. Elastic response was entirely neglected, and materials were assumed to be either perfectly plastic, or to be plastic with strain hardening. Beams were characterized by overall dimensions and plastic yield moment or plastic axial load, rather than by detailed cross-sectional properties. Omissions in Table 2 indicate that the particular loading realm or other parameter was felt to be inapplicable for elements used in this specific design, rather than that that formula could not be developed. The letters N/A in the table indicate that a particular response mode did not apply for that structural element.

TABLE 2. SUMMARY OF AVAILABLE RESPONSE PREDICTIONS

Structural Element	Loading Realm		Response Mode		Plasticity	
	Impulsive	Quasi-Static	Bending	Membrane	Perfect	Strain Hard
One-degree-of freedom	X	X	N/A	N/A	X	---
Simply-supported beam	X	X	X	X	X	---
Clamped-clamped beam	X	X	X	X	X	X
Simply-supported rectangular plate	X	X	X	X	X	X
Clamped circular plate	X	---	X	X	X	---
Cylindrical shell	X	X	N/A	X	X	---

Complete details of development of the limit design formulas are given in Appendix C, together with the design formulas themselves. These formulas are too numerous to repeat here, but will be referred to specifically in results in following sections. Their general character is as follows for all elements, however.

Beam Impulsive Response Formulas

$$\left(\frac{i_o{}^2 b^2}{\rho A P_y}\right) \text{ or } \left(\frac{i_o{}^2 b^2 L}{\rho A M_y}\right) = \text{a finite power series in } \left(\frac{w_o}{L}\right) \tag{2}$$

Beam Quasi-Static Response Formulas

$$\left(\frac{pbL^2}{M_y}\right) \text{ or} \left(\frac{pbL}{P_y}\right) = \text{a constant or a finite power series in } \left(\frac{w_o}{L}\right) \tag{3}$$

Plate Impulsive Response Formulas

$$\left(\frac{i_o{}^2 X^2}{\rho \sigma_y h^4}\right) = \left(\text{a shape factor}\right) \left(\text{a finite power series in } \left(\frac{w_o}{h}\right)\right) \tag{4}$$

Plate Quasi-Static Response Formulas

$$\left(\frac{pX^2}{\sigma_y h^2}\right) = \left(\text{a shape factor}\right) \left(\text{a finite power series in} \left(\frac{w_o}{h}\right)\right) \tag{5}$$

Shell Impulsive Response Formula

$$\left(\frac{i_o{}^2}{\rho \sigma_y h^2}\right) = \text{function of} \left(\frac{w_o}{R}, \frac{R}{L}\right) \tag{6}$$

Shell Quasi-Static Response Formula

$$\left(\frac{p_o R}{\sigma_y h}\right) = \text{function of} \left(\frac{w_o}{R}, \frac{R}{L}\right) \tag{7}$$

In these formulas, i_o is the maximum reflected specific impulse, p is quasi-static pressure, P_y is tensile yield force and M_y plastic bending moment for a beam, while σ_y is yield stress. Element dimensions are beam length L; beam width b; beam, plate or shell thickness h; plate minimum half-width X; and shell radius R. Material mass density is ρ.

The complexity of the multi-layered suppressive structures and multiplicity of choices possible for elements renders optimization of the limit design procedure quite difficult and time-consuming, even given design formulas such as those just discussed. Details of our specific choices, which applied past suppressive structures designs as much as possible, are given in Section VI for both Concept A and Concept B. Results will be given in a following section.

VI. RESULTS

Rectangular Box Structure (Concept A)

The preliminary design of the suppressive structure of rectangular box configuration was accomplished to withstand the impulsive and quasi-static pressure loading of Table 1, Section IV, using primarily the plastic response methods and formulas described in Section V and Appendix C. Standard sizes of structural steel members were used in the design, as much as possible. In most cases, smaller members are also commercially available which are exactly or nearly one-quarter scale models of the prototype structural elements, so that a true dynamic response model can be designed and built without incurring added expense for fabrication of special model members. If a smaller model scale is chosen, say one-tenth scale, most of the model members can be easily made from thin gage sheet material by shearing and bending operations.

The primary material chosen for the structure was ASTM A36 steel. A very wide variety of structural shapes are available in this material, and it is quite ductile and therefore desirable for plastic design. Nominal stress-strain properties are:

Yield stress σ_y = 36,000 psi

Ultimate stress σ_u = 58,000-80,000 psi

Ultimate strain ϵ_u = 30%

In general, the basic plastic design criterion was to limit plastic strain to a value of half of ultimate, i.e., $\epsilon_{max} \leqslant 15\%$. We usually also neglected strain-hardening and used yield stress σ_y = 36,000 psi in the design formulas. Both of these criteria provide a margin of safety of at least 38% in the design.

Details of this preliminary design are given in Appendixes D and E. Vented 10 ft × 10 ft panels are considered in Appendix D, while the framework to support the panels is considered in Appendix E. In the latter appendix we depart somewhat from the plastic design criteria of Appendix C. For structural geometries or loading conditions not covered in Appendix C, load distributions within the structure were computed based on elastic behavior. In these cases, fully plastic section moments were combined with the axial loads and the resulting stresses were allowed to exceed the yield stress. However, stresses were always held to less than the minimum rupture stress of the material. Load redistribution in the structure due to yielding should act to limit stresses to even less than those calculated.

In this preliminary design of the box structure of Concept A, the panels consist of an inner layer of angles, backed by four perforated plate layers. For design purposes angles were assumed to absorb most of the initial blast loading in bending, and the plates were assumed to absorb the quasi-static pressure in membrane action. Because the quasi-static pressure controlled the design, the plates will withstand the dynamic loads also and in the actual design

the *angles can be selected based on a fragment criteria so long as the proper venting area is maintained.*

The framework consists of I-beams and deep section built-up members, referred to in our design as "A", "B", and "C" members. The overall structural configuration and details of framework and panel members are shown in Appendixes D and E. The total weight of steel in the Concept A structure is 799 tons. It is proportioned as follows:

Weight of "A" frame members	190 tons
Weight of "B" frame members	53 tons
Weight of "C" frame members	156 tons
Weight of all panel edge members	16 tons
Weight of all angle panels	229 tons
Weight of uniaxial plate panels	131 tons
Weight of biaxial plate panels	24 tons
TOTAL WEIGHT	799 tons

No foundation weight is included in this total, even though a heavily-reinforced concrete base or a strong steel base structure is required to react loads from the main frame members.*

Horizontal Cylindrical Structure (Concept B)

The cylinder which has been designed to contain a 2500 lb explosion has a radius of 22.3 ft and is 40 ft long. In this manner, a 40 ft by 40 ft gridwork floor fits inside as shown in Figure 1. Instead of being a single cylinder, 4 concentric cylinders are used, each of which is 0.300 inches thick and has a staggered hole venting pattern that is 15% of the area. A fifth wall of angles for stopping fragments would also be located within the cylinders. The fragment stops would be 3-1/2 X 3-1/2 X 1/2 inch angle iron with a 2.415 inch spacing, as in Concept A. These angle irons would run in 40 foot strips longitudinally along the walls of the inner cylinder. A total of 697 angle irons would be used so that α for this inner wall equals 0.5. This combination of cylinders and angle irons yields the same α_{eff} as Concept A; hence, the blast field outside either structure would be essentially the same. The total weight of the Concept B would be 566 tons if we assume that the same ends are used to enclose Concept B as we used on one side of the box containment, Concept A. The weight is proportioned as follows:

Weight of 4 concentric cylinders	117 tons
Weight of all 40-ft angles	155 tons
Weight of 2 end enclosures	294 tons
TOTAL WEIGHT	566 tons

*Foundation design could not be completed within the limits of time and funds for this study.

The cylinders were designed so that the maximum strain was limited to 15%. Equation (C-87) gives the longitudinal strain at $X = \pm L/2$ for a cylinder with clamped ends as

$$\epsilon_{\ell} = \frac{8w_o^2}{L^2} \tag{8}$$

Substituting 0.15 for ϵ_{ℓ} and 40 feet for L into Equation (8), limits the deflection to:

$$w_o = 1.705 \text{ ft} \tag{9}$$

The circumferential strain ϵ_c is given by Equation (C-88). For the w_o of Equation (9) the maximum circumferential strain (at the center of the cylinder) equals

$$\epsilon_c = \frac{w_o}{R} = 0.0764 \tag{10}$$

at $X = 0$

Thus the longitudinal strain governs the allowable deflection of the cylinder. Because the cylinder has a slightly smaller volume than the box in Concept A, the quasi-static pressure rise equals 150 psi. This value for p_o is obtained by substituting for W/V in Figure B-5. The radius of $R = 22.3$ ft and length of $L = 40$ ft permit the cylinder to enclose a volume which is almost the same as that for a cube and a floor space which is identical to that in a cube. Substituting for R, L, p_o and w_o in Equation (C-103) and assuming that the steel has a yield point of 36,000 psi yields an overall cylinder thickness of 1.02 inches. Because we will use 4 concentric cylinders to vent the structure instead of one cylinder, the thickness of each cylinder is 0.255 inch. This thickness would be the proper thickness if the cylinders were unvented, but each cylinder has a venting area of 0.15 times the total area of the cylinder; hence, the final thickness of each cylinder was obtained by ratioing the areas or

$$h = \frac{0.255}{0.85} = 0.300 \text{ inches} \tag{11}$$

Structural weight and material thicknesses could be reduced if ductile high strength steels were used, but the price of such a structure could be higher.

VII. DISCUSSION AND CONCLUSIONS

In this report, we have developed preliminary designs of suppressive structures of two different overall geometries with identical 40 ft X 40 ft floor areas, to suppress the blast from 2500 lb of explosive detonated in a melt kettle. As much as possible, results of past suppressive structure designs and blast measurements have been utilized in prediction of

blast suppression, panel design, internal pressures, etc. Methods have been developed for estimating reflected and quasi-static blast loads within the structures, and a number of limit design formulas for plastic deformation of elements of suppressive structures have been developed and used as the basis for our design.

The structural designs resulting from this study indicate that construction of a suppresive structure for this weight of explosive and size of structure is indeed feasible, for either a rectangular box configuration (Concept A) or a horizontal cylinder configuration (Concept B). Ths structural material is used more efficiently in the latter configuration, resulting in a significantly lower total weight of material. We must, however, emphasize that *neither* structure represents an optimum design, but is instead the result of our best effort for the designs which could be made with limited time and funds. It is almost certain that the designs could be improved with additional effort, and that structural weights would decrease in the process of design refinement.

We have adhered throughout to sound principles of engineering design. Some concepts novel to designers accustomed to elastic design with generous safety factors have undoubtedly been introduced, but these concepts are inherent in limit design and are often verified by experimental data from the literature. When we were uncertain of applied loads or structural responses, we invariably made conservative assumptions. *One such assumption has a very strong influence on the design weights—that is the assumption that the venting process has no significant effect on the quasi-static pressure rise within the structures. Any significant reduction in this pressure which is solidly based on experimental data or well-founded analysis will in turn significantly lower structural weight and cost.*

In addition to tests or analyses to better define the quasi-static pressure within well-vented structures, other efforts are recommended prior to final design and construction of a full-scale structure. At least a second iteration in the design procedure should be made to more nearly optimize the design. Design, construction and test of a scale model of the selected configuration would prove highly desirable. This model should be carefully instrumented to measure internal pressure rises, response of critical structural elements, and external suppressed blast pressures. Testing a single panel in the open is not recommended, because the initial blast loading is also drastically altered by diffraction which would not be present in the final structure.

There seems to be some question regarding the validity of blast loading and structural response scale modeling laws and procedures. Such laws exist and have been well-proven by a variety of model prototype tests, for structures undergoing large plastic deformation (see references 7-10). Exact geometric models employing the same materials as the prototype will respond in a manner allowing accurate prediction of prototype response to blasts from scaled explosive charges detonated within. Assuming that the structure in Concept A is to be modeled, Table 3 shows the proper charge weights and structural weights for prototype scale model proof tests for two model scale factors.

TABLE 3. COMPARISON OF PROTOTYPE AND MODEL TEST CONDITIONS

Structure	Charge Wt, Lb.	Parameter				
		Str. Wt, tons	Time Scale	Pressures, Stresses	Strains	Displace-ments
Prototype	2500	799	1	1	1	1
1/4-Scale Model	39.1	12.5	1/4	1	1	1/4
1/10-Scale Model	2.5	0.799	1/10	1	1	1/10

Not only are final deformations properly scaled, but also entire time histories of pressures, stresses, strains and displacements can be used to accurately predict prototype response. We strongly recommend that either 1/4-scale or 1/10-scale well instrumented tests, using increasing charge weights up to the limit in Table 3, precede construction and test of the full-scale structure.

APPENDIX A
ANALYSIS OF A PLASTIC SPHERICAL SHELL CONTAINMENT STRUCTURE

We have assumed an internal volume $V = 64{,}000\ \text{ft}^3$, which gives an internal radius of the sphere of

$$a = \left(\frac{3V}{4\pi}\right)^{1/3} \tag{A-1}$$

$$a = \left(\frac{3 \times 64{,}000}{4\pi}\right)^{1/3} = 24.8\ \text{ft}$$

Methods for response of this shell are reported in Reference 11, but we will use instead an energy method (which is equivalent). Energy imparted to the shell by the blast impulse and by the static pressure is equated to the strain energy in elastic plus plastic deformation under the pure membrane action which applies for a spherical shell. The assumed stress-strain curve for the material is (see reference 11) shown in Figure A-1.

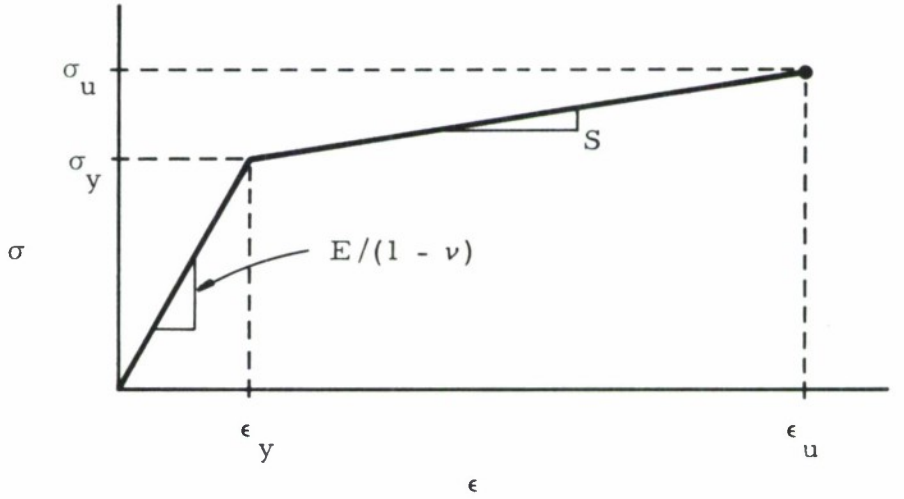

FIGURE A-1. ASSUMED ELASTIC-PLASTIC STRESS-STRAIN CURVE

In this figure, subscript y represents yield and subscript u, ultimate. The area under the stress-strain curve up to any final strain ϵ represents the energy absorbed by the material per unit volume. From Figure A-1, we see that the yield strain ϵ_y is

$$\epsilon_y = \frac{(1-\nu)}{E}\,\sigma_y \tag{A-2}$$

and that the slope S of the strain-hardening part of the curve is

$$S = \frac{(\sigma_u - \sigma_y)}{(\epsilon_u - \epsilon_y)} \tag{A-3}$$

Assume a mild steel with the following properties:

Young's modulus $E = 30 \times 10^6$ psi

Poisson's ratio = $\nu = 1/3$

Yield stress $\sigma_y = 4 \times 10^4$ psi

Ultimate stress $\sigma_u = 6 \times 10^4$ psi

Ultimate strain $\epsilon_u = 30\% = 0.300$

Density $\rho = 7.36 \times 10^{-4}$ lb sec^2/in^4

From Equation (A-2)

$$\epsilon_y = \frac{(1 - 0.333)}{30 \times 10^6} \times 4 \times 10^4 = 0.899 \times 10^{-3}$$

from Equation (A-3)

$$S = \frac{(6 \times 10^4 - 4 \times 10^4)}{(3 \times 10^{-1} - 0.899 \times 10^{-3}} = 6.67 \times 10^4 \text{ psi}$$

A characteristic response time for the shell undergoing plastic deformation is[11]

$$\tau_p = 2\pi/(2S/\rho a^2)^{1/2} \tag{A-4}$$

or

$$\tau_p = 2\pi/(2 \times 6.67 \times 10^4/7.36 \times 10^{-4} \times 298^2)^{1/2} = 0.139 \text{ sec}$$

Blast loading can be calculated from charts in Chapter 6 of Reference 2. Peak pressure is peak normally reflected pressure P_r, and impulse is I_r. From Table 6-1, Reference 2, blast energy is

$$E = W\left(\frac{E}{W}\right) = 2500 \times 20.5 \times 10^6 = 5.125 \times 10^{10} \text{ in-lb}$$

Scaled distance

$$\bar{R} = (Rp_o{}^{1/3})/E^{1/3} \tag{A-5}$$

$$\bar{R} = \frac{298 \times 14.7^{1/3}}{(51.25 \times 10^9)^{1/3}} = 0.195$$

From charts in Chapter 6-1, Reference 2,

$$\bar{P}_r = 157, \bar{I}_r = 0.473$$

$$P_r = 157 \times 14.7 = 2310 \text{ psi}$$

$$I_r = I_r \times p_o^{2/3} \times E^{1/3}/a_o$$

$$= 0.473 \times 14.7^{2/3} \times (51.25 \times 10^9)^{1/3}/1.34 \times 10^4 = 0.792 \text{ psi-sec}$$

Duration of an equivalent triangular pulse is

$$T_r = 2I_r/P_r = 6.86 \times 10^{-4} \text{ sec}$$

This duration is much less than the response time τ_p, so the loading is impulsive.

Using an energy balance, we can now calculate the kinetic energy imparted to the shell by the impulse I_r, and equate this to elastic and plastic strain energy. Kinetic energy is

$$\text{K.E.} = \frac{I_r^2 A^2}{2M} \tag{A-6}$$

where A is shell surface area and M is shell mass. But,

$$A = 4\pi a^2 \tag{A-7}$$

$$M = (4\pi a^2)h\rho \tag{A-8}$$

where h is shell thickness. So,

$$\text{K.E.} = \frac{2I_r^2 \pi a^2}{h\rho} \tag{A-9}$$

Specific strain energy, the area under Figure A-1 up to ultimate stress is

$$D = \frac{\sigma_y \epsilon_y}{2} + \frac{(\sigma_y + \sigma_u)}{2}(\epsilon_u - \epsilon_y) \tag{A-10}$$

$$D = \frac{4 \times 10^4 \times 0.889 \times 10^{-3}}{2} + \frac{(6 \times 10^4 + 4 \times 10^4)}{2}(300 \times 10^{-3})$$

$$= 17.78 + 15{,}000 = 15{,}020 \text{ psi}$$

The *elastic* strain energy, represented by the first term in Equation (A-10), can be seen to be entirely negilgible compared to the *plastic* strain energy.

The volume of shell material is

$$V_s = 4\pi a^2 h \tag{A-11}$$

and total strain energy is

$$\text{S.E.} = V_s D = 4\pi a^2 hD \tag{A-12}$$

Equating (A-9) and (A-12), we can solve explicitly for shell thickness

$$h = (I_r^2 / 2\rho D)^{1/2} \tag{A-13}$$

$$h = \left(\frac{0.792^2}{2 \times 7.36 \times 10^{-4} \times 15{,}020} \right)^{1/2} = 0.168 \text{ in.}$$

The quasi-static pressure rise in the shell can be estimated from work of Proctor and Filler[12], using curves for ΔP versus W/V.

$W/V = 2500/64{,}000 = 3.91 \times 10^{-2}$ lb/ft^3, from which

$\Delta P = 145$ psi

To design to this static pressure, let us limit our stress to the average of σ_y and σ_u, i.e. $\sigma = 5 \times 10^4$ psi. The applicable equation is (Reference 11)

$$h = \frac{(\Delta P)a}{2\sigma} = \frac{145 \times 298}{2 \times 5 \times 10^4} = 0.432 \text{ in.}$$

This is the controlling thickness, and is decoupled from the thickness to withstand the blast loading. The corresponding weight of steel in the shell is:

$$W_s = V_s \rho g = 4\pi a^2 h \rho g \tag{A-14}$$

$$W_s = 4\pi \times 298^2 \times 0.432 \times 7.36 \times 10^{-4} \times 386 = 136{,}000 \text{ lb}$$
$$= 68 \text{ tons}$$

The conclusion of this exercise is that an unvented containment structure, using shell material in the most efficient possible manner by allowing purely membrane action and considerable plastic deformation, is indeed feasible for this structural volume and explosive energy.

APPENDIX B
LOADS OUTSIDE AND WITHIN A BLAST-SUPPRESSION STRUCTURE

Blast Pressures Outside the Structure

The side-on overpressures P_s in the free-field around an explosive charge are given by a functional relationship as expressed in Equation (B-1).

$$P_s = f\left(\frac{R}{W^{1/3}}\right) \qquad \text{(free field)} \qquad \text{(B-1)}$$

where

R = standoff distance

W = charge weight

This functional relationship is the famous Hopkinson blast scaling law for the blast field around geometrically similar sources at sea-level ambient atmospheric conditions[2]. Assume that a cubical blast suppressive structure whose length on any side is X and whose walls are fabricated of a single metal sheet with holes drilled in it is now centered over the explosive charge. The ratio of the vent area of a wall to the total cross-sectional area of the wall will be defined as equaling α. Equation (B-1) for free-field blast will now be modified by the additional geometric parameters defining the size of the suppressive cube X and the vent area ratio α. If we elect to write a modified form for Equation (B-1) in nondimensional terms, a functional equation for predicting blast pressures outside the suppressive structure becomes:

$$P_s = f_1\left(\frac{R}{W^{1/3}}, \frac{X}{R}, \alpha\right) \qquad \text{(suppressive structure equation)} \qquad \text{(B-2)}$$

Equation (B-2) represents a 4-parameter space of nondimensional numbers or pi terms. Although a functional format is not expressed by Equation (B-2), sufficient quantities of experimental data can be used to obtain an empirical relationship. This is precisely what we will do to develop a relationship for predicting blast pressures outside of the suppressive structure; however, before this is done we must realize that most suppressive structures do not have walls which are a single sheet with holes. The vast majority of structures have 3 to 6 wall layers with various staggered venting patterns so fragments will not escape the confinement. This means that, for a multi-walled confinement, we must compute an effective α, α_{eff}, so Equation (B-2) can be used to predict blast pressures. To compute α_{eff} for a multi-walled structure, we have hypothesized that:

$$\frac{1}{\alpha_{eff}} = \frac{1}{\alpha_1} + \frac{1}{\alpha_2} + \ldots\ldots + \frac{1}{\alpha_N} \qquad \text{(B-3a)}$$

where

N = number of elements in a suppressive structure panel. Or,

$$\frac{1}{\alpha_{\text{eff}}} = \sum_{i=1}^{i=N} \frac{1}{\alpha_i} \tag{B-3b}$$

Although no proof of this relationship is presently possible, it does reach the appropriate limits for small and large numbers of plates. For example, if only one plate is present $\alpha_{\text{eff}} = \alpha_1$, as it should. If an infinite number of plates is present, $\alpha_{\text{eff}} = 0$, with the flow completely choked. If one of the plates is solid and thus has a zero α, $\alpha_{\text{eff}} = 0$ as it should. If all plates have the same value for α, $\alpha_{\text{eff}} = \alpha/N$ which is a number smaller than α for a single plate, as would be expected. In each member, α is defined according to Equation (B-4).

$$\alpha = \frac{A_{\text{vent}}}{A_{\text{wall}}} \tag{B-4}$$

For plates the meaning of this definition is obvious; however, in angles and louvres, the definition is less obvious. Figure B-1 defines α in a series of angles.

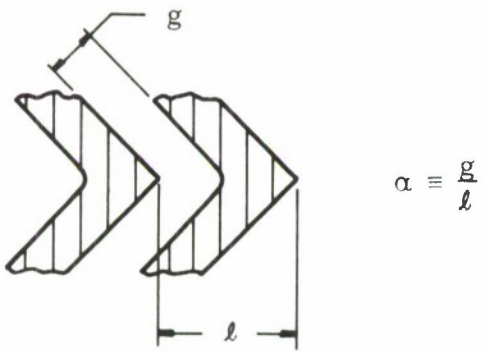

FIGURE B-1. DEFINITION OF α IN A SERIES OF ANGLE MEMBERS

In a louvre, we use a similar definition of α, except that the α, determined on the basis of Equation (B-4), is multiplied by a factor equal to 1/2. This factor was applied because the data of Reference 6 indicate that louvres are more efficient in constricting flow than are plates with holes. Perhaps this is explained by the fact that the entrance of a louvre is perpendicular to the entrance of a hole in a wall. As will be shown later, the factor of 1/2 appears to be justified by a curve fit to the experimental data. Figure B-2 illustrates our definition of α for a louvre.

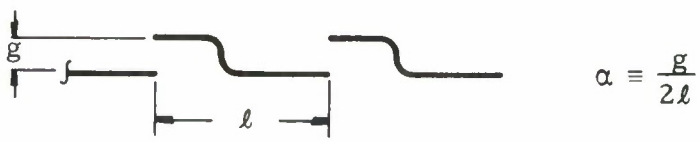

FIGURE B-2. DEFINITION OF α IN A LOUVRE

Now that α_{eff} has been defined, we are prepared to develop a functional format for Equation (B-2). This format was developed by assuming that Equation (B-2) can be expressed as:

$$P_s = A \left(\frac{R}{W^{1/3}}\right)^{N_1} \left(\frac{X}{R}\right)^{N_2} \left(\alpha_{eff}\right)^{N_3} \tag{B-5}$$

If logarithms are taken of both sides of this equation,

$$(\log P_s) = (\log A) + N_1 \left(\log \frac{R}{W^{1/3}}\right) + N_2 \left(\log \frac{X}{R}\right) + N_3 (\log \alpha_{eff}) \tag{B-6}$$

The equation is made linear, and a least-squares curve fit can be developed by stating that:

$$\left[1.0, \log \frac{R}{W^{1/3}}, \log \frac{X}{R}, \log \alpha_{eff}\right] \begin{bmatrix} \log A \\ N_1 \\ N_2 \\ N_3 \end{bmatrix} = \left[\log P_s\right] \tag{B-7}$$

Substituting matrix notation yields:

$$[L]\ [N] = [P] \tag{B-8}$$

and a least squares curve fit results for $\log A$, N_1, N_2, and N_3 or the N matrix when:

$$[N] = [L^T L]^{-1}\ [L^T]\ [P] \tag{B-9}$$

Experimental test data from References (5, 6 and 16) were used to develop this curve fit. The resulting equation is

$$P_s = 976.3 \frac{W^{2/3}\ \alpha_{eff}{}^{1/2}}{R^{3/2}\ X^{1/2}} \tag{B-10}$$

where

P_s = side-on pressure (psi)

W = charge weight (lbs)

R = standoff distance from charge (ft)

X = width of suppressive cube (ft)

α_{eff} = effective vented area ratio (–)

Figure B-3 is a plot of Equation (B-10) versus the experimental data points used to compose this plot. Equation (B-10) appears to experimentally curve fit the test results excellently. One standard deviation for the experimental data about the line in Figure (B-3) equals 18.6% which is only slightly worse than would be obtained for free-field data. Because this is a curve fit to test data, Equation (B-10) should only be used when input conditions fall within variations in individual pi terms. The variations included in test results were:

$$0.0263 \leqslant \alpha_{eff} \leqslant 0.60$$

$$0.323 \leqslant \frac{X}{R} \leqslant 1.77 \qquad \text{(B-11)}$$

$$4.27 \text{ ft/lb}^{1/3} \leqslant \frac{R}{W^{1/3}} \leqslant 17.5 \text{ ft/lb}^{1/3}$$

It is interesting to curve fit free-field side-on blast pressure data from References (5, 6 and 16) using the same procedure over the same range as for the suppressive structure blast field data. The resulting equation for free-field data is:

$$P_s = 976.3 \left(\frac{W^{2/3}}{R^2}\right) \qquad \text{(B-12)}$$

A comparison between Equation (B-12) and the test data points can be seen in Figure B-4. The standard deviation for blast pressures in the free-field is 13.1% which is only slightly better than the standard deviation for the suppressive structure blast field equation. Naturally Equation (B-12) should only be applied whenever $R/W^{1/3}$ is between the limits established by Equation (B-11).

If one compares Equation (B-10) for suppressive structures to Equation (B-12) for free-field blast, it is immediately apparent that the influence of the suppressive structure is to create an effective standoff distance less than the free-field standoff distance at which blast pressures are the same for a given size energy release. This standoff distance with a structure suppressing the blast R_{st} is related to the free-field standoff distance R_f by:

$$R_f^2 = R_{st}^{3/2} \frac{X^{1/2}}{\alpha_{eff}^{1/2}} \qquad \text{(B-13)}$$

or

$$R_{st} = \alpha_{eff}^{1/3} \left(\frac{R_f^{4/3}}{X^{1/3}}\right) \qquad \text{(B-14)}$$

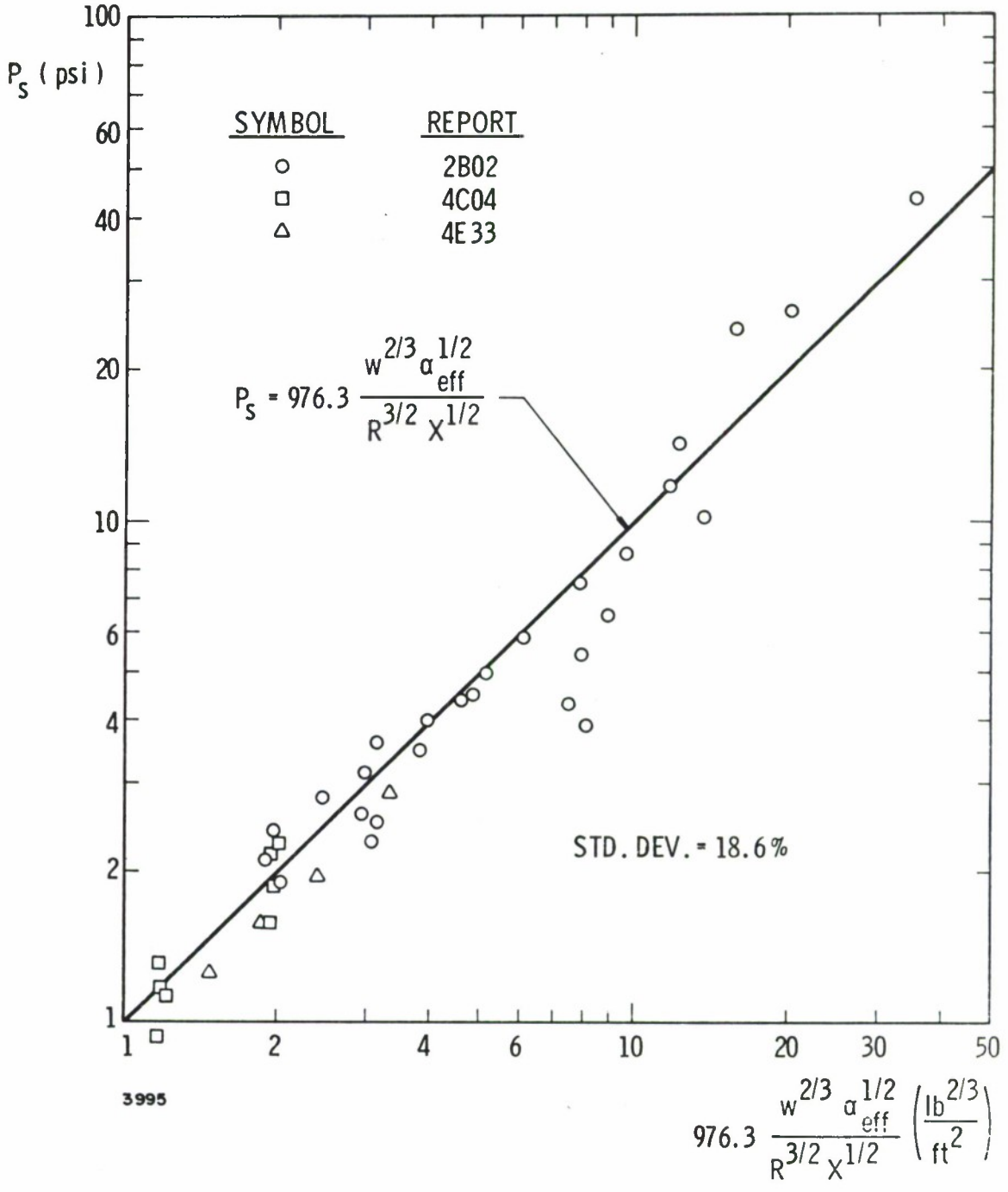

FIGURE B-3. CURVE FIT TO BLAST PRESSURES OUTSIDE SUPPRESSIVE STRUCTURES

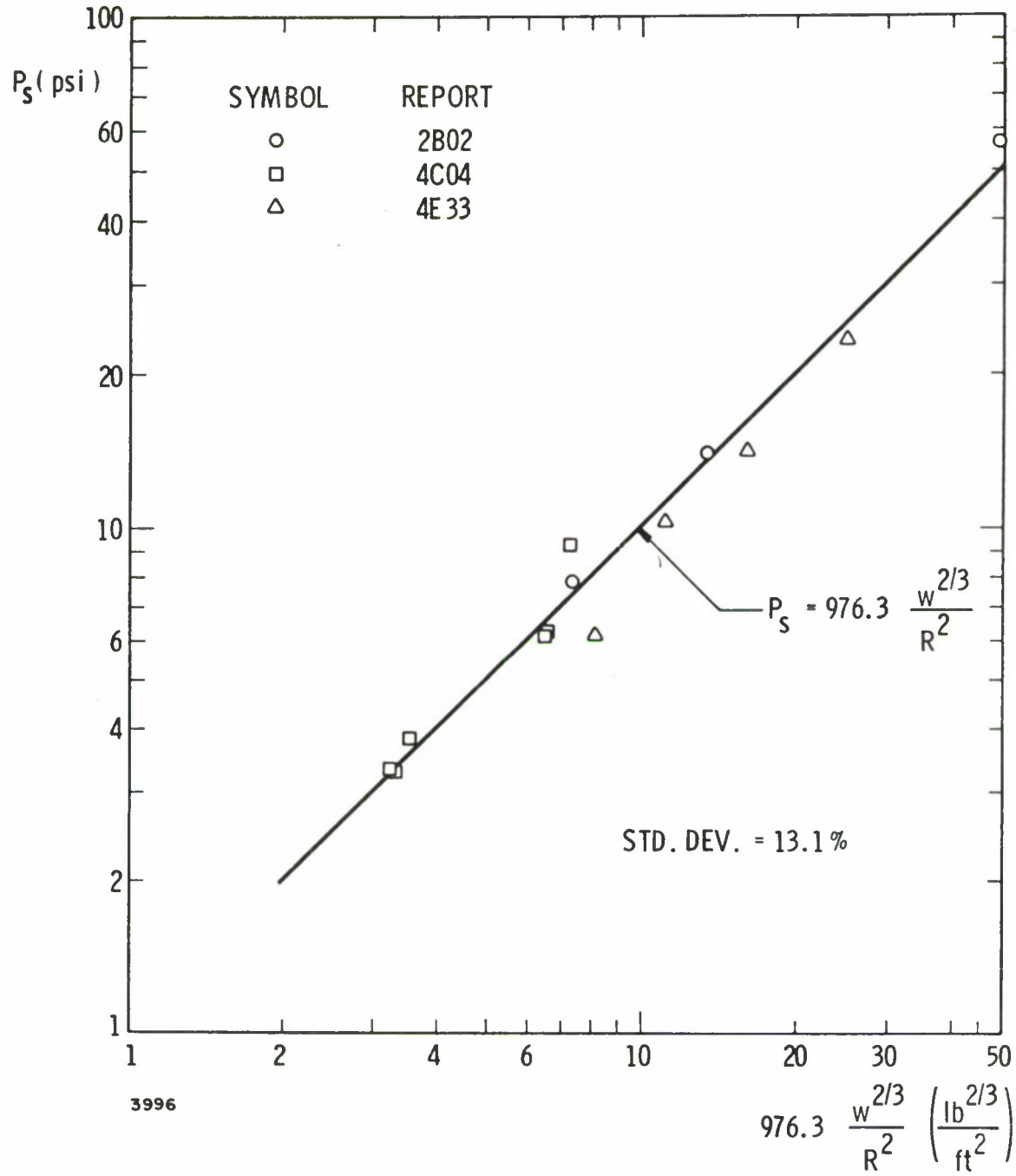

FIGURE B-4. CURVE FIT TO FREE-FIELD BLAST PRESSURES

Pressure Rise Inside Structure

In this section, we will discuss the quasi-static pressure rise within a suppressive structure. To create a solution, we will first perform a model analysis. The problem is envisioned as an instantaneous energy release of magnitude W inside a confined volume V. A vent area ($\alpha_{eff}A$) exists through which internal gases can escape. We are interested in predicting the internal pressure rise and decay of p as functions of time t. Ambient atmospheric pressure p_o exists initially inside and outside the confined volume. To completely define an equation of state for the gases in this problem, we need two additional parameters which will be the ratio of specific heats γ and speed of sound c. The following table summarizes the parameters in this problem and lists their fundamental dimensions in an engineering system of F, L, and T.

PARAMETERS DETERMINING QUASI-STATIC PRESSURE INSIDE VENTED CONTAINMENT VESSEL

Parameter	Symbol	Fundamental Dimensions	Reason for Including
Volume	V	L^3	Describe geometry of boundaries
Vented Area	$(\alpha_{eff}A)$	L^2	
Energy Release	W	FL	Input Energy
Atmospheric Pressure	p_o	F/L^2	Define the State of Air
Sound Speed in Air	c	L/T	
Specific Heat Ratio Air	γ	---	
Pressure Increase	p	F/L^2	Desired Response
Time	t	T	

Several different texts tell how nondimensional numbers or pi terms can be developed from this list of variables. Because no new assumptions are inserted in developing pi terms, we will present only the results and not perform all of the algebra. The assumptions in this analysis are all in the definition of the problem. Phenomena cannot be considered which have no parameter listed in the table. Probably the major assumption is that no thermal effects are considered; in other words the pressures dissipate through the venting and not through the conduction of heat into the walls of the suppressive structure. An acceptable set of pi terms which can result is:

$$\pi_1 = p/p_o$$

$$\pi_2 = \frac{(\alpha_{eff}A)^{3/2}}{V} \qquad \text{(B-15)}$$

$$\pi_3 = \gamma \qquad \text{(B-15) (Cont'd)}$$

$$\pi_4 = \frac{W}{p_o V}$$

$$\pi_5 = \frac{ct}{V^{1/3}}$$

If we assume γ is a constant (as it would be for air), and are only interested in predicting peak pressure, the result would not be dependent upon time or the pi term $ct/V^{1/3}$ and the pi term γ would be invariant. Hence

$$\frac{p_{max}}{p_o} = f\left(\frac{W}{p_o V}, \frac{(\alpha_{eff}A)^{3/2}}{V}\right) \qquad \text{(B-16)}$$

Because p_o is invariant, we can also write a dimensional functional format for Equation (B-16).

$$p_{max} = f\left(\frac{W}{V}, \frac{(\alpha_{eff}A)^{3/2}}{V}\right) \qquad \text{(B-17)}$$

Figure B-5 is a plot of p_{max} versus W/V for various values of $(\alpha_{eff}A)^{3/2}/V$. Provided $(\alpha_{eff}A)^{3/2}/V$ is less than 0.0775 the experimental data indicate that the maximum pressure p_{max} is independent of $(\alpha_{eff}A)^{3/2}/V$. In other words, the maximum pressure is reached before significant venting occurs if $(\alpha_{eff}A)^{3/2}/V$ is less than 0.0775, and:

$$p_{max} = f\left(\frac{W}{V}\right) \quad \text{provided} \quad \frac{(\alpha_{eff}A)^{3/2}}{V} \leq 0.0775 \qquad \text{(B-18)}$$

The data used in developing Figure B-5 come from Reference (15). In addition to presenting their own data which was obtained at the Naval Civil Engineering Laboratory, they also report test data obtained by James Proctor at Naval Ordnance Laboratory. Both groups of experimenters used Comp B explosive, but as can be seen in Figure B-5, their experiments were in different domains of W/V.

The dashed straight lines in Figure B-5 are the asymptotes for complete energy conversion or for p_{max} proportional to (W/V). If (W/V) is too large, insufficient oxygen is available to convert all the energy in the explosive charge; hence the energy release is reduced by the ratio of the heat of detonation divided by the heat of combustion. Figure B-5 implies that for $W/V < 0.003$ complete oxidation occurs; $W/V > 0.1$ the only oxidizer available is that in the explosive itself, and W/V between 0.003 and 0.1 results in partial oxidation. Throughout our structural calculations, we use the normalized data presented in Figure B-5.

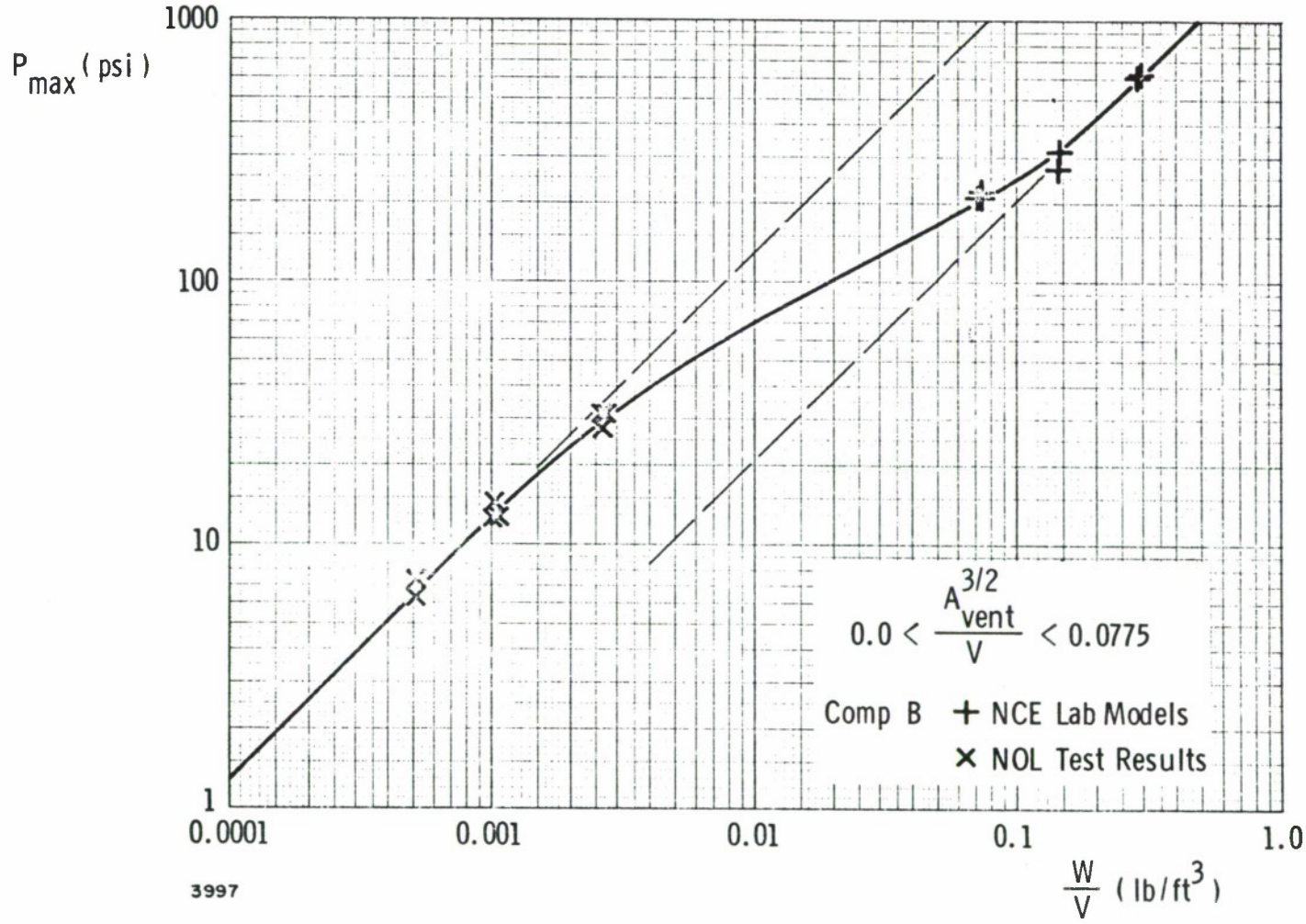

FIGURE B-5. QUASI-STATIC PRESSURE RISE INSIDE AN UNVENTED ENCLOSURE

If the maximum pressure is reached before significant venting occurs, the blow-down time will be independent of $W/p_o V$, and we can write a functional time of blow-down equation.

$$\frac{ct}{V^{1/3}} = f\left(\frac{p}{p_o}, \frac{(\alpha_{\text{eff}}A)^{3/2}}{V}\right) \tag{B-19}$$

Neglecting the invariant ambient gas parameters in Equation (B-19) permits us to write a dimensional form of Equation (B-19).

$$\frac{t}{V^{1/3}} = f\left(p, \frac{(\alpha_{\text{eff}}A)^{3/2}}{V}\right) \tag{B-20}$$

The data used to develop Figure B-5 can also be used to empirically solve Equation (B-20). Figure B-6 is a plot of $t/p^{1/6}V^{1/3}$ versus $(\alpha_{\text{eff}}A)^{3/2}/V$. The ordinate of this graph contains an empirical ovservation that the two pi terms $t/V^{1/3}$ and p can be combined to form $t/p^{1/6}V^{1/3}$. This empirical observation means that we now write Equation (B-20) as Equation (B-21):

$$\frac{t}{p^{1/6}V^{1/3}} = f\left(\frac{(\alpha_{\text{eff}}A)^{3/2}}{V}\right) \tag{B-21}$$

The function format for Equation (B-21) can now be obtained from Figure B-6 .

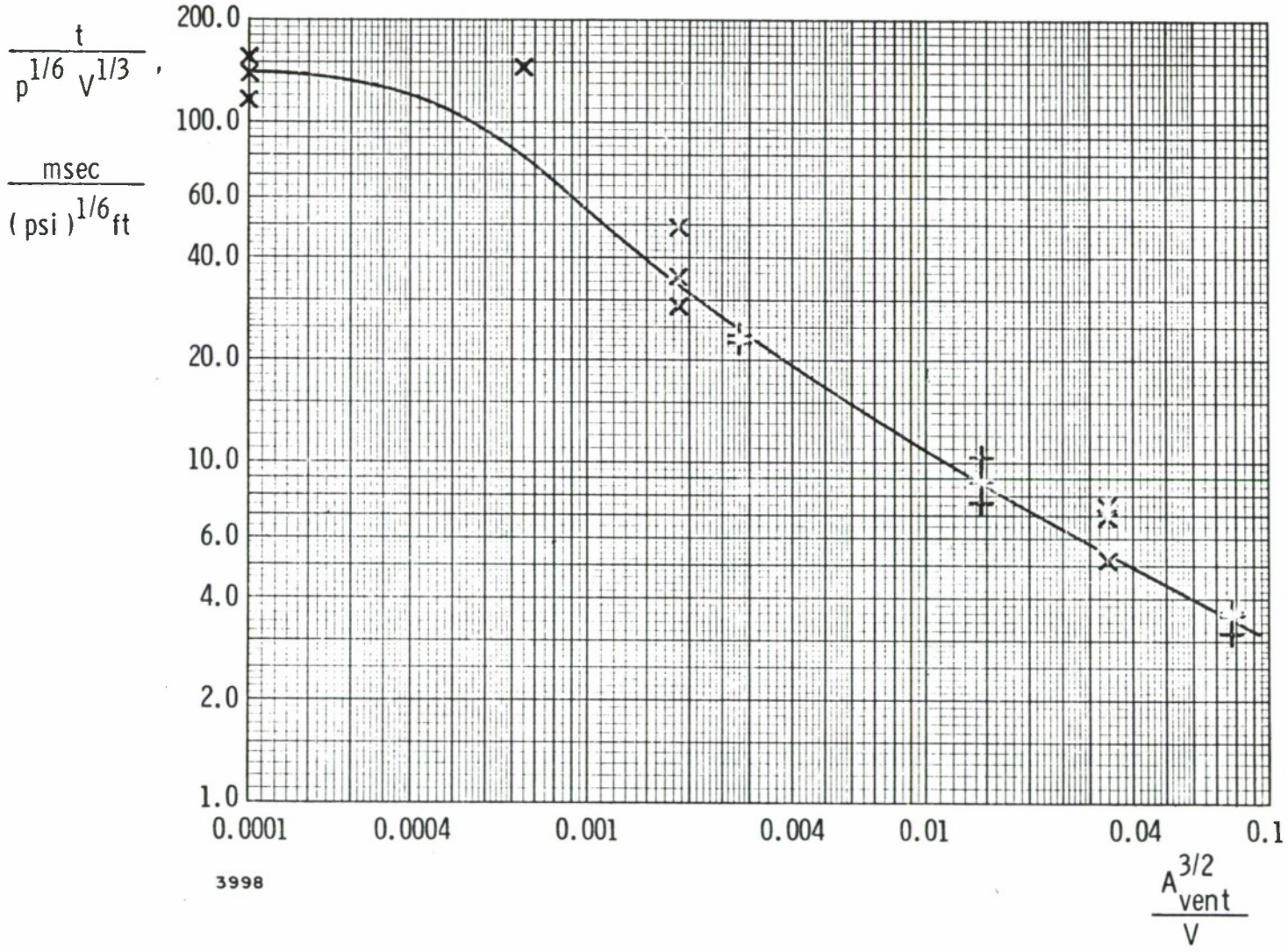

FIGURE B-6. SCALED BLOW-DOWN TIME FOR VENTED STRUCTURE

APPENDIX C
STRUCTURAL ANALYSIS PROCEDURES

Most of the analyses in this Appendix apply to flat panels, or straight members which can be used in flat panels or to support such panels. The final analysis refers to a cylindrical structure. When possible, the analyses are validated by comparison with data for dynamic structural deformations from the literature. But, such comparisons are limited to impulsive response of some simple structural elements.

The basis for all structural analysis of suppressive blast structures will be rigid-plastic, energy balance solutions. To illustrate the validity of this approach consider a single-degree-of-freedom, rigid-plastic system as in Figure C-1a. The motion of the mass m is resisted by a Coulomb friction element f when the load $p(t)$ is applied to the structure. We will approximate a blast loading by assuming that $p(t)$ has an exponential decay as in Figure C-1b, where P is the maximum applied force and T is the time constant associated with the duration of loading. If $P/f \leqslant 1.0$, we have the trivial case that the residual deformation X_{max} equals 0 because the mass never moves.

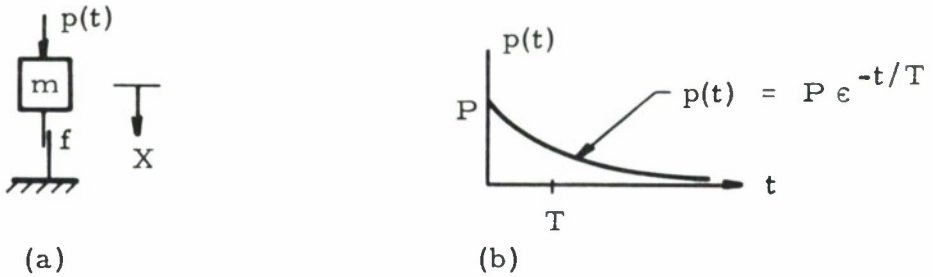

FIGURE C-1. RIGID-PLASTIC, SINGLE-DEGREE-OF-FREEDOM DAMAGE MODEL

If $P/f \geqslant 1.0$, we have the differential equation of motion

$$P\epsilon^{-t/T} - f = m\frac{d^2x}{dt^2} \tag{C-1}$$

or

$$\frac{d^2x}{dt^2} = \frac{P}{m}(\epsilon^{-t/T} - f/P) \tag{C-2}$$

By direct integration, we obtain for the case of zero initial velocity:

$$\frac{dx}{dt} = \frac{PT}{m}\left[1 - \epsilon^{-t/T} - \left(\frac{f}{P}\right)\left(\frac{t}{T}\right)\right] \tag{C-3}$$

Integrating again, we obtain for the case of zero initial displacement:

$$x = \frac{PT^2}{m}\left[\frac{t}{T} + \epsilon^{-t/T} - \frac{1}{2}\left(\frac{f}{P}\right)\left(\frac{t}{T}\right)^2 - 1\right] \tag{C-4}$$

Motion continues until the velocity, Equation (C-3) equals zero or until:

$$\epsilon^{-t/T} + \left(\frac{f}{P}\right)\frac{t}{T} = 1.0 \tag{C-5}$$

One cannot explicitly solve for t/T, so one must assume values of P/f, solve for t/T, and substitute in the displacement equation, Equation (C-4), to obtain X_{max}. The following table is such a calculation.

SOLUTION TO EQUATIONS C-4 AND C-5

t/T	P/f	Xm/PT^2	$(PT)^2/Xmf$
- - -	1.00	0	∞
0.09	1.033	0.001	1033
0.35	1.18	0.003	394
0.50	1.27	0.009	141
0.75	1.42	0.024	59.2
1.00	1.58	0.052	30.3
1.50	1.94	0.143	13.6
2.00	2.31	0.270	8.56
3.00	3.16	0.630	5.02
4.00	4.08	1.06	3.84
6.00	6.01	2.00	3.01
9.00	9.00	3.50	2.57
13.0	13.0	5.50	2.36
20.0	20.0	9.00	2.22
35.0	35.0	16.50	2.12
50.0	50.0	24.0	2.08
75.0	75.0	36.5	2.05
100.0	100.0	49.0	2.04
- - -	∞	- - -	2.00

The maximum displacement X_{max} in the third column of the table has been nondimensionalized by dividing the left and right sides of Equation (C-4) by PT^2/m. A solution can be presented for the maximum displacement by plotting $X_{max}\ m/PT^2$ versus P/f. We have elected to divide P/f by $X_{max}\ m/PT^2$ to form a new fourth column in the table and to plot this new column $(PT)^2/X_{max}\ mf$ versus P/f. The reason for this manipulation is that the product PT equals the applied total impulse I, and in this manner we create a scaled P-I diagram. The solid line in Figure C-2 is this scaled P-I diagram for a rigid plastic model.

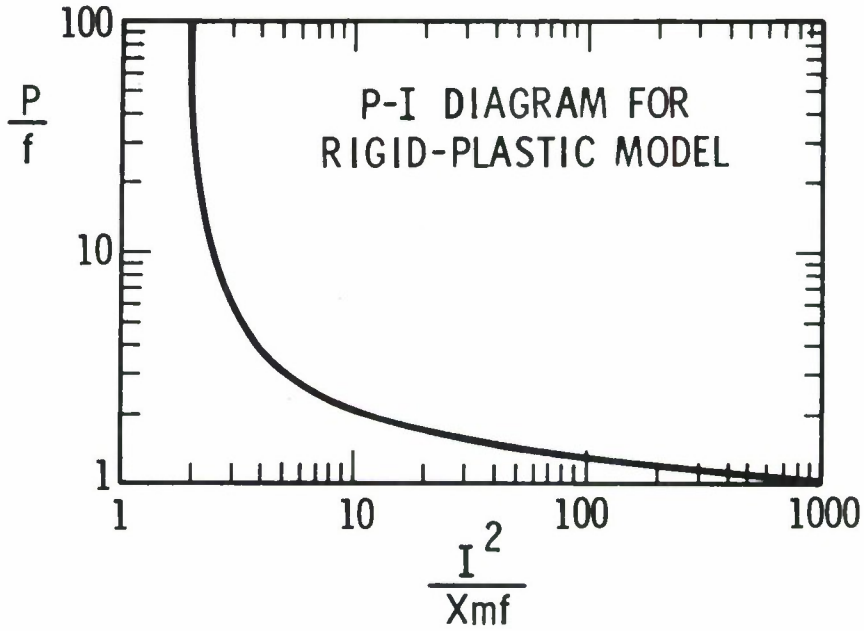

FIGURE C-2. *P-I* DIAGRAM FOR RIGID-PLASTIC SYSTEM

Observe in the table and Figure C-2 that whenever ($I^2/X_{max}\ mf$) is greater than about 60, the duration of loading T is larger than the response time t and P/f equals 1.0. Similarly, whenever P/f is greater than about 20, duration of loading T is smaller than the response time t of the responding structure and $I^2/X_{max}\ mf$ equals 2.0. The energy solutions which we will apply compute both of these asymptotes. We will obtain asymptotes for beams, membranes, plates, and shell structures in various following calculations. To illustrate the principles behind these calculations, we will first calculate the asymptotes for this idealized system.

The strain energy U stored in plastic deformation is given by:

$$U = fX_{max} \tag{C-6}$$

The kinetic energy K.E. imparted to the mass equals:

$$\text{K.E.} = (1/2)mV_o^2 = (1/2)m(I/m)^2 = I^2/2m \tag{C-7}$$

The work Wk done by the maximum force P acting through the distance X_{max} is:

$$Wk = PX_{max} \tag{C-8}$$

Equating the strain energy U, Equation (C-6), to the kinetic energy K.E., Equation (C-7), yields the asymptote for the impulsive loading realm or

$$\frac{I^2}{X_{max}\, mf} = 2.0 \qquad \text{(impulsive loading realm)} \qquad \text{(C-9)}$$

We term this domain the impulsive loading realm because the response of the system depends only upon the maximum applied impulse. The other asymptote is obtained by equating U, Equation (C-6), to the work Wk, Equation (C-8).

$$P/f = 1.0 \qquad \text{(quasi-static loading realm)} \qquad \text{(C-10)}$$

Because the response depends only upon the peak load, we will term this domain the quasi-static loading realm. Now we are prepared to apply these principles to real structural components.

Bending Simply-Supported Beam

Figure C-3 illustrates the bending of a simply-supported beam being loaded with a uniform load. To calculate strain energy in this member we must first assume a deformed shape.

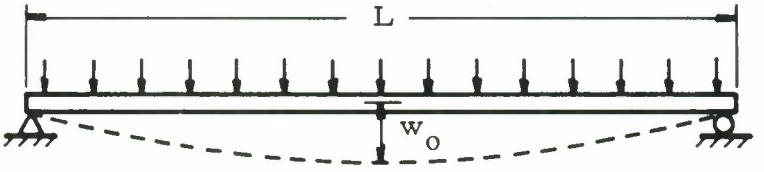

FIGURE C-3. BENDING OF A SIMPLY-SUPPORTED BEAM

Choosing

$$w = w_o \left(1 - \frac{4x^2}{L^2}\right) \qquad \text{(C-11)}$$

as an appropriate deformed shape we find that at $X = 0$, center of the beam, $w = w_o$ and the slope $dw/dx = 0$, while at the ends of the beam, $x = \pm L/2$, the deflections $w = 0$ and the slopes $dw/dx = -8xw_o/L^2$, a maximum value. The strain energy equals the plastic yield moment M_y for the beam cross-section times the change in angle of rotation integrated over the entire beam. Because the beam is symmetric and the change in angle of rotation with respect to x approximately equals $-d^2w/dx^2$, the strain energy U equals:

$$U = -2\int_0^{L/2} M_y \frac{d^2w}{dx^2}\, dx \qquad \text{(C-12)}$$

Substituting Equation (C-11) yields

$$U = +2\int_0^{L/2} M_y \frac{8w_o}{L^2}\,dx \tag{C-13}$$

or

$$U = \frac{8M_y w_o}{L} \tag{C-14}$$

The kinetic energy K.E. is obtained by summing up the impulse squared divided by two times the incremental mass [see Equation (C-7)] over the entire beam. If b is the width of the loaded member, ρ the density, A the cross-sectional areas, and i_o the specific impulse (impulse per unit area), this summation yields the following integration.

$$\text{K.E.} = 2\int_0^{L/2} \frac{i_o{}^2 b^2 (dx)^2}{2\rho A(dx)} \tag{C-15}$$

or

$$\text{K.E.} = \frac{i_o{}^2 b^2 L}{2\rho A} \tag{C-16}$$

Equating U, Equation (C-14), to K.E., Equation (C-16), yields the asymptote for the impulsive loading realm.

$$\frac{i_o{}^2 b^2 L}{\rho M_y A} = 16\left(\frac{w_o}{L}\right) \quad \text{(impulsive realm s.s. beam)} \tag{C-17}$$

The work Wk is obtained by integrating over the length of the beam, the forces times the distance through which they move. This operation is performed by integrating $pb\,dx$ times the assumed deformed shape, Equation (C-11).

$$Wk = 2\int_0^{L/2} pb\, w_o \left(1 - \frac{4x^2}{L^2}\right)dx \tag{C-18}$$

or

$$Wk = \frac{2}{3} pbL\, w_o \tag{C-19}$$

Equating Wk, Equation (C-18), to U, Equation (C-14), yields the quasi-static asymptote.

$$\frac{pbL^2}{M_y} = 12 \qquad \text{(quasi-static realm s.s. beam)} \qquad \text{(C-20)}$$

Bending Clamped Beam

So far these calculations have assumed that the beam is simply-supported and free to rotate at the ends. If the beam is clamped at the ends so no rotation occurs, but can move inwards so that no membrane action is developed, we can use many of the results which have already been developed. To do this, assume that a clamped beam is really two simply-supported beams that have been split and joined end to end as in Figure C-4.

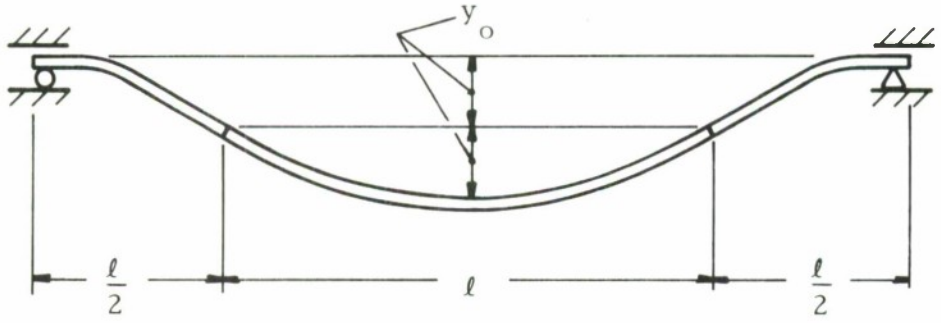

FIGURE C-4. DEFORMED SHAPE OF CLAMPED BEAMS

This new configuration implies that:

$$U = 2U_{ss} = \frac{16M_y Y_o}{\ell} \qquad \text{(C-21)}$$

and that

$$\text{K.E.} = 2\,\text{K.E.}_{ss} = \frac{i_o^2 b^2 \ell}{\rho A} \qquad \text{(C-22)}$$

but $\ell = 1/2L$ and $Y_o = 1/2w_o$, so substituting for ℓ and Y_o and equating U to K.E. yields:

$$\frac{i_o^2 b^2 L}{\rho A M_y} = 32\,\frac{w_o}{L} \qquad \text{(impulsive realm clamped beam)} \qquad \text{(C-23)}$$

Because Equation (C-23) for clamped beams is twice Equation (C-17) for simply-supported beams, we can write

$$\frac{i_o^2 b^2 L}{N\rho A M_y} = 16\,\frac{w_o}{L} \qquad \text{(impulsive realm beam bending)} \qquad \text{(C-24)}$$

where

$N = 1.0$ for simply-supported beams,

$N = 2.0$ for clamped beams

To experimentally demonstrate the validity of this solution, we have plotted experimental data taken by Florence and Firth (Reference 1) and compared these data to Equation (C-24). Because Florence and Firth used beams with rectangular cross sections, $M_y = \sigma_y bh^2/4$. Substituting for M_y, bh for A, and 2ℓ for L (they used half spans) yields:

$$\frac{i_o^{\,2}}{N\rho\sigma_y h^2} = \left(\frac{h}{\ell}\right)\left(\frac{w_o}{\ell}\right) \quad \text{(impulsive realm rectangular beam bending)} \qquad \text{(C-25)}$$

All of the beams tested by Florence and Firth had an ℓ/h ratio of 36, so this comparison is made by plotting $i_o/h\sqrt{N\rho\sigma_y}$ versus w_o/ℓ. All beams are impulsively loaded using sheet explosive. Both clamped and pinned beams made of 2024-T4 aluminum, 6061-T6 aluminum, 1018 cold rolled steel, and 1018 annealed steel are included in this comparison. Figure C-5 demonstrates the validity of Equation (C-25) and this analysis procedure.

To calculate the response of a clamped bending beam in the quasi-static loading realm we must calculate the work Wk on a deformed beam as in Figure C-4. If we use a deformed shape as given by Equation (C-11) for each beam segment, the work Wk equals

$$Wk = 2\int_0^{\ell/2} pbY_o\left[1 + \left(1 - \frac{4x^2}{\ell^2}\right)\right]dx + 2\int_0^{\ell/2} pbY_o\left[1 - \left(1 - \frac{4x^2}{\ell^2}\right)\right]dx \qquad \text{(C-26)}$$

or

$$Wk = 2pbY_o\ell \qquad \text{(C-27)}$$

But $\ell = \frac{L}{2}$ and $Y_o = \frac{w_o}{2}$; hence

$$Wk = \frac{1}{2}\,pb\,w_o L \qquad \text{(C-28)}$$

Equating Equation (C-28) to U in Equation (C-21) yields:

$$\frac{pbL^2}{M_y} = 32 \qquad \text{(quasi-static realm clamped beam)} \qquad \text{(C-29)}$$

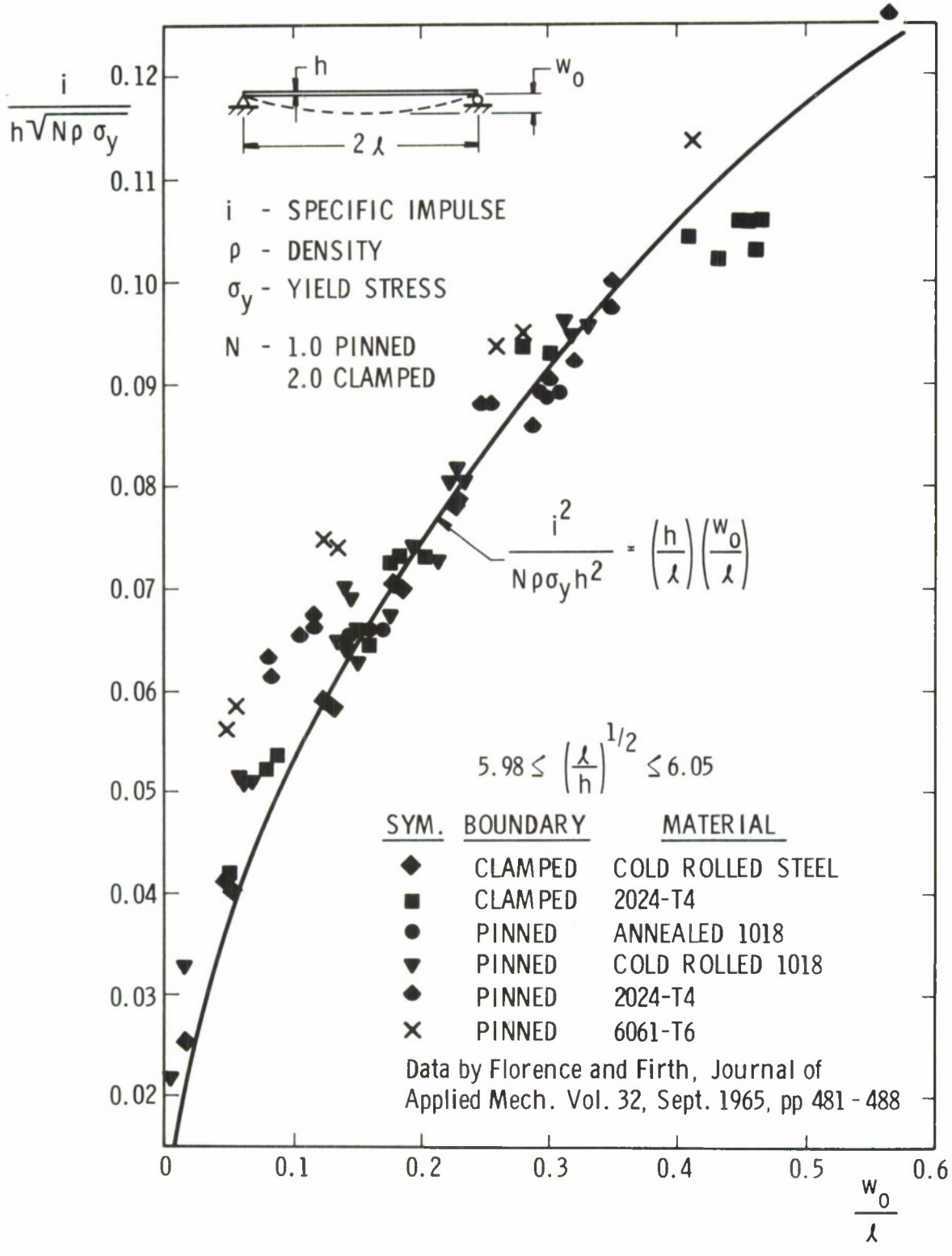

FIGURE C-5. BEAM BENDING IN THE IMPULSIVE REALM

Because Equation (C-29) for clamped beam bending is 8/3 times Equation (C-20) for simply-supported beam bending, we can write:

$$\frac{pbL^2}{M_y} = 12N^{1.415} \qquad \text{(quasi-static realm beam bending)} \quad \text{(C-30)}$$

where

$N = 1$ simply-supported beam

$N = 2$ clamped beam

Although we have no data to verify this analysis, the procedure is precisely the same as that used in the single-degree-of-freedom oscillator analysis. If a beam happens to have a rectangular cross section, Equation (C-30) becomes, after substituting for M_y,

$$\frac{pL^2}{\sigma_y h^2} = 3N^{1.415} \qquad \text{(quasi-static realm rectangular beam bending)} \quad \text{(C-31)}$$

Membrane Action in Beams

The deformed beam sketched in Figure C-3 and the deformed shape presented in Equation (C-11) can also be used to estimate the response of a beam undergoing axial or extensional straining. The strain ϵ in such a member equals:

$$\epsilon = \frac{dL - dx}{dx} \qquad \text{(C-32)}$$

But dL is given by

$$dL = \sqrt{(dw)^2 + (dx)^2} \qquad \text{(C-33)}$$

hence

$$\epsilon = \sqrt{1.0 + \left(\frac{dw}{dx}\right)^2} - 1.0 \qquad \text{(C-34)}$$

Using the binomial expansion and retaining only the first two terms as an approximation yields:

$$\epsilon = \frac{1}{2}\left(\frac{dw}{dx}\right)^2 \qquad \text{(C-35)}$$

Differentiating Equation (C-11) and substituting into Equation (C-35) then gives:

$$\epsilon = \frac{32x^2 w_o{}^2}{L^4} \tag{C-36}$$

But the strain energy per unit volume equals $\sigma d\epsilon$ or for a rigid non-strain-hardening plastic system

$$U = 2\int_0^{L/2} \sigma_y \epsilon A dx \tag{C-37}$$

Substituting Equation (C-36) for ϵ and realizing that $\sigma_y A$ equals the yield load P_y gives:

$$U = \frac{64 w_o{}^2 P_y}{L^4} \int_0^{L/2} x^2 dx \tag{C-38}$$

The integration then yields:

$$U = \frac{8 P_y w_o{}^2}{3L} \tag{C-39}$$

Because the kinetic energy imparted to the member does not depend upon the deformed shape, K.E. is still given by Equation (C-16), and because the deformed shape in this string analysis is the same as the deformed shape in the beam analysis, the work Wk is given by Equation (C-19). Equating U to K.E. yields the impulsive asymptote.

$$\frac{i_o{}^2 b^2}{\rho P_y A} = \frac{16}{3}\left(\frac{w_o}{L}\right)^2 \quad \text{(impulsive realm membrane analysis)} \tag{C-40}$$

The quasi-static asymptote is obtained by equating U to Wk which yields:

$$\frac{pbL}{P_y} = 4\left(\frac{w_o}{L}\right) \quad \text{(quasi-static realm membrane analysis)} \tag{C-41}$$

If the members have rectangular cross sections, Equations (C-40) and (C-41) become:

$$\frac{i_o{}^2}{\rho \sigma_y h^2} = \frac{16}{3}\left(\frac{w_o}{L}\right)^2 \quad \text{(impulsive realm rectangular membrane analysis)} \tag{C-42}$$

$$\frac{pL}{\sigma_y h} = 4\left(\frac{w_o}{L}\right) \quad \text{(quasi-static realm rectangular membrane analysis)} \tag{C-43}$$

Strain hardening can increase the strain energy which is stored in a deforming beam. In bending this increase in stored energy is insignificant because membrane action usually starts to store energy of a much larger magnitude before bending strain energy becomes significant. The extra strain energy from hardening will be given by

$$U = 2\int_0^{L/2} \frac{(E_t\epsilon)(\epsilon)}{2} A\,dx \tag{C-44}$$

Substituting Equation (C-36) for ϵ yields

$$U = \frac{(32)^2 E_t w_o{}^4 A}{L^8} \int_0^{L/2} x^4\,dx \tag{C-45}$$

or

$$U = \frac{32E_t A w_o{}^4}{5L^3} \qquad \text{(strain hardening, membrane action)} \tag{C-46}$$

This hardening term may be added directly to Equation (C-39) to obtain the total strain energy from membrane action. Then the sum of Equations (C-39) and (C-46) can be equated to either Equation (C-16) or Equation (C-19) to obtain respectively the impulsive and quasi-static asymptotes. These asymptotes are:

$$\frac{i_o{}^2 b^2}{\rho P_y A} = \frac{16}{3}\left(\frac{w_o}{L}\right)^2 + \frac{64}{5}\left(\frac{E_t A}{P_y}\right)\left(\frac{w_o}{L}\right)^4 \qquad \text{(impulsive realm membrane equation)} \tag{C-47}$$

$$\frac{pLb}{P_y} = 4\left(\frac{w_o}{L}\right) + \frac{48}{5}\left(\frac{E_t A}{P_y}\right)\left(\frac{w_o}{L}\right)^3 \qquad \text{(quasi-static realm membrane equation)} \tag{C-48}$$

Beams in Bending and Membrane Action

We will superimpose bending and membrane strain energies by adding the two expressions to obtain a total strain energy in the structure whenever both mechanisms are significant. Although it is very difficult to show that this is a correct procedure in plastic analysis of irregular cross sections (I-beams, angles, etc.), it is easy to show that in elastic rectangle members this procedure is rigorously correct. The strain in an elastic rectangle member is given by:

$$\epsilon = \frac{P}{EA} + \frac{Mc}{EI} \tag{C-49}$$

where

c = distance from neutral axis (can be negative)

P = load

M = moment

A = cross section area

I = second moment of area.

But the strain energy per dx length of beam is given by

$$U/dx = \int_{-h/2}^{+h/2} \frac{E\epsilon^2}{2} bdc \tag{C-50}$$

Or upon substituting Equation (C-49)

$$\frac{U}{dx} = \int_{-h/2}^{+h/2} \left(\frac{bM^2 c^2 dc}{2EI^2} + \frac{bP^2 dc}{2EA^2} + \frac{MPcdc}{EIA} \right) \tag{C-51}$$

This integration yields

$$\frac{U}{dx} = \frac{M^2}{2EI} + \frac{P^2}{2EA} + 0 \tag{C-52}$$

The term $\int_{-h/2}^{+h/2} \frac{MPcdc}{EIA}$ equals 0 because this coupling term is an even experssion. The other two terms when Equation (C-52) is multiplied by dx are respectively the sum of the bending strain energy and the membrane strain energy. Hence Equation (C-52) states that no coupling occurs and the strain energy in the structure U is:

$$U = U_{\text{bending}} + U_{\text{membrane}} \tag{C-53}$$

Summing Equations (C-39), (C-46), and either Equation (C-14) or (C-21) depending upon boundary conditions yields the strain energy which can be equated to the kinetic energy as expressed by either Equation (C-14) or (C-21) (these equations are the same) to obtain the impulsive loading realm asymptote. Equation (C-54) is this equality.

$$\frac{i_o{}^2 b^2 L}{2\rho A} = \frac{8NM_y w_o}{L} + \frac{8P_y w_o{}^2}{3L} + \frac{32E_t A w_o{}^4}{5L^3} \tag{C-54a}$$

or

$$\frac{i_o^2 b^2}{\rho A P_y} = 16N\left(\frac{M_y}{P_y L}\right)\left(\frac{w_o}{L}\right) + \frac{16}{3}\left(\frac{w_o}{L}\right)^2 + \frac{64}{5}\left(\frac{E_t A}{P_y}\right)\left(\frac{w_o}{L}\right)^4 \qquad \text{(C-54b)}$$

(impulsive realm)

In the quasi-static loading realm, the strain energy is equated to the work Wk given by either Equation (C-19) or Equation (C-28) dependent upon boundary conditions. This equality yields:

$$\frac{2}{3N^{0.415}} pbLw_o = \frac{8NM_y w_o}{L} + \frac{8P_y w_o^2}{3L} + \frac{32E_t A w_o^4}{5L^3} \qquad \text{(C-55a)}$$

or

$$\frac{pbL}{P_y} = 12N^{1.415}\left(\frac{M_y}{P_y L}\right) + 4N^{0.415}\left(\frac{w_o}{L}\right) + \frac{48N^{0.415}}{5}\left(\frac{E_t A}{P_y}\right)\left(\frac{w_o}{L}\right)^3 \qquad \text{(C-55b)}$$

(quasi-static realm)

Humphreys (Reference 2) presents experimental data on clamped rectangular strips whose boundaries cannot move together when loaded with an impulse. For a rectangular member, we substitute $M_y = \sigma_y bh^2/4$, $P_y = \sigma_y bh$, and $A = bh$ into Equation (C-54b) to obtain:

$$\frac{i_o^2}{\rho\sigma_y h^2} = 4N\left(\frac{h}{L}\right)\left(\frac{w_o}{L}\right) + \frac{16}{3}\left(\frac{w_o}{L}\right)^2 + \frac{64}{5}\left(\frac{E_t}{\sigma_y}\right)\left(\frac{w_o}{L}\right)^4 \qquad \text{(C-56)}$$

(impulsive realm rectangular beam)

Because Humphreys plots $\left[\frac{i_o L}{(\rho\sigma_y)^{1/2} h^2}\right]$ versus $\left[\frac{2w_o}{h}\right]$ we have multiplied all terms in Equation (C-56) by L^2/h^2 and set $N = 2$ to obtain:

$$\left[\frac{i_o L}{h^2(\rho\sigma_y)^{1/2}}\right]^2 = 4\left(\frac{2w_o}{h}\right) + \frac{4}{3}\left(\frac{2w_o}{h}\right)^2 + \frac{4}{5}\left(\frac{E_t h^2}{\sigma_y L^2}\right)\left(\frac{2w_o}{h}\right)^4 \qquad \text{(C-57)}$$

Figure (C-6) is a comparison of Humphreys' data with Equation (C-57). The data includes tests on 1020 mild steel, cold-rolled steel, and 4130 N steel. As can be seen in Figure C-6, the data would appear to verify this analysis. The two lines in Figure C-6 are plots of Equation (C-57) with and without the strain hardening term. For very large deflections,

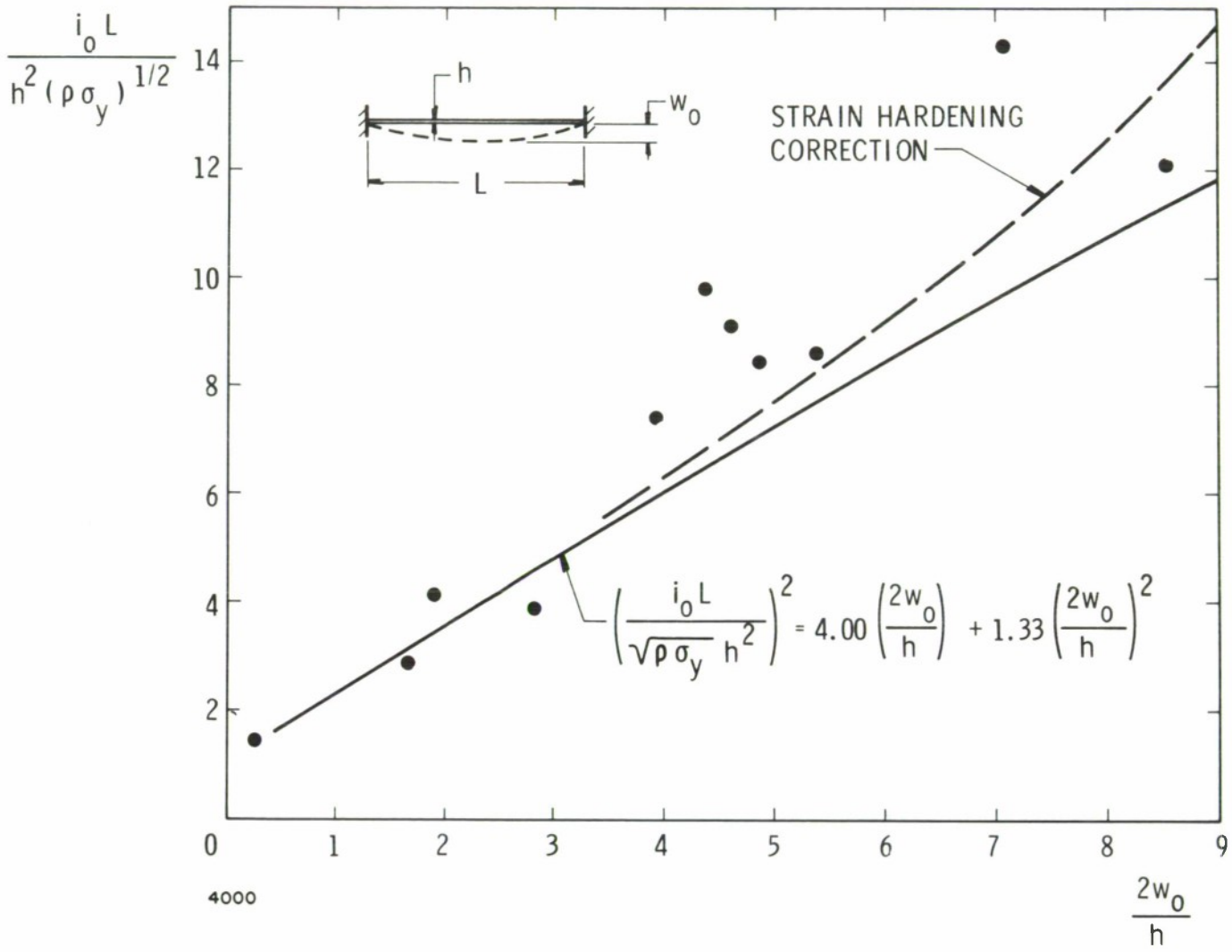

FIGURE C-6. COMPARISON OF EQUATION (C-57) WITH HUMPHREY'S DATA

the term is left out of an analysis, Figure C-6 indicates that an energy analysis would overestimate deflections.

Plates in Bending and Membrane Action

The strain energy per unit volume in a structural element under a biaxial state of stress is

$$\frac{U}{\text{Vol.}} = \int_{\text{strains}} \left[\sigma_{11} d\epsilon_{11} + 2\sigma_{12} d\epsilon_{12} + \sigma_{22} d\epsilon_{22}\right] \tag{C-58}$$

Assume a rigid-perfectly plastic stress-strain law without strain hardening. Then Mohr's circle of stress for any strain is a point on the horizontal normal stress axis, and no shearing stress occurs. This observation means that Equation (C-58) simplifies and becomes

$$\frac{U}{\text{Vol.}} = \sigma_y \epsilon_x + \sigma_y \epsilon_y \tag{C-59}$$

The bending strain energy and the membrane strain energy can now be calculated for the plastic deformation of a plate if we assume a deformed shape for the plate. For a plate bounded on all four sides but free to rotate along the edge, we will assume

$$w = w_o \left(1 - \frac{x^2}{X^2}\right) \left(1 - \frac{y^2}{Y^2}\right) \tag{C-60}$$

where

X & Y are half spans

x & y are a rectangular coordinate system at the center of the plate

w_o is the mid-plate deflection

This assumed deformed shape is symmetric, has the maximum deflection at the center of the plate, has no deflection along the boundaries, has no slope in the center of the plate, has the maximum slope at the edge of the plate, and has curvature throughout most of the plate. Our ability to meet all these conditions with Equation (C-60) infers that the assumed deformed shape is an appropriate one for a simply-supported plate.

The bending strain energy U_b is estimated by substituting $-z \dfrac{\partial^2 w}{\partial x^2}$ for ϵ_x and $-z \dfrac{\partial^2 w}{\partial y^2}$ for ϵ_y in Equation (C-59) and integrating to obtain:

$$U_b = -8\int_0^{h/2} dz \int_0^X dx \int_0^Y dy \left(\sigma_y z \frac{\partial^2 w}{\partial x^2} + \sigma_y z \frac{\partial^2 w}{\partial y^2}\right) \tag{C-61}$$

Differentiating Equation (C-60) and substituting it into Equation (C-61) yields:

$$U_b = 16\sigma_y w_o \int_0^{h/2} \int_0^X \int_0^Y \left[\frac{z}{X^2}\left(1 - \frac{y^2}{Y^2}\right) + \frac{z}{Y^2}\left(1 - \frac{x^2}{X^2}\right)\right] dz\, dx\, dy \tag{C-62}$$

or

$$U_b = \frac{4\sigma_y w_o h^2}{3}\left(\frac{Y}{X} + \frac{X}{Y}\right) \tag{C-63}$$

The membrane strain energy U_m is estimated by substituting $\frac{1}{2}\left(\frac{\partial w}{\partial y}\right)^2$ for ϵ_x and $\frac{1}{2}\left(\frac{\partial w}{\partial y}\right)^2$ for ϵ_y in Equation (C-59) and integrating to obtain:

$$U_m = 4\int_{-h/2}^{+h/2} dz \int_0^X dx \int_0^Y dy \left[\frac{\sigma_y}{2}\left(\frac{\partial w}{\partial x}\right)^2 + \frac{\sigma_y}{2}\left(\frac{\partial w}{\partial y}\right)^2\right] \tag{C-64}$$

Differentiating Equation (C-60) and substituting it into Equation (C-64) yields:

$$U_m = 8\sigma_y {w_o}^2 \int_{-h/2}^{+h/2} \int_0^X \int_0^Y \left[\frac{x^2}{X^4}\left(1 - \frac{y^2}{Y^2}\right)^2 + \frac{y^2}{Y^4}\left(1 - \frac{x^2}{X^2}\right)^2\right] dz\, dx\, dy \tag{C-65}$$

or

$$U_m = \frac{64\sigma_y {w_o}^2 h}{45}\left(\frac{X}{Y} + \frac{Y}{X}\right) \tag{C-66}$$

The kinetic energy K.E. imparted to a plate is obtained by integrating the impulse squared divided by two times the incremental mass [see Equation (C-7)] for a dx by dy differential element in the surface of a plate. This manipulation yields:

$$\text{K.E.} = 4\int_0^X \int_0^Y \frac{{i_o}^2 (dx)^2 (dy)^2}{2\rho h (dx)(dy)} \tag{C-67}$$

or

$$\text{K.E.} = \frac{2i_o^2 XY}{\rho h} \tag{C-68}$$

The work Wk performed on a deforming plate is obtained by

$$Wk = \int_A pwdA \tag{C-69}$$

Substituting our assumed deformed shape, Equation (C-60), for w and dx plus dy for dA yields:

$$Wk = 4pw_o \int_0^X \int_0^Y \left(1 - \frac{x^2}{X^2}\right)\left(1 - \frac{y^2}{Y^2}\right) dx\, dy \tag{C-70}$$

or

$$Wk = \frac{16}{9} pw_o XY \tag{C-71}$$

Equating Equations (C-63) plus (C-66), the sum of the strain energies, to Equation (C-68), the kinetic energy, yields the impulsive asymptote for a deforming simply-supported plate.

$$\frac{2i_o^2 XY}{\rho h} = \frac{4\sigma_y w_o h^2}{3}\left(\frac{Y}{X} + \frac{X}{Y}\right) + \frac{64\sigma_y w_o^2 h}{45}\left(\frac{Y}{X} + \frac{X}{Y}\right) \tag{C-72}$$

or

$$\frac{i_o^2 X^2}{\rho \sigma_y h^4} = \left[1 + \left(\frac{X}{Y}\right)^2\right]\left[\frac{2}{3}\left(\frac{w_o}{h}\right) + \frac{32}{45}\left(\frac{w_o}{h}\right)\right]^2 \quad \text{(impulsive realm s.s. plate)} \tag{C-73}$$

Equating the strain energy to the work, Equation (C-71), yields the quasi-static asymptote for a deforming simply-supported plate.

$$\frac{16}{9} pw_o XY = \frac{4\sigma_y w_o h^2}{3}\left(\frac{Y}{X} + \frac{X}{Y}\right) + \frac{64\sigma_y w_o^2 h}{45}\left(\frac{Y}{X} + \frac{X}{Y}\right) \tag{C-74}$$

or

$$\frac{pX^2}{\sigma_y h^2} = \left[1 + \left(\frac{X}{Y}\right)^2\right]\left[\frac{3}{4} + \frac{4}{5}\left(\frac{w_o}{h}\right)\right] \quad \text{(quasi-static realm s.s. plate)} \tag{C-75}$$

We have no data to demonstrate the validity of this solution on rectangular or square plates; however, Florence (Reference 3) presents deformation data on clamped circular plates loaded with a uniformly distributed impulse. To demonstrate the validity of this analysis philosophy, we developed an energy solution for clamped circular plates. The assumed deformed shape was:

q

$$w = w_o \left(1.0 - \frac{3r^2}{R^2} + \frac{2r^2}{R^3}\right) \tag{C-76}$$

This deformed shape has zero radial slope at the edges and center of the plate, no deflection at the edges of the plate and a maximum deflection of w_o in the center of the plate. Radial moments exist with opposite signs at the edge and center of the plate because the radial plate curvatures change signs in these locations. Because of symmetry, $\partial w/\partial\theta$ and $\partial^2 w/\partial\theta^2$ equal zero as they should in such a plate. Using an $ry\theta$ spherical coordinate system permits us to estimate the kinetic energy as:

$$\text{K.E.} = \int_0^R \frac{i_o{}^2 (2\pi r)^2 (dr)^2}{2\rho h (2\pi r)(dr)} \tag{C-77}$$

or

$$\text{K.E.} = \frac{\pi i_o{}^2 R^2}{2\rho h} \tag{C-78}$$

The membrane strain energy is given by:

$$U_m = \int_0^R 2\pi r dr h \sigma_y \frac{1}{2}\left(\frac{\partial w}{\partial r}\right)^2 = \int_0^R \pi r dr h \sigma_y w_o{}^2 \left(-\frac{6r}{R^2} + \frac{6r^2}{R^3}\right)^2 \tag{C-79}$$

or

$$U_m = 1.885\, \sigma_y h w_o{}^2 \tag{C-80}$$

The bending strain energy is given by:

$$U_b = 2\int_0^{h/2}\int_0^R (2\pi r)\, \sigma_y z \frac{\partial^2 w}{\partial r^2} dz\, dr = 4\pi\sigma_y \int_0^{h/2}\int_0^R w_o \left(-\frac{6}{R^2} + \frac{12r}{R^3}\right) z dz r dr \tag{C-81}$$

or

$$U_b = 1.751\ \sigma_y h^2 w_o \tag{C-82}$$

Equating the kinetic energy, Equation (C-78) to the sum of the strain energies, Equations (C-80) and (C-82) then yield:

$$\frac{\pi}{2}\frac{i_o{}^2 R^2}{\rho h} = 1.571\ \sigma_y h^2 w_o + 1.885\ \sigma_y h w_o{}^2 \tag{C-83}$$

or

$$\frac{i_o{}^2 R^2}{\rho \sigma_y h^4} = \left(\frac{w_o}{h}\right) + \frac{6}{5}\left(\frac{w_o}{h}\right)^2 \qquad \text{(impulsive realm clamped circular plate)} \tag{C-84}$$

Notice that the only difference between a clamped circular plate and a simply-supported rectangular plate is that the characteristic half span R replaces X and the numerical coefficients in front of the (w_o/h) and $(w_o/h)^2$ terms are slightly different. Figure C-7 is a plot of Florence's data from experiments on 6061-T6 aluminum and 1018-cold rolled steel clamped circular plates. The solid line in Figure C-7 is Equation (C-84) which appears to fit the data excellently.

We have not developed the equations for clamped rectangular plates as there was no need to use this relationship in our analysis. The only difference between clamped and simply-supported plates would be in the numerical coefficient preceding the bending or (w_o/h) term. If deflections are very large the membrane term dominates and boundary conditions which influence the bending term would make insignificant differences in the solution.

Spherical Containment

Energy and force balance methods are used in Appendix A to estimate plastic response of a spherical containment shell.

Cylindrical Shell Elements

In one of the design concepts, a large part of the suppressive structure consists of a layered cylindrical shell with flat ends. Each layer of the shell will absorb plastic energy largely by membrane action, so bending will be neglected. The shell will be placed in a state of biaxial tension by the internal loads, but the stress state is different from that in the spherical shell discussed in Appendix A. For a short, stubby cylinder which is clamped at the edges so they cannot deflect, we can assume a deformed shape of the form:

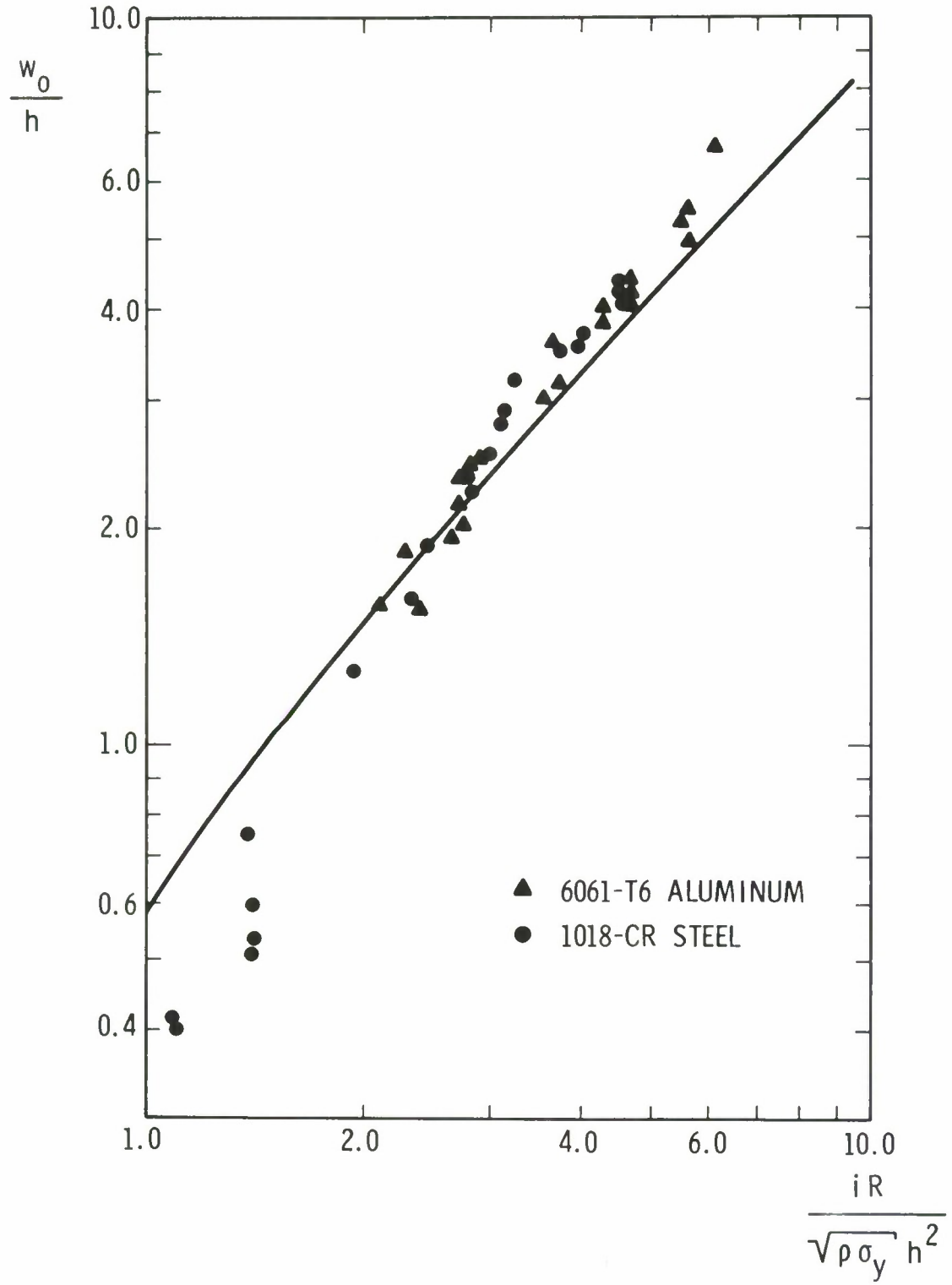

FIGURE C-7. COMPARISON OF EQUATION (C-84) WITH EXPERIMENTAL PLATE DATA

$$w = w_o \left(1 - \frac{4x^2}{L^2}\right) \tag{C-85}$$

This deformed shape has a maximum displacement w_o and zero slope in the middle of the cylinder where $x = 0$ and zero displacement at the ends of the shell, $x = \pm L/2$. The longitudinal strains ϵ_ℓ in such a cylinder are given by:

$$\epsilon_\ell = \frac{1}{2}\left(\frac{dw}{dx}\right)^2 \tag{C-86}$$

Differentiating Equation (C-85) and substituting into Equation (C-86) yields:

$$\epsilon_\ell = \frac{32x^2 w_o{}^2}{L^4} \tag{C-87}$$

The circumferential strain ϵ_c in the cylinder is given by:

$$\epsilon_c = \frac{2\pi(R + w) - 2\pi R}{2\pi R} = \frac{w}{R} \tag{C-88}$$

Substituting Equation (C-85) into Equation (C-88) then yields:

$$\epsilon_c = \frac{w_o}{R}\left(1 - \frac{4x^2}{L^2}\right) \tag{C-89}$$

Because the cylinder is a symmetric shell, these strains and the stresses associated with them must be the principle strains and stresses. This observation means then no shear stresses exist on a rectangular differential element where faces are perpendicular to longitudinal and circumferential axes. Because the strain energy per unit volume is given by:

$$\frac{U}{\text{Vol.}} = \Sigma\, \sigma_{ij}\, d\epsilon_{ij} \tag{C-90}$$

and no shearing strains exist, Equation (C-90) for a rigid-plastic stress strain law without strain hardening becomes:

$$\frac{U}{\text{Vol.}} = \sigma_y \epsilon_c + \sigma_y \epsilon_\ell \tag{C-91}$$

The volume of a differential hoop of dx width equals:

$$\text{Vol.} = 2\pi R h dx \tag{C-92}$$

Substituting Equation (C-89) for ϵ_c, Equation (C-87) for ϵ_ℓ, and Equation (C-92) for vol. permits one to estimate the strain energy in the cylinder by integrating

$$U = 2\int_0^{L/2} \left[\frac{\sigma_y w_o}{R}\left(1 - \frac{4x^2}{L^2}\right) + \frac{32\sigma_y x^2 {w_o}^2}{L^4}\right]\left(2\pi R h dx\right) \tag{C-93}$$

or

$$U = \frac{16\pi\sigma_y R h {w_o}^2}{3L} + \frac{4\pi}{3}\sigma_y h L w_o \tag{C-94}$$

The work Wk put into the cylinder equals:

$$Wk = 2\int_0^{L/2} p_o(2\pi R dx)w \tag{C-95}$$

Substituting Equation (C-85) for w yields:

$$Wk = 4\pi R w_o p_o \int_0^{L/2} \left(1 - \frac{4x^2}{L^2}\right) dx \tag{C-96}$$

or

$$Wk = \frac{4\pi}{3} p_o R w_o L \tag{C-97}$$

The kinetic energy K.E. imparted to the cylinder is obtained by substituting into Equation (C-97) and integrating

$$\text{K.E.} = 2\int_0^{L/2} \frac{{i_o}^2 (2\pi R)^2 (dx)^2}{2\rho(2\pi R)h(dx)} \tag{C-98}$$

or

$$\text{K.E.} = \pi \frac{{i_o}^2 R L}{\rho h} \tag{C-99}$$

The asymptote for the impulsive loading realm is obtained by equating the kinetic energy, Equation (C-99) to the strain energy, Equation (C-94).

$$\pi \frac{i_o^2 RL}{\rho h} = \frac{16\pi\sigma_y R h w_o^2}{3L} + \frac{4\pi}{3}\sigma_y h L w_o \tag{C-100}$$

or

$$\frac{i_o^2}{\rho\sigma_y h^2} = \frac{16}{3}\left(\frac{w_o}{R}\right)^2\left(\frac{R}{L}\right)^2 + \frac{4}{3}\left(\frac{w_o}{R}\right) \quad \text{(impulsive realm cylinder)} \tag{C-101}$$

The asymptote for the quasi-static loading realm is obtained by equating the work, Equation (C-97) to the strain energy, Equation (C-94).

$$\frac{4\pi}{3} p_o R w_o L = \frac{16\pi\sigma_y R h w_o^2}{3L} + \frac{4\pi}{3}\sigma_y h L w_o \tag{C-102}$$

or

$$\frac{p_o R}{\sigma_y h} = 4\left(\frac{R}{L}\right)^2\left(\frac{w_o}{R}\right) + 1 \quad \text{(quasi-static realm cylinder)} \tag{C-103}$$

Notice that for very short cylinders (R/L very large) Equation (C-103) equals Equation (C-43) for membrane action in rectangular strips, and Equation (C-101) equals Equation (C-42). On the other hand, if the cylinder is very long (R/L very small), Equation (C-103) yields the familiar static relationship.

$$\frac{p_o R}{\sigma_y h} = 1.0 \tag{C-104}$$

and Equation (C-101) reaches the less familiar impulsive loading realm relationship.

$$\frac{i_o^2}{\rho\sigma_y h^2} = \frac{4}{3}\left(\frac{w_o}{R}\right) \tag{C-105}$$

These limits are the correct asymptotes if the boundaries of the cylinders are unclamped so membrane action cannot be developed in the longitudinal direction. In our cylindrical shell analysis, we will assume that the boundaries are clamped and Equations (C-101) and (C-103) will be applied.

Although a number of design formulas have been developed here, several qualifying statements apply, as follows:

(1) Energy methods for the quasi-static loading realm yield force balance equations. Because the strain energies have been computed for uncoupled, fully-plastic membrane plus bending, some care should be exercised to ensure that the final state of

stress will react the applied loads without exceeding the rupture stress of the material. Future equations for the quasi-static loading should couple the stresses due to axial loads and bending moments to limit the combined plastic stress to some selected level.

(2) Results for quasi-static loading have not been compared with experiment. Assumed deformed shapes, which are shown to be suitable for dynamic loading, by virtue of comparisons with experiments, may not be the best selections for response to quasi-static loading.

(3) Energies due to quasi-static and dynamic loading should not be combined for this problem because the loadings occur at significantly different times.

APPENDIX D
PANEL ANALYSIS

Each panel to be used in this structure will be vented and will consist of 10 ft × 10 ft assemblies. The panels will consist of two subassemblies, the inner one containing a set of angles with $\alpha = 0.5$ (see Appendix B), and the outer one containing four perforated plates with one pair having $\alpha = 0.3$ and the other $\alpha = 0.1$. Angle panels will be bordered with four channels while plate panels will be mounted in angles. The plate panel edge members will be welded to the frame during assembly described in Appendix E.

Since the vent area of the angle panel is 50%, the predominant loading will be the dynamic impulse generated by the centrally located explosive in the structure. The large venting area will not allow any appreciable quasi-static pressure to act on the angles. On the other hand the plates have considerably less venting so that the effective venting of the four plates in series is such that it will be assumed that the entire quasi-static pressure build-up is contained only by the plates. It is probable that this pressure will dictate the thickness of these plates. However, a check will be made using the dynamic impulsive loading to ensure that the plates will take it.

The angles to be used in these panels will be sized using the equations derived in Appendix C. The angle panels will be attached to the frame such that membrane action will not be developed. Therefore, they will be sized entirely on bending with simply-supported ends.

The perforated plate panels will be attached to the frame in two different ways. Those for use on the sides of the structure will be able to develop uniaxial membrane stresses. Those for the roof of the structure, where cross members are required on the frame, will be designed for biaxial membrane stresses. Thus, two different design equations will be used.

All panel members to be designed will be, as much as possible, standard structural shapes of ASTM A36 steel. The yield stress σ_y for this steel is 36,000 psi and the ultimate tensile strength σ_u ranges between 58,000 and 80,000 psi (reference 20). Thus, in all cases where σ_y is required a value of 36,000 psi will be used. Also, the strain-hardening term will be neglected in all design calculations, so the results will be slightly conservative providing a small safety margin.

Angles

The angles will be assembled as shown in Figure D-1. The response to dynamic impulse loads is given by Equation (C-24)

$$\frac{i_o^2 b^2 L}{2\rho A} = \frac{8mM_y w_o}{L} \qquad \text{where } m = 1 \text{ for simply-supported ends}$$

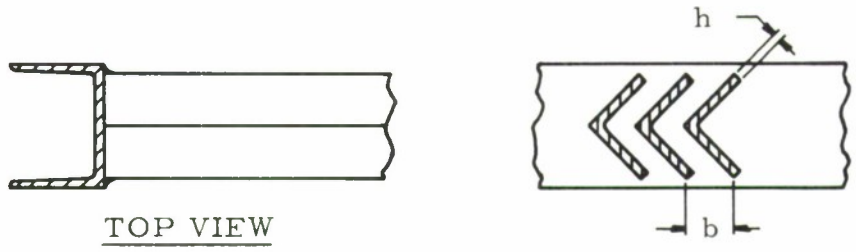

FIGURE D-1. ANGLE PANEL

From Table 1, Section 1V, i_o = 0.91 psi sec.* The other parameters are:

b = 2.415 in. for h = 0.5 in. ($b = h/0.207$)

L = 116 in.

ρ = .283/386 lb-sec^2/in^4

w_o = 0.15 L in.

A = cross-section area of beam member

M_y = plastic modulus

$$\frac{(.91 \text{ psi-sec})^2 (2.415 \text{ in})^2 (116 \text{ in})}{2(.283/386 \text{ lb-sec}^2/\text{in}^4) A \text{ in}^2} = \frac{8(1) M_p (.15\ L)}{L}$$

$$382073 = 1.2 M_y A$$

$$(M_y A)_{\text{Req'd}} \geqslant 318{,}394$$

For L 3-1/2 X 3-1/2 X 1/2 A36 steel angle, M_y = 17,200 lb-ft A = 3.25 in^2. Therefore, $(M_y A)$ = (11,200)(12)(3.25)

$$= 436{,}800 \gtrsim 318{,}394$$

Other angles can be selected with the required cross-sectional area and plastic moment. However, since h was picked to be 0.5 initially, the 3-1/2 in. leg is the smallest that will meet the requirements. If other angle thicknesses are desired, a new b must first be computed and a check must be made to ensure that the necessary leg length will provide sufficient overlap. In this case the overlap is $OL = (3.5 + 0.5)(.707) - 2.415$

$$OL = 0.413 \text{ in.}$$

*As noted earlier, this value should be multiplied by 1.630 to be correct. All succeeding calculations should be modified accordingly.

The weight of these angles in one panel is:

$$\text{No. Angles} = \frac{116}{2.415} = 48$$

$$W_A = \frac{(48)(11.1 \text{ lb/ft})(116 \text{ in.})}{(12 \text{ in/ft})} = 5{,}150 \text{ lb}$$

For this size angle and to provide sufficient bearing surface in assembling the panels to the frame, MC6 X 15.3 channels are selected to fabricate the angle panels. The weight of these channels is

$$W_c = \frac{(4)(15.3 \text{ lb/ft})(116 \text{ in})}{12 \text{ (in/ft)}} = 592 \text{ lb}$$

Thus the total weight of one angle panel is

$$W_{TA} = 5{,}742 \text{ lb}$$

Plates—Uniaxial Membrane Action

To analyze a strip from the plate to quasi-static loading equation (C-7.5) is used

$$\frac{P_{\max} X}{\sigma_y h^2} = \left[1 + \left(\frac{X}{Y}\right)^2\right]\left[\frac{3}{4} + \frac{4}{5}\left(\frac{w_o}{h}\right)\right]$$

Strain hardening has been neglected and the ends are simply supported. For this problem of membrane action in one direction only:

Y = Long half-span of plate and $\rightarrow \infty$

$P_{\max}$ = 145 psi

σ_y = 36,000 lb/in^2 for A36 steel

L = 116 in

w_o = .15 L in.

X = Short half span = $L/2$

$$\frac{(145)(58)^2}{36{,}000\, h^2} = \frac{3}{4} + \frac{4}{5}\frac{(0.15)(116)}{h}$$

$$\frac{13.55}{h^2} = 0.75 + \frac{13.92}{h}$$

$$h^2 + 18.56\,h - 18.07 = 0$$

$$h = \frac{-18.56 \pm 20.41}{2}$$

$$h = 0.927$$

Since the load will be distributed among four plates and the membrane action is predominant ($18.56\,h >> h^2$), each plate thickness becomes simply

$$h_p = \frac{h}{4}$$

$$h_p = 0.232 \text{ in.}$$

The actual thicknesses are then

For $\alpha = 0.3$, $h_A = \dfrac{0.232}{0.7} = 0.331$ in. $\therefore$ Use 5/16 plate

For $\alpha = 0.1$, $h_A = \dfrac{0.232}{0.9} = 0.258$ in. $\therefore$ Use 1/4 plate

To obtain the specified venting areas

For $\alpha = 0.3$, $A_{\text{Total}} = (116)^2 = 13456 \text{ in}^2$

$A_{\text{Vent}} = A_T \alpha = 4036.8 \text{ in}^2$

Using 1/4″ holes $A_{\text{Hole}} = \pi(1/8)^2 = 0.0491 \text{ in}^2$

No. of Holes = 4036.8/0.0491 = 82,237 or for square panel

No. of Holes per side for square array = 287

℄ Spacing = 116/287 = 0.405 in. Therefore, use 7/16 in. on the 5/16″ plate, with the holes staggered.

For $\alpha = 0.1$ $\quad A_{Vent} = 1345.6\ in^2$

No. of Holes = 1345.6/o.0491 = 27,405

No. of Holes per side for square array = 166

℄ Spacing = 116/166 = 0.699. Therefore, use 11/16 in. on the 1/4" plate, with the holes staggered.

The weights for these plates are

$$W_\alpha = 0.3 = \frac{(2)(12.75)(116)^2(0.7)}{(12)^2} = 1{,}688\ lb$$

$$W_\alpha = 0.1 = \frac{(2)(10.20)(116)^2(0.9)}{(12)^2} = 1{,}716\ lb$$

The plates will be made up into panels using L 4 X 4 X 3/4 angles as shown in Figure D-2.

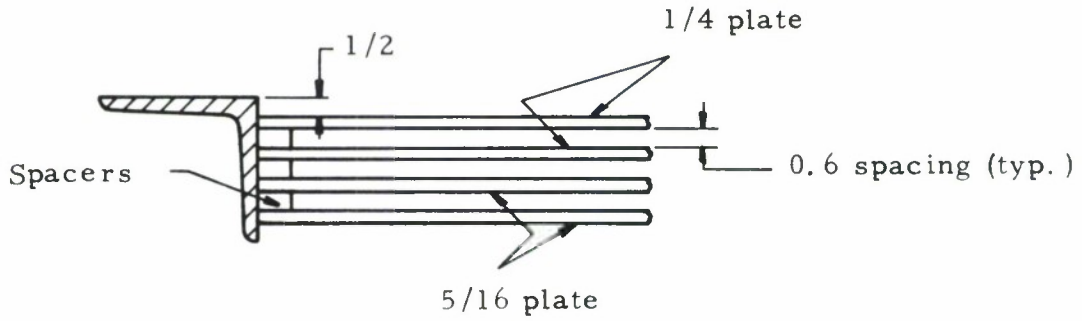

FIGURE D-2. PLATE PANEL

The weight of the angles around the perimeter of the plate panel is

$$W_A = \frac{(4)(18.5\ lb/ft)(116\ in.)}{(12\ in/ft)} = 715\ lb$$

Therefore, the total panel weight is W_{TP} = 4,099 lb.

To check for dynamic loading as if the angle panels were not present, the plates will also be sized using Equation (C-73) for simply-supported ends.

$$\frac{i_o^2 X^2}{\rho \sigma_y h^4} = \left[1 + \left(\frac{X}{Y}\right)^2\right]\left[\frac{2}{3}\left(\frac{w_o}{h}\right) + \frac{32}{45}\left(\frac{w_o}{h}\right)^2\right]$$

$$\frac{(0.91)^2(58)^2(386)}{(.283)(36{,}000)(h^4)} = \frac{2}{3}\frac{(.15)(116)}{h} + \frac{32}{45}\left[\frac{(.15)(116)}{h}\right]^2$$

$$\frac{105.54}{h^4} = \overbrace{\frac{11.6}{h}}^{\text{(Bending)}} + \overbrace{\frac{215.3}{h^2}}^{\text{(Membrane)}}$$

$$h^3 + 18.56h^2 = 9098$$

For $h = 0.69$, $0.3285 + 8.8364 = 9.165 \approx 9.098 \therefore h_T = 0.69$ inches

Since four plates have been selected for use and the membrane portion of the equation is predominant ($18.56\,h^2 >> h^3$) the required plate thickness for one of the set of four is $h = 0.69/4 = 0.1725$.

For $\alpha = 0.3$, $h_A = \dfrac{h}{0.7} = 0.246 <$ For Quasi-Static Case

For $\alpha = 0.1$, $h_A = \dfrac{h}{0.9} = 0.192 <$ For Quasi-Static Case

Thus, the plate panel will handle the dynamic as well as the quasi-static loading.

Plates—Biaxial Membrane Action

From Equation (C-75), for simply-supported ends

$$\frac{P_{\max} X^2}{\sigma_y h^2} = \left[1 + \left(\frac{X}{Y}\right)^2\right]\left[\frac{3}{4} + \frac{4}{5}\frac{w_o}{h}\right]$$

which includes the effects of bending and membrane contributions to the load reaction.

σ_y = 36,000 lb/in^2

$X = Y$ = 116/2 in.

L = 116 in.

$P_{\max}$ = 145 psi

w_o = 0.15 L = 0.3 X

$$\frac{(145)(58)^2}{(36{,}000)h^2} = 2\left[\frac{3}{4} + \frac{(4)(0.15)(116)}{(5)h}\right]$$

$$13.55 = 1.5h^2 + 27.84h$$

$$h^2 + 18.55h - 9.03 = 0$$

$$h = \frac{-18.55 \pm 19.5}{2}$$

$$h = 0.475 \text{ in.}$$

Since membrane action is predominant ($18.55\,h >> h^2$) the thickness of each plate is $h = 0.475/4 = 0.119$ in. The actual thicknesses and weights are then

For $\alpha = 0.3$ $\quad h_A = h/0.7$, use 3/16″ plate

$$W_T = (7.65 \text{ lb/ft}^2)\left(\frac{115}{12}\right)^2 \text{ ft}^2 (0.7) = 492 \text{ lb/plate}$$

For $\alpha = 0.1$ $\quad h_A = h/0.9 = 0.132$, use 3/16″ plate

$$W_T = 632 \text{ lb/plate}$$

The panels from these plates will be essentially the same as in Figure D-2 except that the spacing between plates will now be 0.69 in. The same angles will be used around the perimeter. Therefore the total panel weight for these is

$$W_{TP} = 2{,}963 \text{ lb}$$

APPENDIX E
FRAME ANALYSIS

The general frame arrangement is shown schematically in Figure E-1. Internal dimensions of 40 ft X 40 ft X 40 ft have been maintained. As indicated in Appendix D, the vented panels were designed for two different loading conditions, for biaxial membrane stresses and for uniaxial membrane stresses. Panels designed for biaxial membrane stresses are for the roof of the structure where cross members are required anyway to react the loads at the roof induced by the A-member. Panels designed for uniaxial membrane action are used in the side of the structure so that no cross members are required (Figure E-1b). Although the frame elements were checked for dynamic loads, the quasi-static pressure loading predominated in sizing the members as it did for the plate panels and for the spherical and cylindrical suppressive structures.

A mild steel ASTM A36 was assumed for the framing members. From the Steel and Aluminum Stock List (Reference 20) properties of A36 are

$$\sigma_y = 36{,}000 \text{ psi (minimum)}$$

$$\sigma_u = 58{,}000 \text{ psi-}80{,}000 \text{ psi}$$

Unless otherwise specified, the design is based on fully plastic cross-sections at the yield stress, σ_y.

Detailed analyses of joints were not performed, but we attempted to choose members which could be assembled in the field without hidden welds, etc. Also local stiffeners may be required for some I-beam flanges to prevent excessive bending deformations and also for some plates and I-beam webs to prevent local buckling. These details were not checked. Rather, overall dimensions were determined to give an indication of the overall structural size and weight. In some cases trusses rather than beams might represent a more efficient design, but, again, these details are left for later analyses.

MEMBER LOADS

A-Member

Pressure loads from the internal explosion are transferred primarily through membrane action in the panels to the large A and C members in the frame. This is demonstrated for the walls of the structure in Figure E-2. The maximum quasi-static pressure is from Appendix B. Figure E-3 shows the load transfer through the A-members (other than those at the corners). The quasi-static pressure acting over a 10 ft span produces the uniform distributed load of 17,400 lb/in. Reactions at the base and at the roof are computed for member A using relationships for an elastic beam simply supported at one end and fixed at the other. The

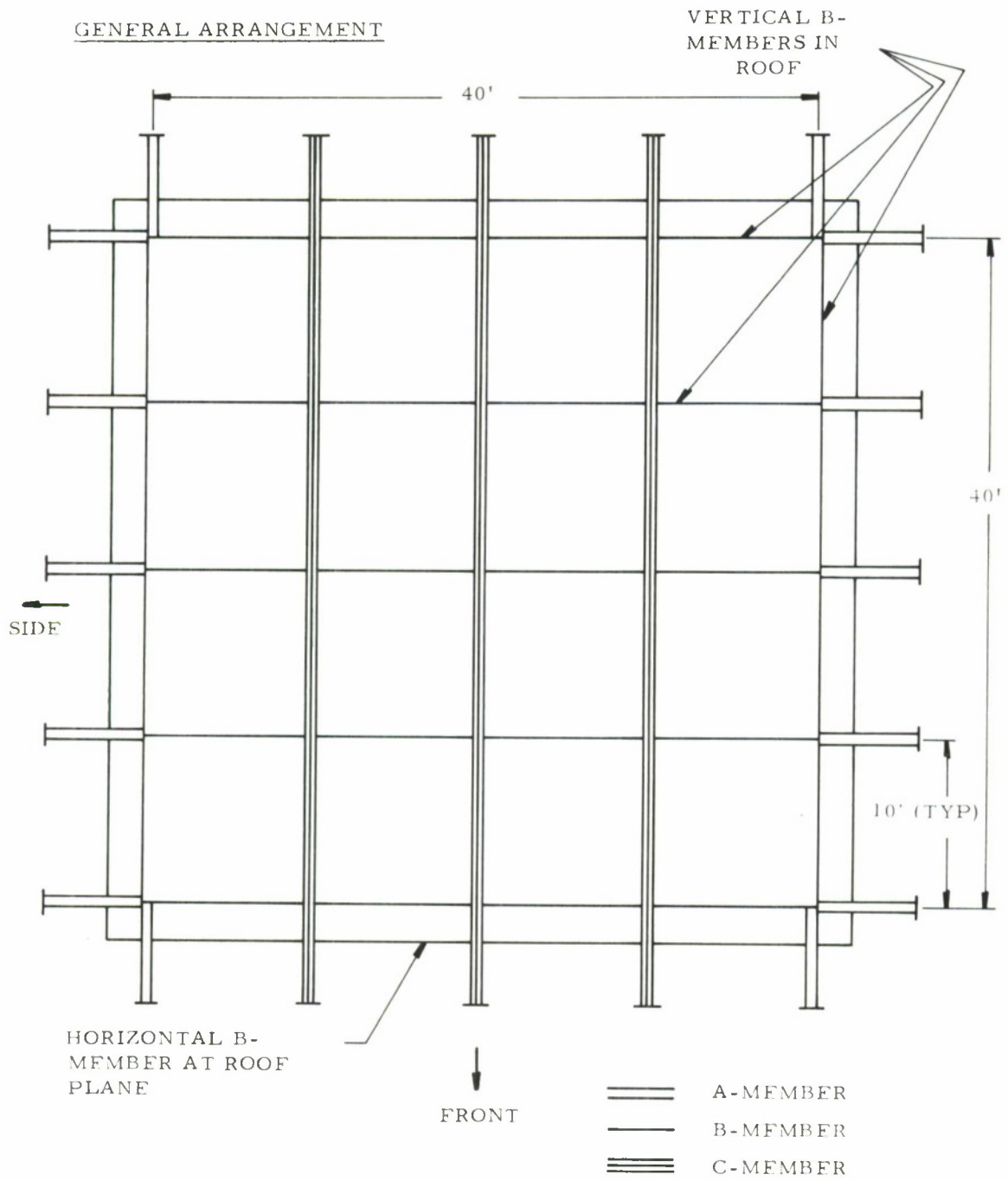

FIGURE E-1a. TOP VIEW OF FRAMING

GENERAL ARRANGEMENT (CONT'D)

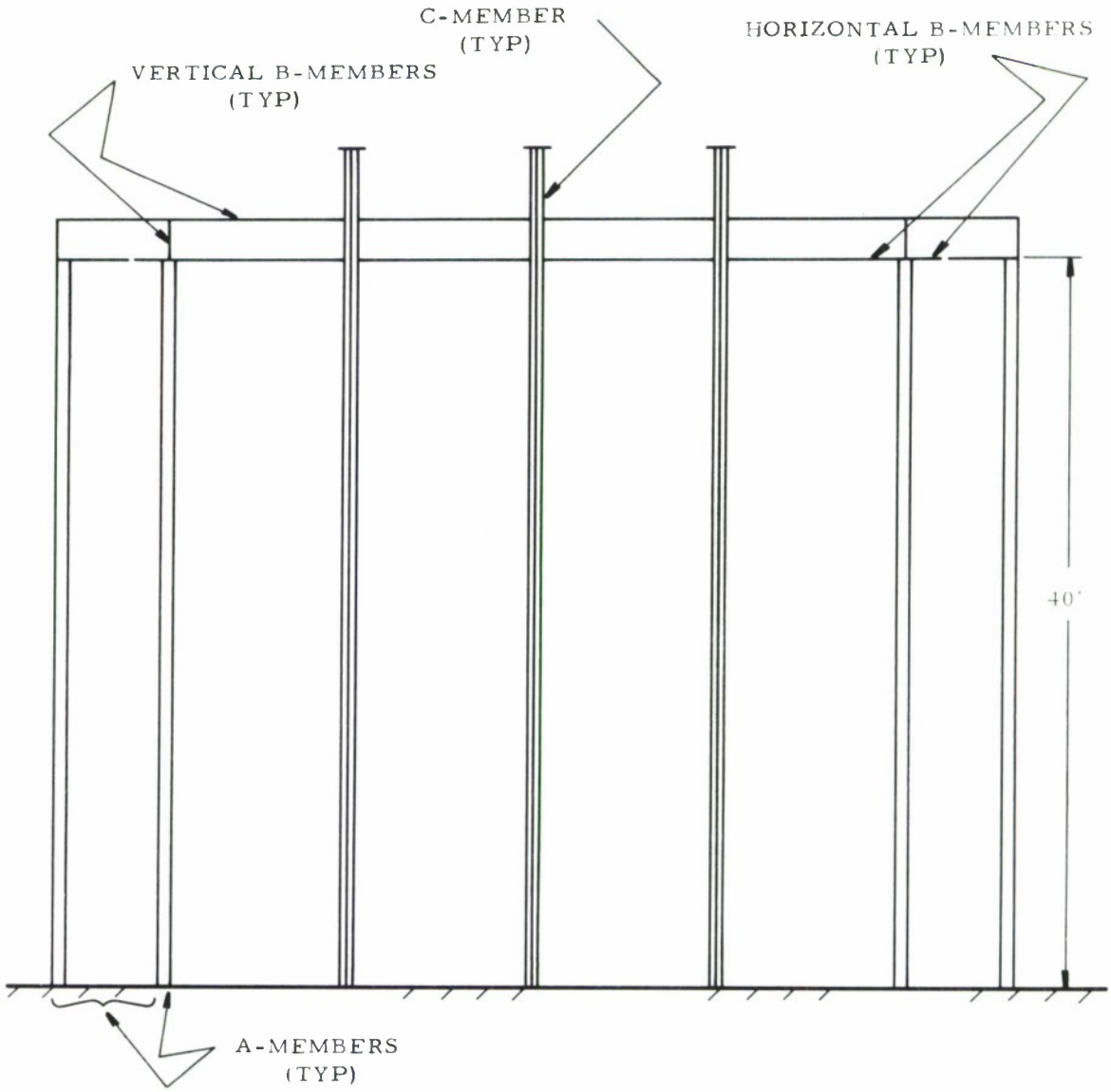

FIGURE E-1b. FRONT VIEW OF FRAMING

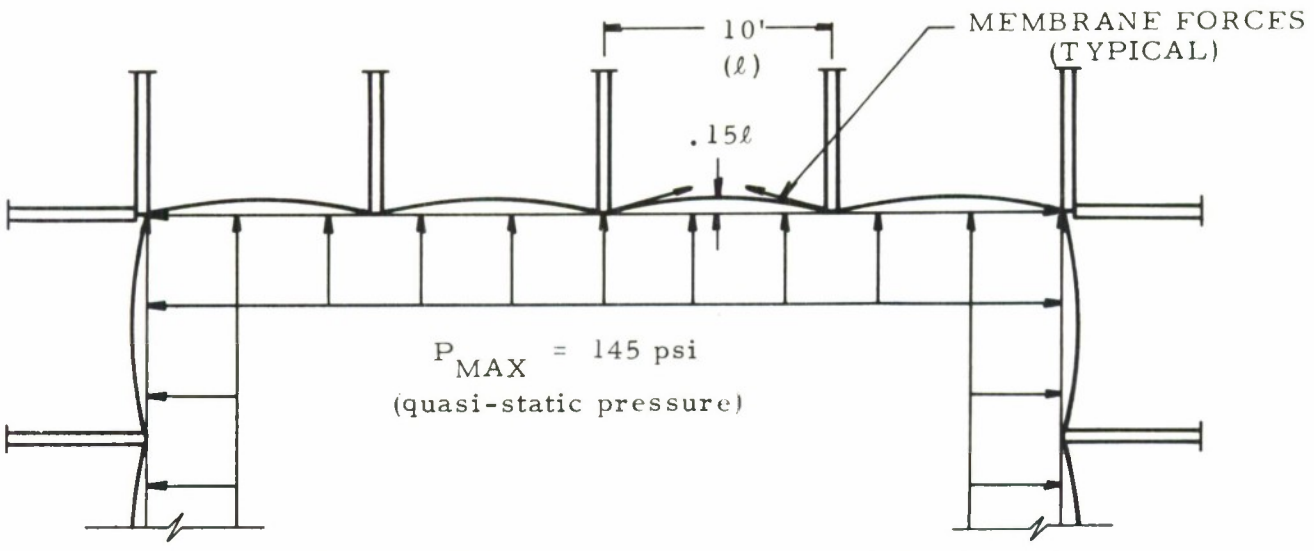

FIGURE E-2. LOAD TRANSFER FROM PANELS IN WALLS TO "A" AND "C" MEMBERS

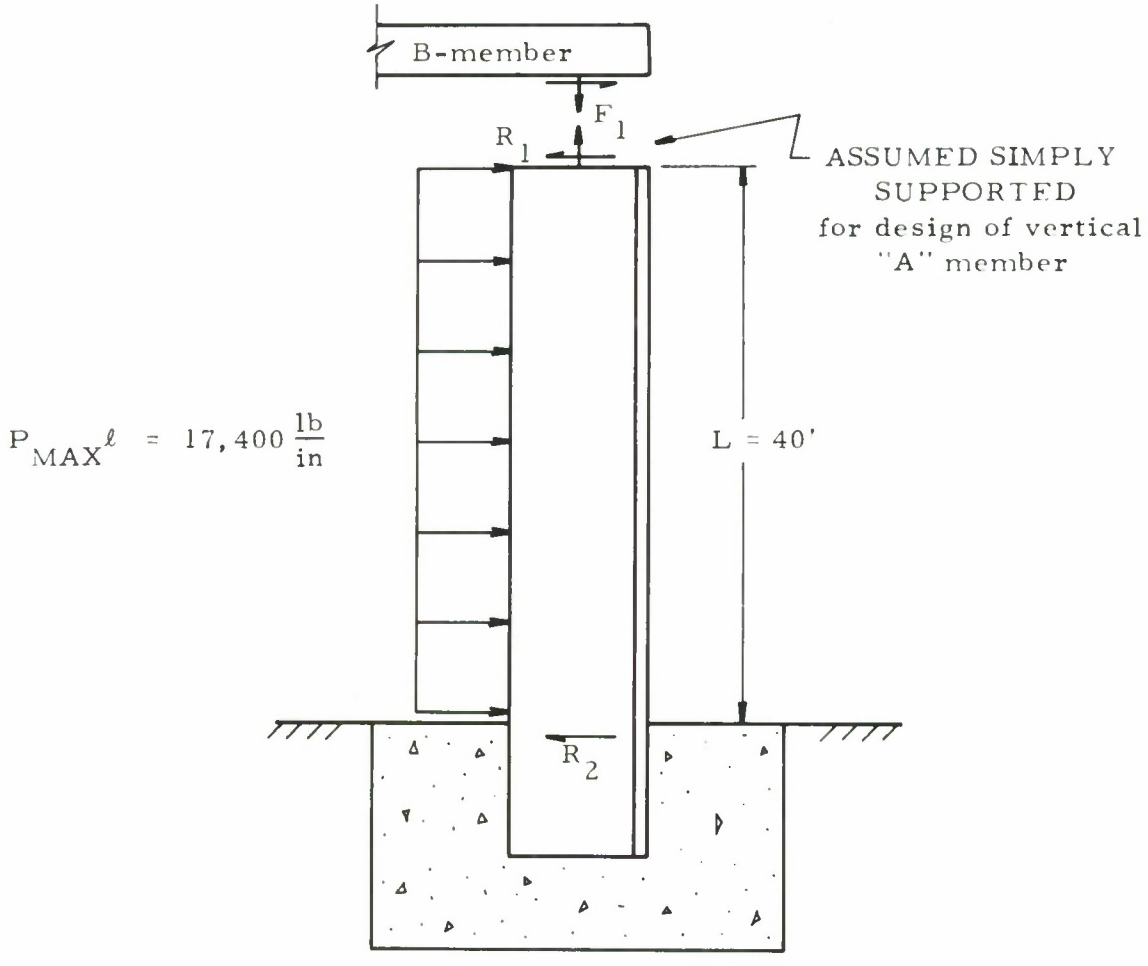

FIGURE E-3. LOAD TRANSFER THROUGH INTERIOR A-MEMBER

simply supported end condition was assumed at the top because the B-member will be much more flexible than the A-member. Roark (reference 21) gives the reactions as

$$R_1 = \frac{3}{8} WL = \frac{3}{8} (17{,}400 \text{ lb/in})(480 \text{ in}) = 3.132 \times 10^6 \text{ lb} \qquad \text{(E-1)}$$

$$R_2 = \frac{5}{8} WL = \frac{5}{8} (17{,}400)(486) = 5.22 \times 10^6 \text{ lb} \qquad \text{(E-2)}$$

The force R_2 is transferred to the foundation and the force R_1 is reacted in the roof by member B. An axial force, F_1, also acts on member A but it is relatively small as will be discovered when deriving the loads for member B. These loads act on the vertical A-members other than those at the corners of the structure. For the corner members the loads are those required to develop the membrane stresses in the panels. If the corner members were not included, the intersecting panels at the corners would attempt to deform into a constant radius cylindrical section producing large rotations at the junction of the panels. The junction could not withstand the resulting large strains without failure, and thus the corner members are required.

Loads on the corner members are derived from Figure E-4. Panel dimensions were determined for a center deflection of 15% of the panel width (see Appendix D). For this condition, and the assumed deflection curve of the membrane, the angle θ at the boundary of the membrane can be determined. For uniaxial membrane action, the deflection shape (see Appendix C) was taken as

$$W = w_o \left(1 - \frac{4X^2}{L^2}\right) \qquad \text{(E-3)}$$

Differentiating,

$$\tan \theta = \frac{dW}{dX} = -w_o \frac{8X}{L^2} \qquad \text{(E-4)}$$

where $X = 0$ at the plate center and $L/2$ at the boundary. Substituting $X = L/2$ and $w_o = -.15\ L$

$$\tan \theta = -(-.15\ L) \frac{8 \left(\frac{L}{2}\right)}{L^2} = .60$$

$$\theta = 31°$$

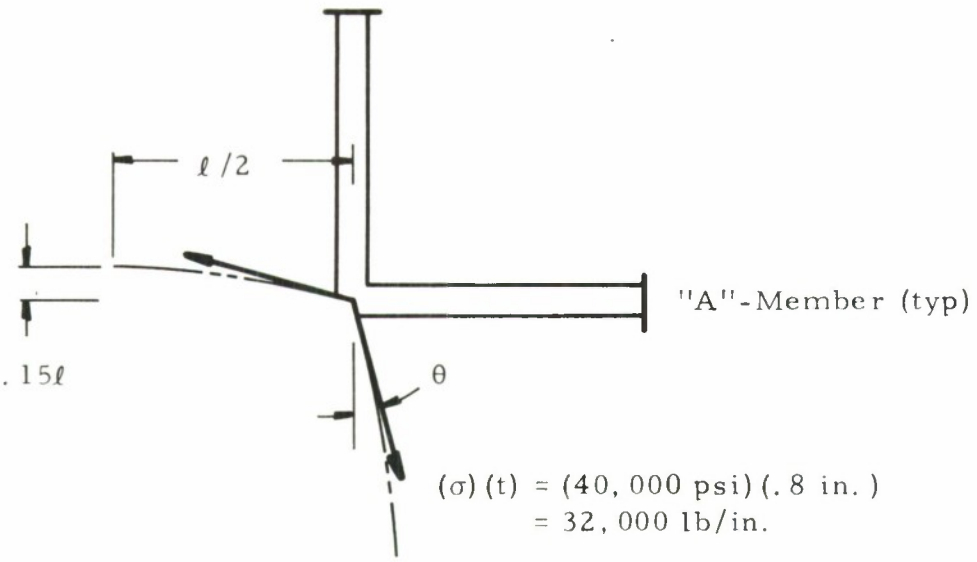

FIGURE E-4. LOADS ON CORNER A-MEMBERS

Summing forces along either side yields

$$N = (32{,}000 \text{ lb/in})(\cos 31 - \sin 31\ ) = 10{,}948 \text{ lb/in}$$

If the deflections are somewhat less than anticipated, or the rotations at the corners somewhat less than predicted by the assumed deflection equation for the same membrane stress, the loads would increase. For example $\theta = 20°$

$$N = 32{,}000 \text{ lb/in}\,(\cos 20 - \sin 20) = 19{,}200 \text{ lb/in}$$

Therefore, it is reasonable to expect a load for the corner members equivalent to that for which the interior members are to be designed. Thus the corner members will be taken to be the same as the interior members and designed for the loads shown in Figure E-3.

B-Member

In addition to the axial load induced into member B by the reaction R_1 at the top of member A, member B must react the pressure loads transferred to it by membrane stresses in the roof panels. Except for the members at the edge of the roof, these loads are determined by consideration of Figure E-5. The distributed load is approximated by assuming that the pressure acting over the shaded area is distributed linearly over the length of the member. Because the B-member is continuous across the C-member and because the vertical A-member is stiff relative to the B-member, the B-member can be considered as having its ends fixed against rotation over the 10 ft span between members.

Consider now the B-members at the edge of the roof. As for the vertical A-members at the corners, these members act to develop the membrane stresses in the intersecting

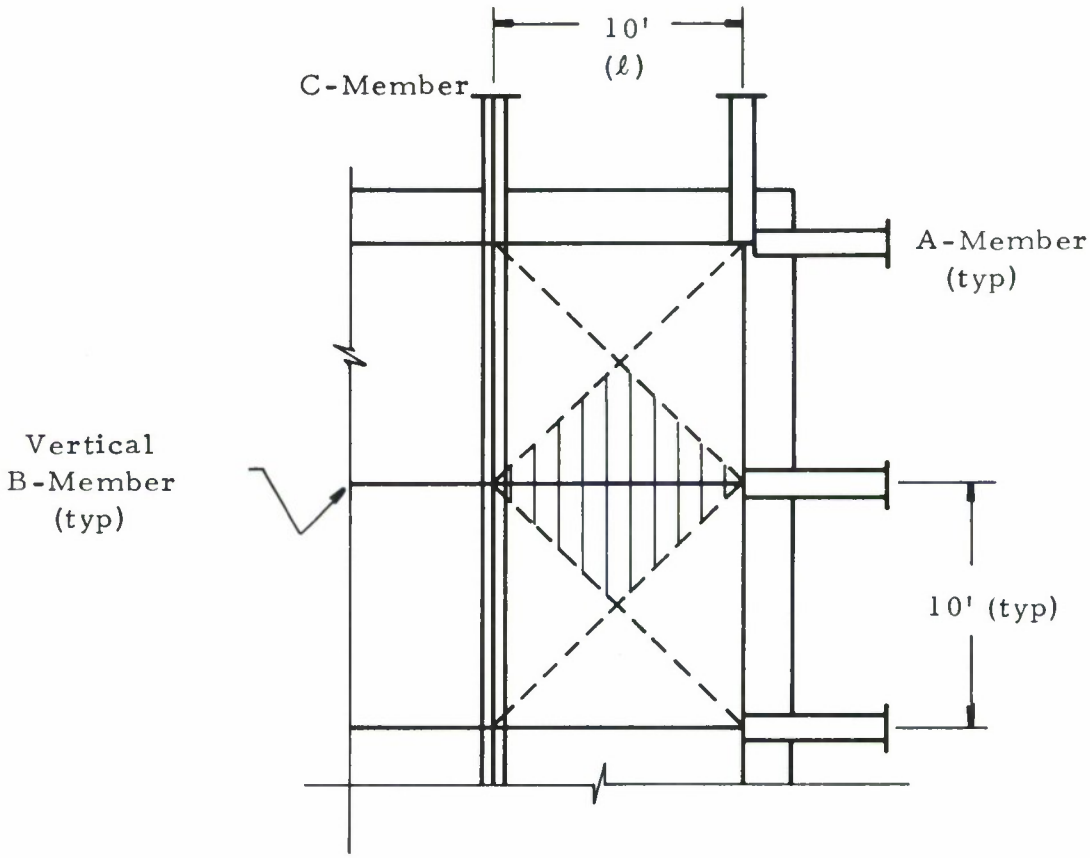

(a) Area for Computing Distributed Load

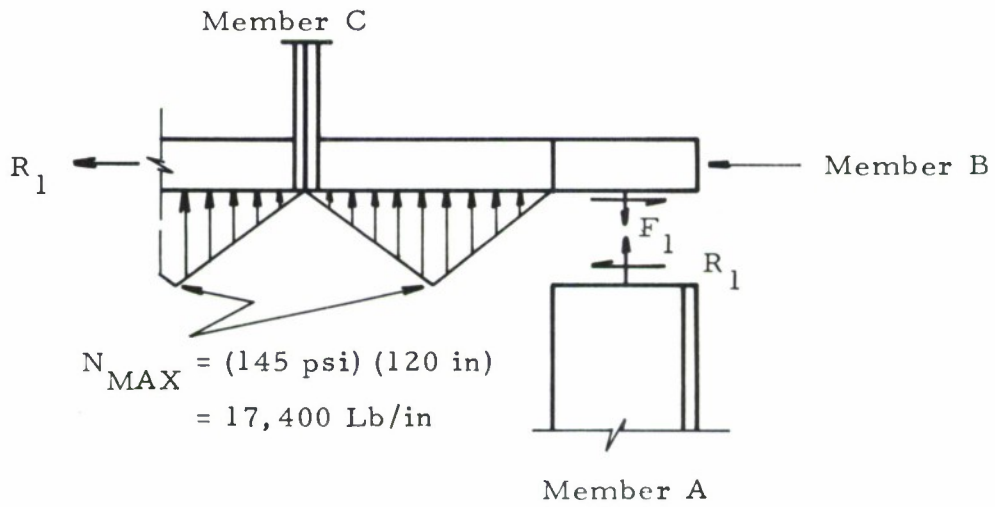

(b) Equivalent Distributed Load

FIGURE E-5. LOADS ON VERTICAL B-MEMBERS IN ROOF (EXCEPT FOR EDGE MEMBERS)

panels while preventing excessive edge rotations at the junction of the panels. The peak distributed load is determined exactly as it was for the corner A-members (see Figure E-4) and will have the same magnitude (see above). However, because biaxial membrane stresses are developed in the panels intersecting at the edges of the roof, the membrane stress will not be constant but will have a distribution similar to the linear assumed for the interior B-members (see Figure E-5). Thus the corner B-members will be sized for the same loads as the interior B-members just as was the case for the A-members.

It should also be noted that the net load on the edge members is directed inward, parallel to the wall or roof for each member, rather than outward as for the interior members in the roof. One result of this condition is that the net vertical reaction where the B-members intersect at the edge of the roof is approximately zero. This is the vertical reaction F_1 shown between the A- and B-members in Figures E-3 and E-5b.

C-Members

As shown in Figure E-6 the three C-members are assumed to be continuous across the structure and will behave as a frame with a uniformly distributed load. The fact that the B-members intersect the C-members and will cause the load to peak at the intersections and be smaller between the B-members will be neglected. The total load will not be affected.

MEMBER SIZES

B-Member

Because the B-member will be incorporated into the design of the larger built-up A- and C-members, it will be sized first. The loads are shown in Figure E-5 and the axial load R_1 is given by Equation (E-1). The loading and restraint are depicted schematically below.

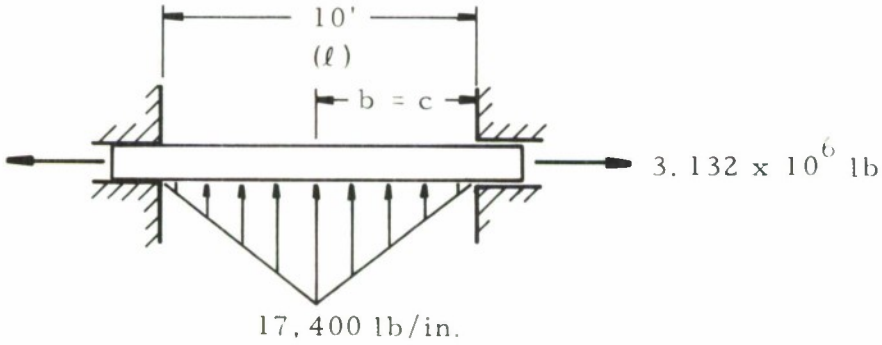

FIGURE E-7. B-MEMBER LOADING AND SUPPORT CONDITIONS

To resist the axial load alone requires a total cross-section area of

$$A = \frac{3.132 \times 10^6 \text{ lb}}{36{,}000 \text{ psi}} = 87 \text{ in}^2$$

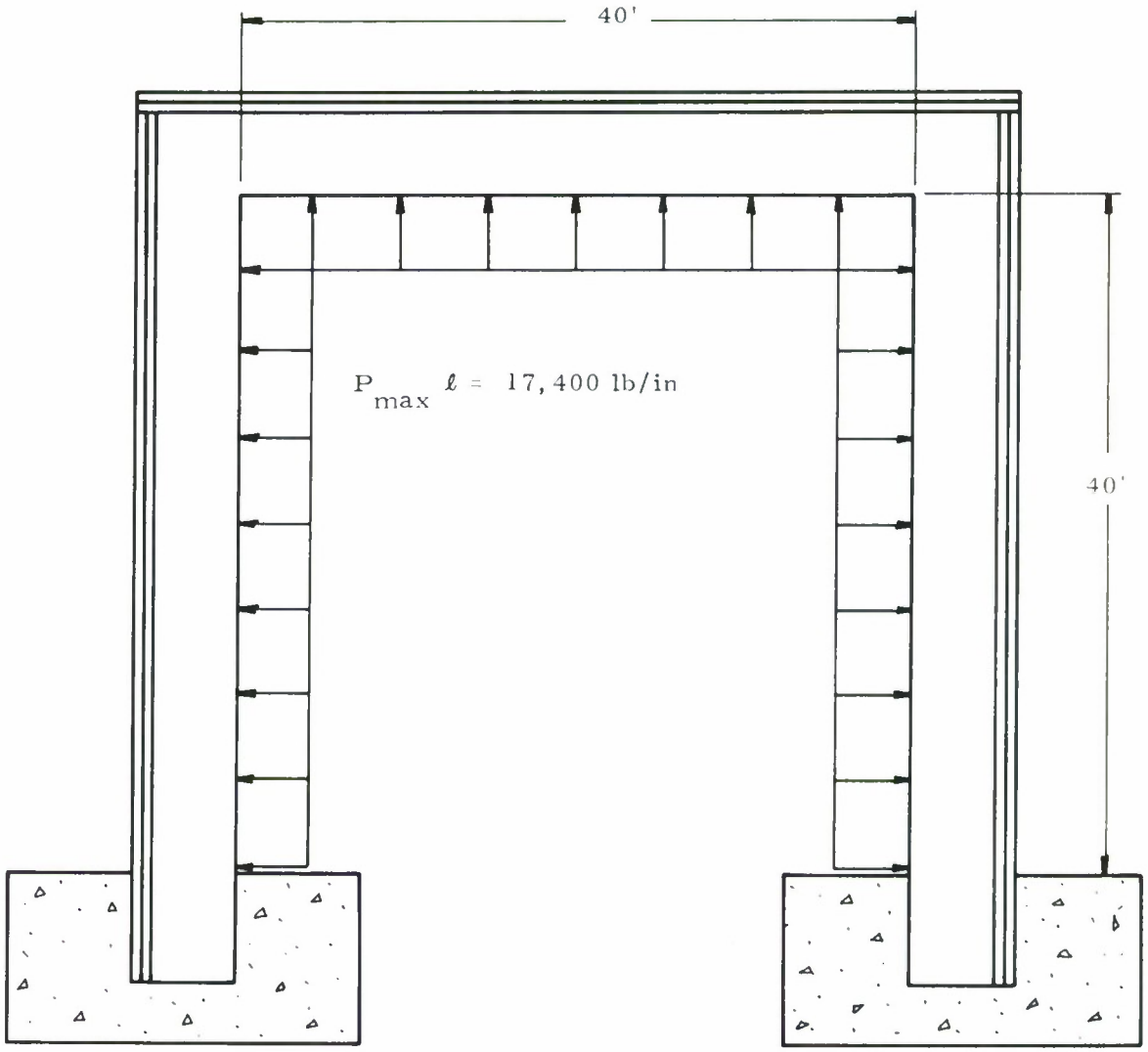

FIGURE E-6. DISTRIBUTED LOADS ON THE C-MEMBERS

Because the angle members in the panel edge are welded directly to the B-member as shown in Figure E-8, the members will contribute to the required area.

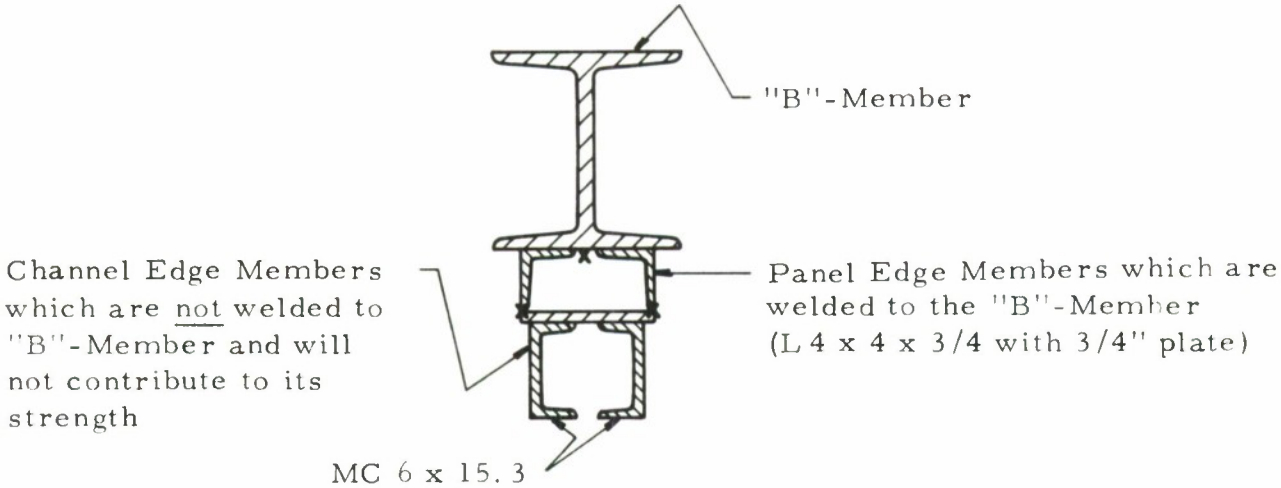

FIGURE E-8. B-MEMBER CONFIGURATION

This contribution is

$$A = 2(5.44\ \text{in}^2) + (8\ \text{in})(.75\ \text{in}) = 16.88\ \text{in}^2$$

Therefore the required area for the I-beam is

$$A_{\text{net}} = 87 - 16.9 = 70.1\ \text{in}^2$$

From the *Steel and Aluminum Stock List* (reference 20) no stock I-beams were found which give the required area. Hence, a non-stock I-beam was selected from the *Manual of Steel Construction* (reference 22). The properties are

$W = 14 \times 237$

$A = 69.7\ \text{in}^2$

Elastic Section Modulus, $S = 382\ \text{in}^3$

Plastic Section Modulus, $Z_p = 445\ \text{in}^3$

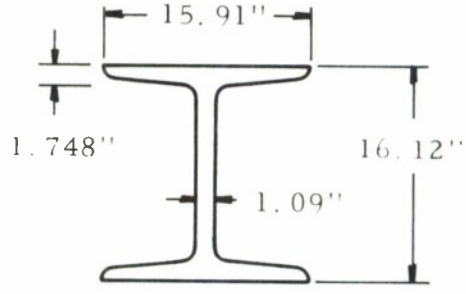

Bending moments can be determined for an elastic beam, neglecting the effect of the axial load on these moments, using formulas in Roark (reference 21). For the load distribution shown in Figure E-7 the end moments are

$$M_{END} = \frac{W}{\ell}\left(2\frac{d^3}{\ell} + \frac{3}{18}C^2 + \frac{51}{405}\frac{C^3}{\ell} - \frac{1}{3}\frac{C^2 b}{\ell} - 3d^2 + d\ell\right) \qquad \text{(E-6)}$$

where $d = 5/6\ \ell$ and $W = 1/2\ N_{MAX}$. For the parameters given

$$M_{ENDS} = 9.383 \times 10^6 \text{ in-lb}$$

This moment produces a fully plastic stress in the I-beam (neglecting the contribution of the edge member) of

$$\sigma = \frac{M}{Z_p} = \frac{9.383 \times 10^6 \text{ in-lb}}{445 \text{ in}^3} = 21{,}000 \text{ psi}$$

Combined with the axial stress of 36,000 psi (area chosen based on yield stress of 36,000)

$$\sigma = 36{,}000 + 21{,}000 = 57{,}000 \text{ psi}$$

which is just under the minimum rupture stress of the material (σ_u = 58,000 psi — 80,000 psi). Because the load distributions were based upon an elastic analysis and because the contribution of the panel edge members was neglected in computing the bending stress, the I-beam chosen is judged adequate to resist the applied loading for the B-members.

A-Member

The loads on the A-member are shown in Figure E-3. For the support condition of one end fixed and one end simply supported the relationship between the applied quasi-static loading and the beam plastic bending moment is given by Equation (E-7).

$$\frac{pbL^2}{M_y} = 15.825 \qquad \text{(E-7)}$$

For this problem

pb = 17,400 lb/in

L = 40 ft

M_y = plastic beam moment, M_p

Z_p = plastic modulus

The required plastic moment is found to be

$$M_p = \frac{(17{,}400 \text{ lb/in})(480 \text{ in})^2}{15.825} \qquad \text{(E-8)}$$

$$= 2.53 \times 10^8 \text{ in-lb}$$

A composite beam (or truss) is required to resist a moment of this magnitude. Using the I-beam selected for the B-member a composite beam is formed as shown schematically in Figure E-9. Location of the neutral axis of the member, $\bar{y}$, and the plastic section modulus, Z_p, are expressed in terms of the I-beam separation distance, a. For a 1.0 in. web the equations are solved to find the overall dimensions of the A-member required to resist the applied moment.

The neutral axis of the B-member plus the plate panel edge members is given by

$$\bar{y}' = \frac{(8.06)(69.7) + (17.39)(10.88) + (20.495)(6)}{69.7 + 10.88 + 6}$$

$$\bar{y}' = \frac{873.96}{86.58} = 10.1 \text{ in.}$$

Now, the overall neutral axis location can be expressed as

$$\bar{y} = \frac{(86.58)(26.2 + a) + (a)(16.12 + a/2) + (69.7)(8.06)}{(86.58) + (a) + (69.7)}$$

$$\bar{y} = \frac{2830.2 + 102.7a + 0.5a^2}{156.3 + (a)(1)} \qquad \text{(E-9)}$$

In terms of $\bar{y}$ the plastic section modulus for the composite beam is

$$Z_p = 2\left[(y - 16.12 + 8.06)(69.7) + (y - 16.12)^2/2\right] = \frac{M_p}{\sigma_y} \qquad \text{(E-10)}$$

Substituting σ_y = 36,000 psi and $M_p = 2.53 \times 10^8$ lb-in into Equation (E-10)

$$\bar{y}^2 + 107.4\,\bar{y} - 7{,}896 = 0$$

$$\bar{y} = \frac{-107.4 \pm 207.7}{2}$$

$$\bar{y} = 50.1 \text{ in.}$$

From Equation (E-9) the value of "a" can now be determined.

$$\therefore 7830.6 + 50.1a = 2830.2 + 102.7a + 0.5a^2$$

$$a^2 + 105.2a - 10{,}000 = 0$$

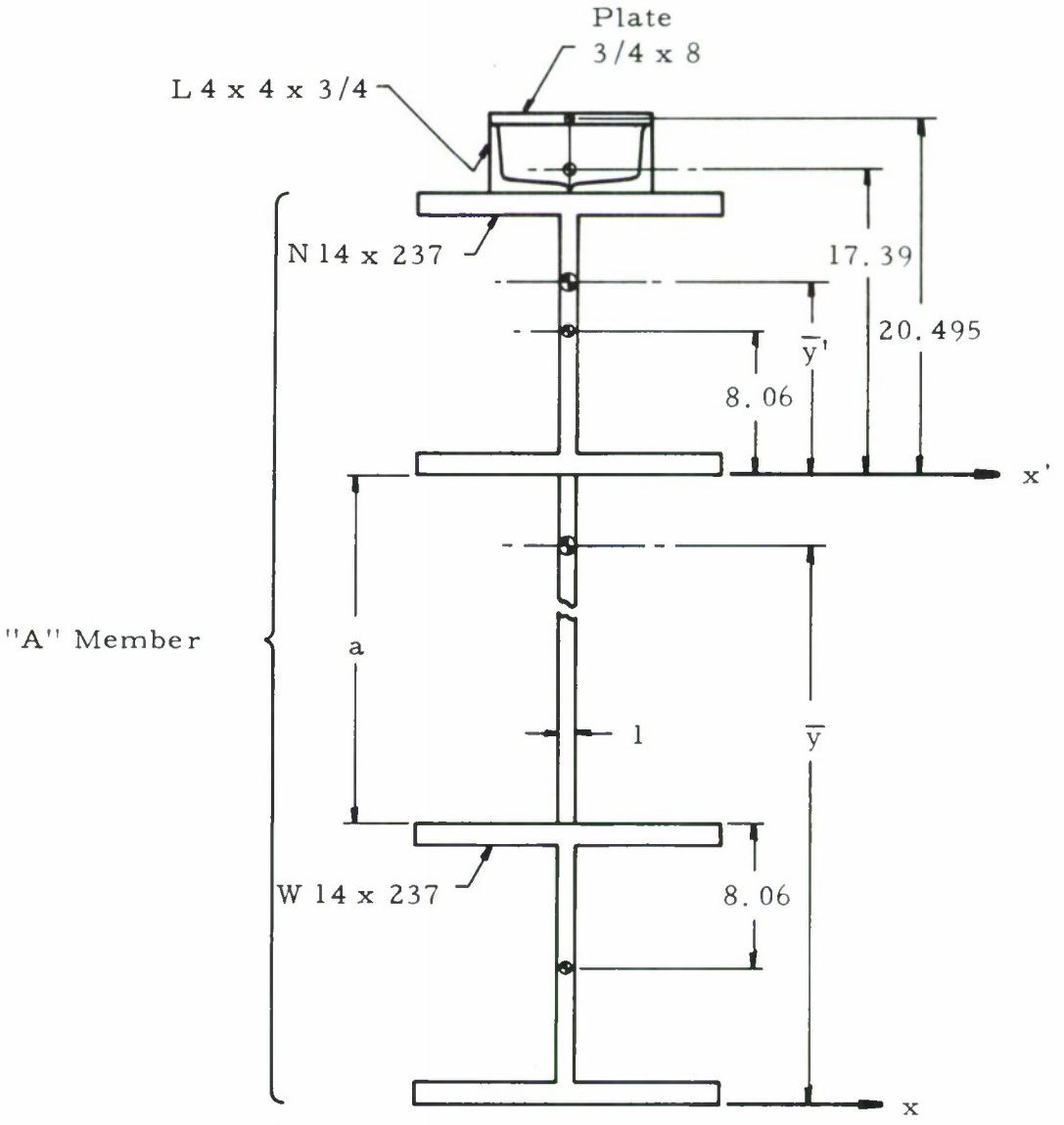

FIGURE E-9. A-MEMBER

$$a = \frac{-105.2 \pm 226}{2}$$

$$a = 60.4 \text{ in.}$$

Areas of the beam are

$$A_{\text{Total}} = 216.7 \text{ in}^2$$

and the area of A-member = 199.8 in^2.

Axial loads in the beam are neglible as explained when deriving the loads on the B-members. Shear at the base should be checked, however, for the base reaction R_2 (see Figure E-3 and Equation E-2). For the area of the A-member

$$\sigma_s = \frac{5.22 \times 10^6 \text{ lb}}{180 \text{ in}^2} = 29{,}000 \text{ psi}$$

The shearing strength of the member can be estimated as

$$\sigma_{sy} \approx .6\sigma = .6(36{,}000) = 21{,}600 \text{ psi}$$

$$\sigma_{su} \approx .6(58{,}000 - 80{,}000)$$

$$34{,}000 \text{ psi} - 48{,}000 \text{ psi}$$

Therefore, the member should be adequate to carry the maximum shearing force at the base and the bending moments for the quasi-static bending moments.

Response to dynamic loading will also be checked for the A-member. The dynamic impulse, found in Appendix B, is 0.91 psi-sec.* From Equation (C-24), the plastic moment for dynamic loading in bending is computed for the A-member assuming it to be simply supported.

$$(0.707)\frac{i_o{}^2 b^2 L}{2(m + \rho A)} = \frac{8M_y w_o}{L}$$

$$m = \frac{(5742 + 4099) \text{ lb-sec}^2}{(116) \text{ in } (386) \text{ in}} = 0.2198 \text{ lb-sec}^2/\text{in}^2$$

A = 199.8 in^2

i_o = 0.91 lb-sec/in^2

*As noted earlier, this number should be multiplied by 1.630 to be correct. All succeeding calculations should be modified accordingly.

b = 120 in.

L = 480 in.

$$\rho = \frac{0.283}{386} = .0007332 \text{ lb-sec}^2/\text{in}^4$$

$w_o = 0.15\ L$

$$\frac{(0.707)(0.91)^2(120)^2(480)}{(2)0.2198 + (0.0007332)(199.8)} = (8)(0.15)M_y$$

$M_y = 4.603 \times 10^6$ lb-in

which is very much lower than the plastic moment required for quasi-static loading (2.53×10^8 lb-in). No further check on other members will be made for the dynamic loading.

C-Member

If the structure is assumed to behave elastically, the distributions of forces within the frame can be found from equations in Reference 21.

Case 45, p. 116 yields the following equations:

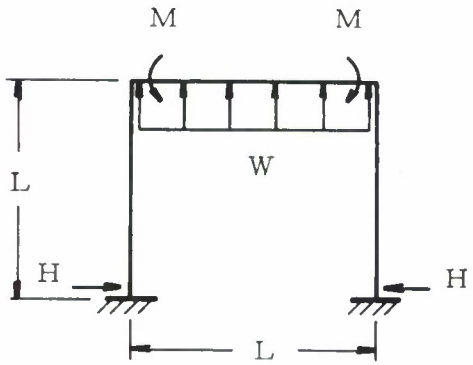

$$M = \frac{2}{3} HL \qquad \text{(E-11)}$$

$$3M - HL = \frac{1}{12} WL \qquad \text{(E-12)}$$

Equations (E-11) and (E-12) give

$$H = \frac{1}{12} W = -.0833\ W \qquad \text{(E-13)}$$

$$M = \frac{1}{18} WL = -.0556\ WL \qquad \text{(E-14)}$$

Case 46, p. 116 yields the following equations

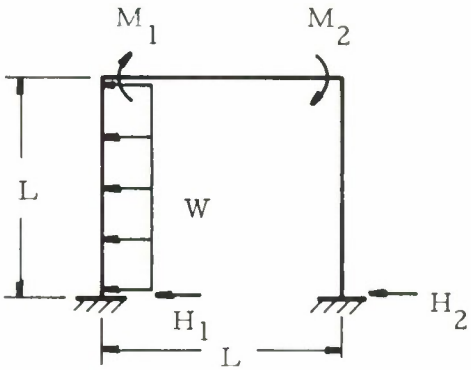

$$\frac{1}{2}M_2 - \frac{1}{2}M_1 - \frac{2}{3}H_2 L = -\frac{1}{8}WL \qquad \text{(E-15)}$$

$$\frac{4}{3}M_1 - \frac{1}{6}M_2 + \frac{1}{2}H_2 L = \frac{1}{6}WL \qquad \text{(E-16)}$$

$$\frac{1}{6}M_1 - \frac{4}{3}M_2 + \frac{1}{2}H_2 L = 0 \qquad \text{(E-17)}$$

From Equations (E-15) through (E-17) M_1, M_2 and H_2 are found to be

$$M_2 = -\frac{43}{504}WL = -.0853WL \qquad \text{(E-18)}$$

$$M_1 = -\frac{1}{7}WL - M_2 = -.0576WL \qquad \text{(E-19)}$$

$$H_2 = \frac{1}{L}\left(\frac{8}{3}M_2 - \frac{1}{3}M_1\right) = -.208W \qquad \text{(E-20)}$$

Now $H_1 = -W - H_2 = -.792W.$

Combining these forces we obtain for the fully loaded frame:

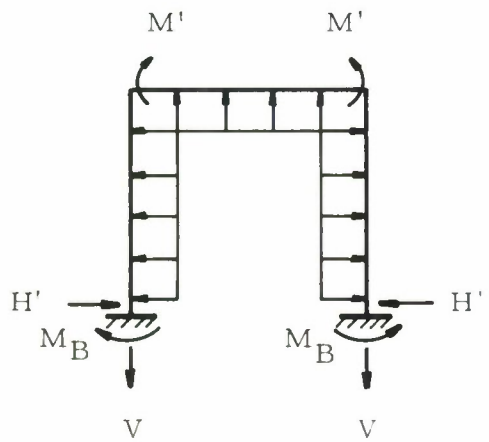

$$\begin{aligned} H' &= H - H_1 - H_2 \\ &= -.0833W - (-.792W) + (-.208W) \\ &= .501W \end{aligned} \qquad \text{(E-21)}$$

$$M' = -M + M_1 - M_2$$
$$= -(-.0556WL) + (-.0576WL) - (-.0853WL)$$
$$= .0833WL \qquad \text{(E-22)}$$

From consideration of equilibrium we also find:

$$V = \frac{1}{2}W = .5W \qquad \text{(E-23)}$$

$$M_B = M' + W\frac{L}{2} - (W - H')L$$

$$= .0833WL + .5WL - .499WL$$

$$= .0843WL \qquad \text{(E-24)}$$

Note that the axial load in the top member is approximately $.5W$ so that all members elements of the frame experience equal loads. For this problem (see Figure E-6)

$$L = 40 \text{ ft}$$

$$W = (17{,}400 \text{ lb/in})(480 \text{ in}) = 5.352 \times 10^6 \text{ lb}$$

The end moments and axial loads are therefore

$$M = .084WL = 3.368 \times 10^8 \text{ in-lb}$$

$$V \approx H = .5(5.352 \times 10^6) = 2.676 \times 10^6 \text{ lb}$$

We will first check to see if the A-member combined with the plate panel edge members (see Figure E-9) is adequate for these loads. The plastic section modulus for the A-member is

$$Z_p = \frac{M_p}{\sigma_y} = \frac{2.53 \times 10^8 \text{ in-lb}}{36{,}000 \text{ lb-in}^{-2}} = 7028 \text{ in}^3$$

and the total area is

$$A = 216.7 \text{ in}^2$$

Computing the stress for the combined bending and axial loads

$$\sigma = \frac{2.676 \times 10^6 \text{ lb}}{216.7 \text{ in}^2} + \frac{3.368 \times 10^8 \text{ in-lb}}{7028 \text{ in}^3}$$

$$= 12{,}349 + 47{,}923 = 60{,}272 \text{ psi}$$

This stress exceeds the minimum ultimate stress for the A36 material. Therefore, the A-member will be slightly enlarged, by increasing a, to form the C-member. For bending only let the allowable stress be

$$\sigma_y = 36{,}000 \text{ psi}$$

Using Equation (E-10),

$$Z_p = \frac{3.368 \times 10^8 \text{ in-lb}}{36{,}000 \text{ psi}} = 2\left[(\bar{y} - 16.12 + 8.06)(69.7) + (\bar{y} - 16.12)^2/2\right]$$

$$\bar{y}^2 + 107.16\,\bar{y} - 10{,}219.3 = 0$$

$$\bar{y} = \frac{-107.16 \pm \sqrt{(107.16)^2 - 4(-10{,}219.3)}}{2}$$

$$= \frac{-107.16 \pm 228.82}{2}$$

$$\therefore \bar{y} = 60.83 \text{ in.}$$

and from Equation (E-9):

$$(60.83)(156.3 + a) = 2830.2 + 102.7a + .5a^2$$

$$\frac{1}{2}a^2 + 41.87a - 6677.85 = 0$$

$$a = \frac{-41.87 \pm \sqrt{(41.87)^2 - 4(1/2)(-6677.85)}}{2(1/2)}$$

$$= -41.87 \pm 122.92$$

$$\therefore a = 81.05 \text{ in.}$$

Total Area = $156.3 + 81.05(1) = 237.35 \text{ in}^2$

Now the combined stress is

$$\sigma = 36{,}000 + \frac{2.676 \times 10^6}{237.35} = 47{,}274 \text{ psi}$$

This stress is significantly less than the ultimate and will be adequate for this design. Shearing stresses were not specifically calculated but will be equal in magnitude to the tension stresses due to the axial load.

SUMMARY OF MEMBER DIMENSIONS
(Without Contribution of Panel Edge Members)

A-Member

Unit wt = 2 X 237 + (60.4)(1)(12)(.283)
=
= 679 lb/ft

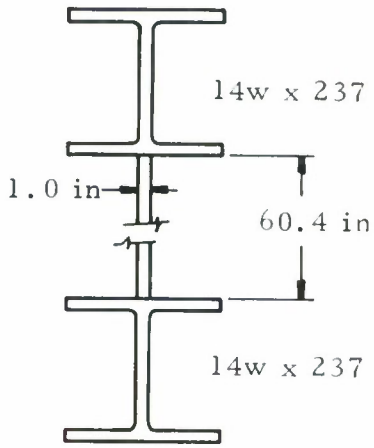

B-Member

Unit wt = 237 lb/ft

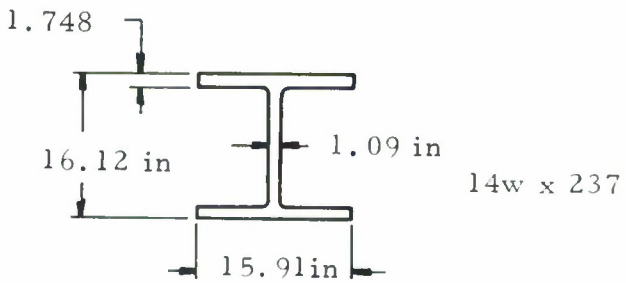

C-Member

Unit wt = 2 X 237 + (81.05)(1)(12)(.283)

= 749 lb/ft

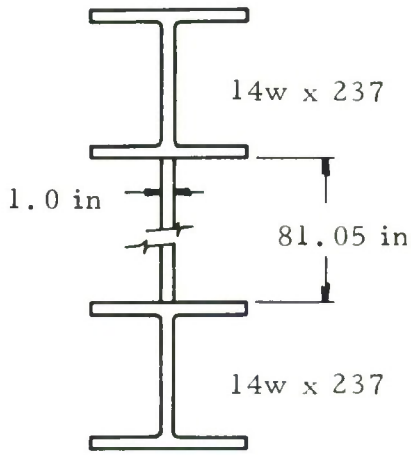

REFERENCES

1. DOD Manual 4145.27M, "DOD Ammunition and Explosives Safety Standards," Dept. of Defense, Off. of the Asst. Sec'y. of Defense (Installations and Logistics), March 1969.

2. W.E. Baker, *Explosions in Air*, Univ. of Texas Press, Austin, Texas, 1973.

3. Report EA1002, "Study of Suppressive Structures Applications to an 81 mm Automated Assembly Facility," prepared for Manufacturing Technology Directorate, Chemical and Plants Division, Edgewood Arsenal, 16 April 1973.

4. Report EA-FR-2B01, "Static Pressure Investigations for the Chemical Agent Munition Demilitarization System," 30 June 1973.

5. Report EA-4E33, "81 mm Suppressive Shielding Technical Data Package," January 1974.

6. Report EA-FR-2B02, "Final Report Application of Suppressive Structure Concepts to Chemical Agent Munition Demilitarization System (CAMDS)," July 27, 1973.

7. W.E. Baker, "Modeling of Large Transient Elastic and Plastic Deformations of Structures Subjected to Blast Loading," *Jour. of Appl. Mech.*, 27, Series E, Sept. 1960, pp. 521-527.

8. W.E. Baker, "Laws for Model Scaling of Interaction of Structures with Blast Waves," *Proc. of 3rd Int. Symp. on Military Applications of Blast Simulators*, 19-21 Sept. 1972, pp.D6-1 through D6-9.

9. H. Schardin, "Dimensionlose Kennzahlen der Hydro- und Aerodynamik," (undated).

10. W.E. Baker, P.S. Westine and F.T. Dodge, *Similarity Methods in Engineering Dynamics*, Hayden Book Co., Inc., Rochelle Park, N.J., 1973 (see Chapts. 4 and 6).

11. W.E. Baker, "The Elastic-Plastic Response of Thin Spherical Shells to Internal Blast Loading," *Jour. of Appl. Mech.*, 27, Series E, 1, Mar. 1960, pp. 139-144.

12. J.F. Proctor and W.S. Filler, "A Computerized Technique for Blast Loads from Confined Explosions," 14th Annual Expl. Safety Seminar, New Orleans, La., 8-10 Nov. 1972, pp. 99-124.

13. J.F. Proctor, "Internal Blast Damage Mechanisms Computer Program," 61 JTCG/ME-73-3, Joint Technical Coordinating Group for Munitions Effectiveness, 10 April 1973.

14. R.G.S. Sewell and G.F. Kinney, "Internal Explosions in Vented and Unvented Chambers," 14th Annual Expl. Safety Sem., New Orleans, La., 8-10 Nov. 1972, pp. 87-98.

REFERENCES (Cont'd)

15. W.A. Keenan and J.E. Tancreto, "Effects of Venting and Frangibility on Blast Environment from Explosions in Cubicles," *Minutes of the Fourteenth Explosives Safety Seminar*, New Orleans, November 1973, pp. 125-161.

16. A.H. Lasseigne, "Static and Blast Pressure Investigation for the Chemical Agent Munition Demilitarization System:Sub-Scale," Report EA-FR-4C04, November 30, 1973.

17. A.L. Florence and R.D. Firth, "Rigid-Plastic Beams Under Uniformly Distributed Impulses," *Jour. of Appl. Mech*, 32, Series E, 3, September 1965, pp. 481-488.

18. J.S. Humphreys, "Plastic Deformation of Impulsively Loaded Straight Clamped Beams," *Jour. of Appl. Mech.*, 32, Series E, 1, March 1965, pp. 7-10.

19. A.L. Florence, "Circular Plate Under a Uniformly Distributed Impulse," *Jour. Solids & Structures*, 2, 1966, pp. 37-47.

20. *Steel and Aluminum Stock List and Reference Book, No. 71* Earle M. Jorgensen Co., Copyright 1971.

21. R.J. Roark, *Formulas for Stress and Strain*, 4th Edition, McGraw-Hill Book Company, 1965, pp. 110 and 116.

22. *Manual of Steel Construction*, 7th Edition, American Institute of Steel Construction, June 1970.

DISTRIBUTION OF SUPPRESSIVE SHIELDING REPORTS

Addressee	No. of Copies
Commander Rocket Propulsion Laboratory Attn: Mr. M. Raleigh Edwards Air Force Base, CA 93523	1
Commander HQ, Armament Development Test Center Attn: DOM/Mr. S. Reither Eglin Air Force Base, FL 32542	1
Commander Hill Air Force Base Attn: MMNTR/Mr. Cummings Clearfield, UT 84406	1
Commander Norton Air Force Base Attn: AFISC-SEV/Mr. K. Collinsworth San Bernardino, CA 92409	1
Commander Air Force Civil Engineering Center Attn: AFCEC-DE/LTC Walkup Tyndall Air Force Base Panama City, FL 32401	1
Commander HQ Air Force Logistics Command Attn: MMWM/CPT D. Rideout IGYE/Mr. K. Shopher Wright-Patterson Air Force Base Dayton, OH 45433	1 ea
Commander Naval Ordnance Systems Command Attn: Code ORD 43B/Mr. A. Fernandes Washington, DC 20360	1
Commander Explosives Safety Attn: ADTC/SEV (Mr. Ron Allen) Eglin Air Force Base, FL 32542	1

Commander Bureau of Naval Weapons Attn: Code F121/Mr. H. Roylance Department of the Navy Washington, DC 20360	1
Commander Naval Ship Research & Development Center Attn: Code 1747/Mr. A. Wilner Bethesda, MD 20034	1
Commander Naval Explosive Ordnance Disposal Facility Attn: Code 501/Mr. L. Wolfson Indianhead, MD 20640	1
Commander Naval Ordnance Systems Command NAPEC Naval Ammunition Depot Attn: ORD-04M/B/X-5/Mr. L. Leonard Crane, IN 47522	1
Commander US Naval Surface Weapons Center Attn: Mr. J. Proctor Whiteoak, MD 20904	1
Chairman DOD Explosives Safety Board Attn: COL P. Kelly, Jr. Forrestal Building GB-270 Washington, DC 20314	5
Joint Army-Navy-Air Force Conventional Ammunition Production Coordinating Group USA Armament Command Attn: Mr. Edward Jordan Rock Island, IL 61201	5
HQDA (DAEN-MCC-I/Mr. L. Foley) Washington, DC 20314	1
HQDA (DAEN-MCE-D/Mr. R. Wight) Washington, DC 20314	1
Director USAMC Field Safety Activity Attn: AMXOS-TA/Mr. Olson Charlestown, IN 47111	1

Commander US Army Materiel Command Attn: AMCCG AMCRD/Dr. Kaufman AMCSF/Mr. W. Queen AMCPM-CS/COL Morris 5001 Eisenhower Ave. Alexandria, VA 22333	1 ea
Office of the Project Manager for Munition Production Base Modernization and Expansion Attn: AMCPM-PBM-E/Mr. Dybacki USA Materiel Command Dover, NJ 07801	3
Commander US Army Armament Command Attn: AMSAR-EN/Mr. Ambrosini AMSAR-SC/Dr. C. Hudson AMSAR-SF/Mr. J. Varcho AMSAR-TM/Mr. Serlin, Mr. T. Fetter, Mr. S. Porter AMSAR-MT/Mr. A. Madsen, Mr. G. Cowan, CPT Burnsteel Rock Island Arsenal Rock Island, IL 61201	1 ea
Commander USAMC Ammunition Center Attn: Mr. J. Byrd AMXAC-DEM/Mr. Huddleston Mr. Sumpterer Savanna, IL 61074	1 ea
Commander Frankford Arsenal Attn: Mr. F. Fidel, Mr. E. Rempler Bridge and Tacony Sts. Philadelphia, PA 19137	1 ea
Commander Picatinny Arsenal Attn: Mr. Saffian Mr. J. Cannovan Mr. Hickerson Mr. I. Forsten Dover, NJ 07801	3 1 ea

Commander USA Test and Evaluation Command Attn: AMSTE-NB Aberdeen Proving Ground, MD 21005	1
Commander Dugway Proving Ground Attn: Dr. Rothenburg Mr. P. Miller Dugway, UT 84022	1 ea
Commander Cornhusker Army Ammunition Plant Grand Island, NE 68801	1
Commander Indiana Army Ammunition Plant Charleston, IN 47111	1
Commander Iowa Army Ammunition Plant Burlington, IA 52502	1
Commander Joliet Army Ammunition Plant Joliet, IL 60436	1
Commander Kansas Army Ammunition Plant Parsons, KS 67357	1
Commander Longhorn Army Ammunition Plant Marshall, TX 75671	1
Commander Lone Star Army Ammunition Plant Texarkana, TX 75502	1
Commander LA Army Ammo Plant P. O. Box 30,058 Shreveport, LA 71130	1
Commander Milan Army Ammunition Plant Milan, TN 38358	1
Commander Radford Army Ammunition Plant Radford, VA 24141	1

Commander Sunflower Army Ammunition Plant Lawrence, KS 66044	1
Commander Lake City Army Ammunition Plant Attn: Mr. John Jacobi Independence, MO 64056	1
Commander Ravenna Army Ammunition Plant Ravenna, OH 44266	1
Commander Pine Bluff Arsenal Pine Bluff, AR 71601	1
Director US Army Materiel Systems Analysis Activity Aberdeen Proving Ground, MD 21005	3
Director US Army Ballistics Research Laboratories Attn: Mr. R. Vitali Aberdeen Proving Ground, MD 21005	5
Division Engineer US Army Engineer Division, Huntsville Attn: HNDED-R/Mr. Dembo Mr. W. Char P.O. Box 1600, West Station Huntsville, AL 35807	1 ea
US Army Engineer Division Waterways Experimental Station P.O. Box 631 Vicksburg, MS 39180	1
Director USAMC Intern Training Center Attn: Dr. G. Chiang Red River Depot Texarkana, TX 75502	1
Dr. Robert D. Siewert NASA Lewis Laboratory 21000 Brook Park Rd Cleveland, OH 44135	1

Mr. George Pinkas 1
Code 21-4
NASA Lewis Laboratory
21000 Brook Park Rd
Cleveland, OH 44135

Mr. W. H. Jackson 1
Deputy Manager for Engineering
Atomic Energy Commission
P.O. Box E
Oak Ridge, TN 37830

Mr. Erskine Harton 1
US Department of Transportation
Washington, DC 20315

Dr. Jean Foster 1
US Department of Transportation
Washington, DC 20315

Mr. Frank Neff 1
Mound Laboratory
Monsanto Research Corp.
Miamisburg, OH 45342

Ms. Trudy Prugh 1
Mound Laboratory
Monsanto Research Corp.
Miamisburg, OH 45342

Commander 1
Naval Weapons Laboratory
Attn: Mr. F. Sanches
Dahlgren, VA 22448

Dr. W. E. Baker 1
Southwest Research Institute
San Antonio, TX 78284

Division Engineer 1
US Army Engineer Division, Fort Belvoir
Fort Belvoir, VA 22060

Commander 1
Naval Sea Systems Command
Washington, DC 20315

Mr. Billings Brown Hercules, Inc. Box 98 Magna, UT 84044	1
Mr. John Komos Defense Supply Agency Cameron Station Alexandria, VA 22030	1
Office of the Project Manager for Chemical Demilitarization and Installation Restoration Edgewood Arsenal Aberdeen Proving Ground, MD 21010	2
Edgewood Arsenal Technical Director Attn: SAREA-TD-E Foreign Intelligence Officer Chief, Legal Office Chief, Safety Office CDR, US Army Technical Escort Center Author's Copy, Manufacturing Technology Directorate Aberdeen Proving Ground, MD 21010	 1 1 1 1 1 3
Edgewood Arsenal Director of Biomedical Laboratory Attn: SAREA-BL-M SAREA-BL-B SAREA-BL-E SAREA-BL-H SAREA-BL-R SAREA-BL-T Aberdeen Proving Ground, MD 21010	 1 1 1 1 1 1
Edgewood Arsenal Director of Chemical Laboratory Attn: SAREA-CL-C SAREA-CL-P Aberdeen Proving Ground, MD 21010	 1
Edgewood Arsenal Director of Development & Engineering Attn: SAREA-DE-S Aberdeen Proving Ground, MD 21010	 4

Edgewood Arsenal Director of Manufacturing Technology Attn: SAREA-MT-TS SAREA-MT-M Aberdeen Proving Ground, MD 21010	 2 1
Edgewood Arsenal Director of Product Assurance Attn: SAREA-PA-A SAREA-PA-P SAREA-PA-Q Aberdeen Proving Ground, MD 21010	 1 1 1
Edgewood Arsenal Director of Technical Support Attn: SAREA-TS-R SAREA-TS-L SAREA-TS-E Aberdeen Proving Ground, MD 21010	 2 3 1
Aberdeen Proving Ground Record Copy CDR, APG Attn: STEAP-AD-R/RHA APG-Edgewood Area, BLDG E5179 Aberdeen Proving Ground, MD 21005	1
Aberdeen Proving Ground CDR, APG Attn: STEAP-TL APG, Aberdeen Area Aberdeen Proving Ground, MD 21005	1
DEPARTMENT OF DEFENSE Administrator Defense Documentation Center Attn: Accessions Division Cameron Station Alexandria, VA 22314	 12
Commander Edgewood Arsenal Attn: SAREA-DM Aberdeen Proving Ground, MD 21010	 1